ABSTRACT

BATIKH, AKRAM. Development of a Transient Benchmark for the Transient Reactor Test Facility (TREAT). (Under the direction of Dr. Ayman I. Hawari)

A transient benchmark based on the Transient Reactor Test Facility (TREAT) M2 Calibration experiment (M2-CAL) is under development. TREAT, at Idaho National Laboratory, is a graphite-moderated air-cooled research reactor which has been used extensively for fuel material testing under extreme and accident conditions. Accurate benchmark models are a beneficial component in the operations, experimental planning, and development of TREAT. In this work, we present a transient benchmark model for the M2-CAL experiment core loading. The benchmark model incorporates the coupling between the Monte Carlo Code Serpent and the computational fluid dynamics code OpenFOAM to capture the temperature feedback mechanism. The temperature distribution in the core is obtained by solving the heat conduction equation in OpenFOAM after transferring the volumetric power distribution calculated in Serpent. Given the short duration of the transient (~11 s), the adiabatic approximation was imposed in OpenFOAM. The M2-CAL transient 2580 was simulated in this work. The benchmark uncertainties for the calculated values of interest were determined by only taking into account the major core parameters contributing to the uncertainty in k_{eff} in the steady-state model. The steady-state benchmark uncertainties in k_{eff} were calculated by performing a $\pm 1\sigma$ perturbation for each variable in the core and calculating the total impact in a quadrature sum. The major objective of this transient test was to determine the power coupling (PCF) and transient correction factors (TCF) in the flux wire before the start of the M2 and M3 tests. A pre-transient analysis was performed to determine the optimum core composition and conditions before the beginning of the transient. The analysis was validated against historic TREAT kinetic measurements and the worth of the transient rod T-2. The steady-state benchmark model was used to determine the PCF and the axial power distribution obtained using U-Zr flux wire measurements. The PCF was calculated in the flux

wire by assigning track-length estimator detectors in the wire, where the fission rates are counted. The PCF was found to be 0.412 ± 0.008 compared to an experimental value of 0.492 ± 0.065. This 16% deviation is attributed to the large uncertainty in the hydrogen concentration. The model was then used to simulate the M2-CAL transient 2580 experiment based on the reported pre-transient and transient conditions. Several transient observables were calculated and compared to the experiment. The model shows good agreement with the experimental power traces, period, and average increase of power at the power ramp (time > 7.8 s in the experiment). The value of the integral worth reported at 16 inch is 1.111%, contrasted with 1.128% calculated by the model. The PCF for the transient test was found to be 0.379 ± 0.001, contrasted with an experimental value of 0.4262 ± 0.0564. The TCF was determined by calculating the ratio of the PCF in steady-state to that of the transient, and was found to have a value of 0.921 ± 0.017 compared to an experimental value of 0.87 ± 0.17. Inverse point kinetics analysis was performed during the period of the power ramp for the model and the experiment. Based on that, the temperature feedback component was isolated and contrasted with the experimental feedback. The deviation in the feedback reactivity compared to the experiment was found to be 16%, which may be attributed to the implementation of the adiabatic approximation. The maximum temperature calculated by the model was found to be 6.79 K higher than that reported in the experiment.

Development of a Transient Benchmark for the Transient Reactor Test Facility (TREAT)

by
Akram S. Batikh

A thesis submitted to the Graduate Faculty of
North Carolina State University
in partial fulfillment of the
requirements for the degree of
Master of Science

Nuclear Engineering

Raleigh, North Carolina

2022

APPROVED BY:

_____	_____
Dr. Ayman I. Hawari Committee Chair	Dr. Nam Dinh

_____
Dr. Paul Huffman

BIOGRAPHY

Akram Batikh was born in the countryside of Kafr El-Shaikh, Egypt in 1993. After finishing high school, Akram Joined the department of Nuclear and Radiation Engineering at Alexandria University. In his undergraduate studies, he came top of his class in each year. After graduating with a B.Sc in nuclear and radiation engineering, Akram was conscripted in the Air Defense Forces of the Egyptian military for one year. He received a fellowship from Alexandria University to work as a teaching assistant in the department of Nuclear and Radiation Engineering. By Fall 2019, Akram begin to pursue a Master's degree in the field of nuclear engineering at NC State University. Akram has done research on the transient analysis and benchmarking of the Transient Reactor Test Facility (TREAT) under the supervision of Dr. Ayman Hawari. During his free time, Akram enjoys reading about anthropology and astrophysics.

ACKNOWLEDGMENTS

I would like to express my deepest gratitude to my advisor, Dr. Ayman I. Hawari, for his guidance throughout this academic journey. I really like to thank him for his guidance and insight during my research and graduate studies. Dr. Hawari's patience and motivation have been inspirational during my studies, and I aspire to emulate his dedication throughout my own career.

I would like to thank Dr. Nam Dinha and Dr. Paul Huffman for graciously serving on my committee. I am grateful for their valuable inputs, advice, and feedback on the research work and thesis. I would like to express my sincere thanks to Dr. Colby Fleming for her assistance and valuable insights.

I am utterly grateful for the continuous support, encouragement, and inspiration my family and my friends have provided over the past years.

TABLE OF CONTENTS

LIST OF TABLES

LIST OF FIGURES

ABBREVIATIONS

TREAT: Transient Reactor Test Facility

PCF: Power Coupling Factor

TCF: Transient Correction Factor

LLSS: Low Level Steady-State

pcm: Per cent milli rho (ρ)

ppm: Part per Million

neg.: Negligible

IGF: Inert Gas fusion

NDIR: Non-Dispersive Infrared Detector

TC: Thermal Conductivity

Combustion-IR: Combustion Infrared Detection

Inhr : Inhour (inverse hour)

1 INTRODUCTION

The Transient Reactor Test Facility (TREAT), located at Idaho National Laboratory (INL), is part of the Materials and Fuels Complex (MFC) and was originally designed to evaluate reactor fuels and structural materials. The TREAT reactor is a high enriched, air cooled, graphite moderated, and graphite reflected core. This thermal spectrum reactor is heavily influenced by the graphite material properties. The fuel is dispersed in a graphite matrix which provides a large thermal feedback safety mechanism as well as the ability to dissipate large amounts of heat from the fuel and into the graphite. These characteristics are necessary for the transient operations for which TREAT has been historically used. For transient operation, up to eight transient rods can be used in the core. These highly accurate and rapid reactivity insertions result in high power transients during which experiments can be examined. A maximum core power around 18 GW is possible along with periods as short as ±100 ms. This allows for a range of transients and even fuel-failure accident scenarios to be tested. The core can be used to apply large amounts of direct heat for experiments, test reactor fuels in extreme accident scenarios, and also for large-scale neutron radiography.

To be able to conduct such experiments, the center of the core is open and accessible for experiment insertion. This hole is large enough for reactor fuel pins and bundles to be inserted for testing. To the north and south, the core can be configured with slotted assemblies to allow for a clear view of the experimental vehicle from outside the core. The fast neutron hodoscope, located at the north opening of the reflector, collimates fast fission neutrons which are observed by a range of detectors providing the ability to monitor experimental fuels during a transient exercise. To the west, the neutron radiography facility can be used for steady state operations, able to handle assemblies up to 15 ft. in length. A general overview of TREAT and some of these features can be seen in Figure 1-1.

TREAT, which first started up in 1959, operated continuously for 35 years before being shutdown in 1994. Under the U.S. Department of Energy (DOE) initiative to resume transient testing, TREAT was successfully

restarted in 2017 with testing of transient capabilities resuming in 2018. During its 35 years of operation, a series of experiments termed the M-series were conducted. The last experiments of this series (the M8 experiments) were scheduled; however, the facility was placed into long-term shutdown prior to the completion of M8. The earlier M2 and M3 experiments were finished. These were designed to test metal fuel during a slow transient overpower (TOP) excursion to support the Integral Fast Reactor (IFR) program. These TOP excursions are characteristic of IFR reactivity-insertion ramps. Fifteen M2 and M3 calibration (M2/M3CAL) experiments were conducted from 1984 to 1985 to determine the steady state power coupling factor (PCF) and the transient coupling factor (TCF) for the three fuel pins to be tested in the M2 and M3 experiments. These power coupling factors quantify the relationship between the experiment power and core power. The core configuration and experimental vehicle are the same for both the M2 and M3 calibration experiments. The core configuration features a fully slotted, north-to-south core with the experimental vehicle placed in the center where the test pins or flux wires would be irradiated. A fully slotted core was used to attempt to reduce the amount of back scattering that could contaminate the image produced by the hodoscope.

The power coupling factor was determined using fresh EBR-II Mark-II driver fuel pins which were irradiated at low-level, steady-state power (LLSS) within a neutronically "equivalent" test vehicle. This test vehicle was designed to shape the flux profile so that test pins with lengths on the order of inches could represent full-length test pins with lengths on the order of feet. The test pins used for the M2 and M3 tests (M2/M3 TEST) ranged from fresh fuel to approximately 8% burnup EBR-II Mark-II driver fuel pins with sodium coolant. The actual test transients were overpower-without-scram tests where the time and location of cladding breach would be observed along with fuel motion after the initial failure. Accurate coupling factors from the M2/M3CAL experiments were required to determine the heat generation in the fuel pins for the subsequent test experiments. The results from the M2/M3CAL would then contribute directly to the safety analysis and preparation for the M2/M3 tests.

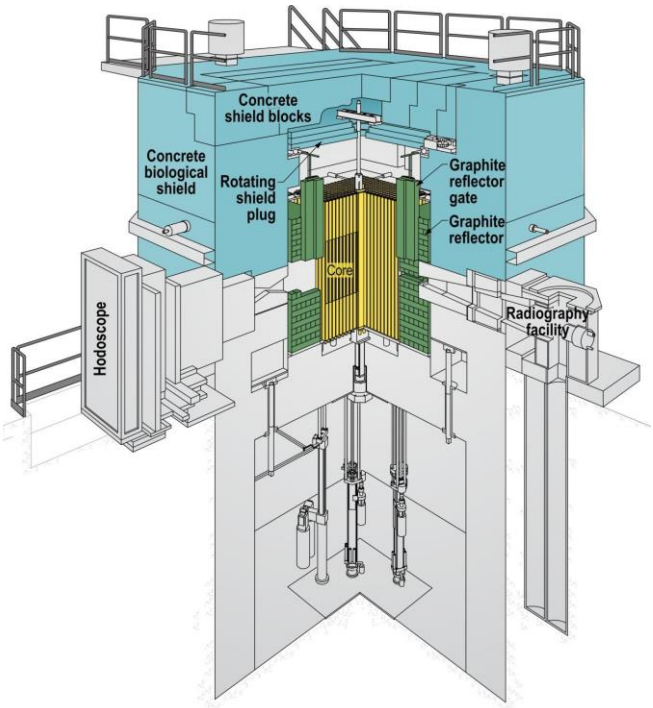

Figure 1-1. TREAT Reactor General Configuration [1]

The transient coupling factors were determined based on uranium-zirconium flux wire irradiations under LLSS conditions and then also transient conditions to determine the axial power profiles at the test pin locations. The flux wires were then compared to the LLSS test pin irradiations to approximate the conditions for the test pins during the experimental transients.

This work will be addressing the M2CAL 2580 Transient experiment which is one of the M2CAL transient tests. The M2 2580 transient test is described in detail in References [2-4]. Many of the reactor details specific to TREAT and not to the particular experiment are taken from reference [1]. This work is a part of a broad effort to develop accurate benchmark models in support of the operation and planning of transient experiments in TREAT. The project also aims at establishing and benchmarking the coupling scheme of Serpent/OpenFOAM as a more convenient alternative to conducting calibration experiments before transient tests. Moreover, this benchmark could lead to the reevaluation of the uncertainties in core compositions.

2 DESCRIPTION OF THE EXPERIMENTAL CONFIGURATION AND MEASURMENTS

2.1.1 Overview of Experiment

The M2 and M3 calibration core configuration and experiments are evaluated for this benchmark due to similarity of core configuration and operation. The M2CAL 2580 experiment was conducted on September 21, 1984 at Idaho National Laboratory's TREAT Reactor as a part of partial energy wire trail transients. First, the experiment began with establishing the pre-transient (critical) conditions for M2CAL 2580 transient test with an estimated power of 50W. The transient is then initiated by ejecting the transient rod T-2 following a pre-planned rod dynamic. The transient lasted approximately 10 seconds from initial rod withdrawal to shutdown [13]. Following the transient, the flux wire positioned in the experimental vehicle was cut into segments and the activity of each segment was measured. The PCF and TCF were then determined by measuring the absolute fission rate in the wire.

2.1.2 Geometry of the Experiment Configuration and Measurement Procedure

The TREAT core is comprised of highly-enriched uranium dioxide (UO_2) dispersed in a graphite matrix, surrounded both radially and axially with a graphite reflector. The core is air cooled and arranged in a 19x19 square lattice for a total of 361 assembly locations. Each of the standard assemblies is 3.960 inch square and comprised of a 4 feet fuel section in the middle with 2 feet of graphite above and below. The assemblies are chamfered such that square air channels are formed at the corners of the assemblies, and the assemblies are arranged on a 4-inch lattice to also allow an air gap between the assembly flat edges. Modified versions of the standard assemblies were created for the source assembly and control rod assemblies. In the middle of the core, the M2/M3CAL configuration features a full slot from north to south where the standard fuel assemblies are replaced with slotted assemblies containing only the graphite top and bottom reflectors but

with no fuel. The middle of the core is then loaded with the experimental vehicle which was designed to be the neutronic equivalent of the subsequent tests. The core configuration, displayed in Figure 2-2, was used for both the M2 and M3 calibrations. The exerts to the right of the core configuration detail the specific assemblies used in this loading.The M2/M3CAL experiments were conducted using core loading 1370 shown in Figure 2-2. The core contained 325 fuel elements, 16 - 48 inch slotted elements, and 2 - 48 inch half slotted elements. In addition, there were 16 fueled control elements of which 4 have transient rods and 12 have control/shutdown rods. In the north east corner is one source assembly, and the experimental vehicle is placed in the center of the core.

The assemblies are arranged on a steel grid plate. Surrounding the core sides is a 2-foot graphite reflector. A 2-inch air gap separates the assemblies and the reflector. The graphite reflector has several blocks removed for external access to the core specifically for the power detectors. Outside the graphite reflector is a 5 feet concrete biological shield. Again, a 2-inch air gap separates the reflector and shield. On the east face of the core, the concrete is replaced with graphite to form a thermal column. To the north, part of the hodoscope instrumentation is inserted into the cutout in the bioshield. To the west, the neutron radiography instrumentation is located in the shielding. Above the core, a large air gap exists from which air is pulled when the pumps are used for forced cooling. Above the air gap is an additional concrete shielding with boral sections. Below the grid plate, some space remains to allow for the placement of the assemblies, but below this point, the base of the reactor concrete forms a floor which also serves as shielding. Penetrations for the control rods go through the concrete base. A subpile room which houses the control rod machinery is located directly below the core and shielding. These details are seen in both Figure 2-2 previously but also in Figure 2-1 below.

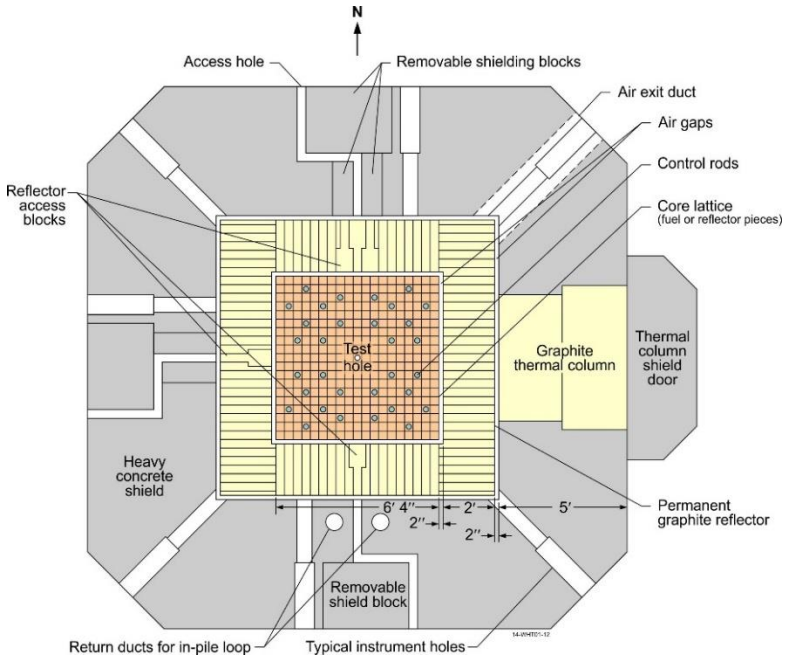

Figure 2-1. TREAT Reactor Core Overview from the Top Down [1].

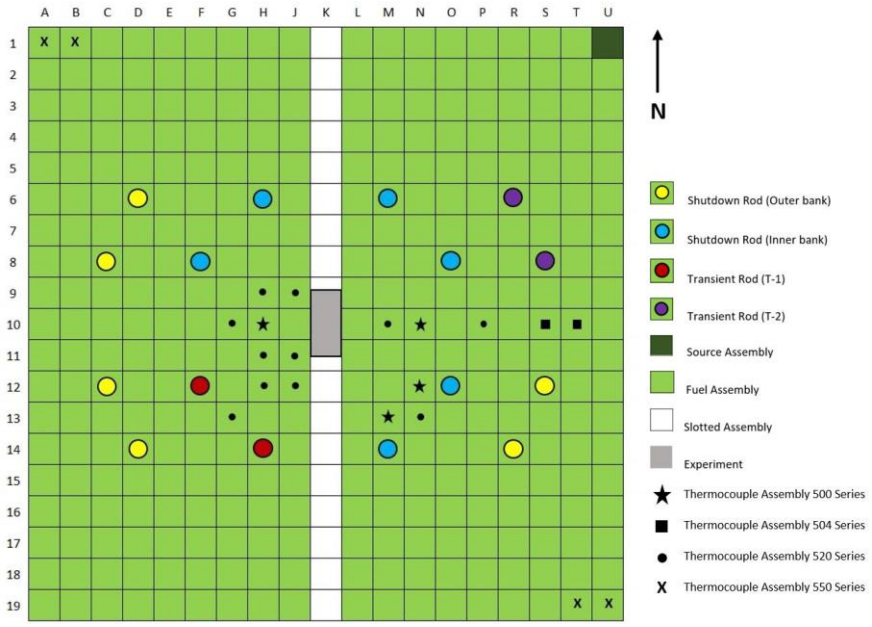

Figure 2-2. M2 and M3 Core Configuration [1].

Core loading 1370 has two banks of shutdown rods, an inner bank and an outer bank. In addition, there are two sets of transient rods (T1 and T2). The inner shutdown rod bank is fully withdrawn at a height of

59 inches, and the outer shutdown rod bank is withdrawn to 32.5 inches. Transient rods T1 are fully withdrawn at 40 inches, and transient rods T2 are withdrawn to 13.86 inches to achieve criticality.

In the central test vehicle, relative activity measurements were taken to characterize the flux distributions axially in the core and relative to core power. These measurements done with test pins (95% uranium, 5% fissium) under LLSS power and U-Zr wires under LLSS and transient conditions contribute directly to the power coupling factor. The flux wires traverse the entire core height while the test pin fuel section is only 13.5 inches long, and both are located centrally in the core. The flux wires or test pins (depending on the experiment) were surrounded with a dysprosium collar to shape the flux profile.

2.1.2.1 ***TREAT Reactor Core Components***

The following assemblies and reactor components are generic to TREAT, and these are the building blocks used for the M2/M3CAL core configuration. Modified or special TREAT assemblies were designed to be variations of the standard TREAT fuel assembly. The modified assemblies share many of the design features present in the standard TREAT fuel assembly.

2.1.2.1.1 Standard Fuel Assembly

The standard fuel assembly with applicable drawings is shown in Figure 2-3. The fuel assemblies are comprised of chamfered top and bottom graphite reflector sections with chamfered fuel blocks containing high-enriched UO_2 dispersed in a graphite matrix. Zircaloy-3 cans hold the fuel blocks while aluminum cans are used for the top and bottom graphite reflectors.

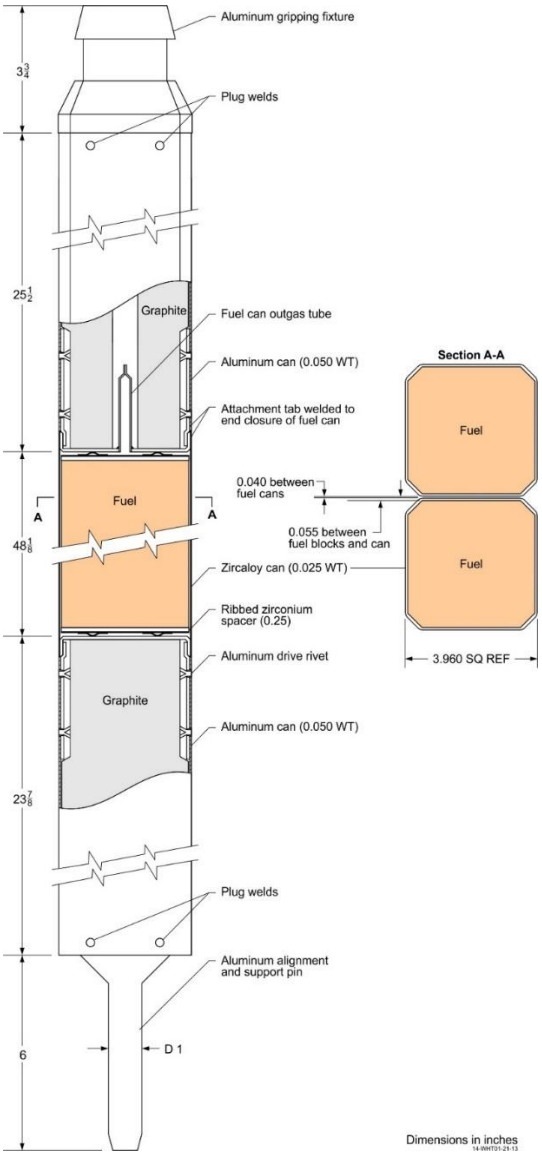

Figure 2-3. Standard TREAT Fuel Assembly (DWG# RE-1-21094.

2.1.2.1.2 Control Rod Fuel Assembly

Control rod fuel assemblies are essentially standard fuel assemblies with a hole through the middle to allow for the vertical insertion and removal of a graphite-boron control rod. Specific details for the modified parts are included in the following figures. Of note, the control rod tube is a Zy-2 component with outer diameter of 2-1/4 inches shown in Figure 2-4 [5].

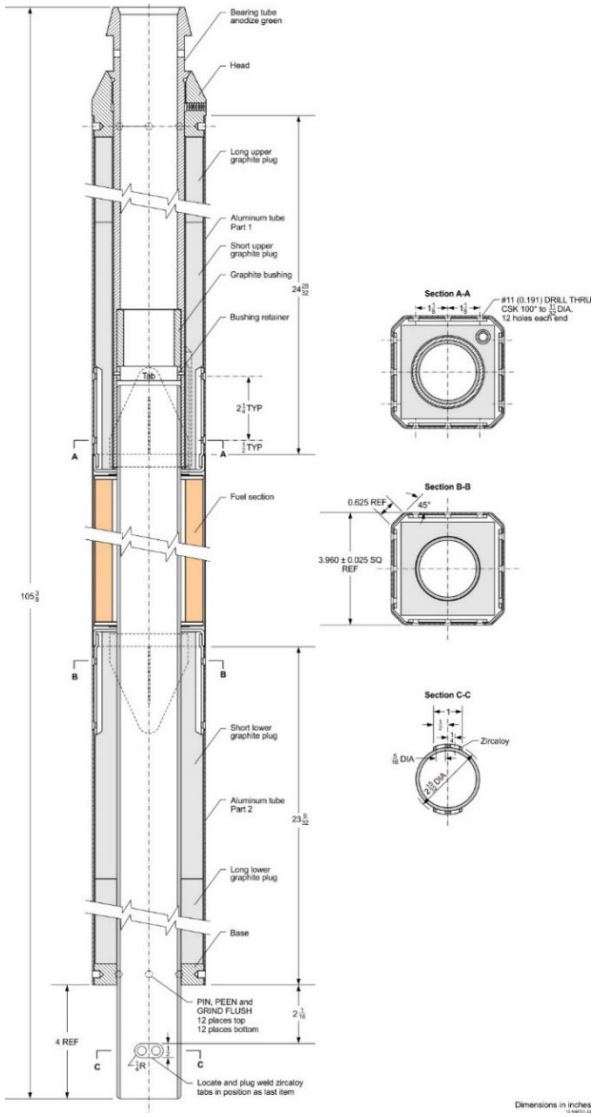

Figure 2-4. Control Rod Fuel Assembly (DWG# RE-1-22602) [1].

2.1.2.1.3 Control Rod / Transient Rod

The control rod consists of an upper poison (B_4C) section with a steel cladding followed by graphite clad in Zy-3 and then two graphite sections clad in steel [1]. Other references incorrectly report the cladding to be Zy-2 rather than Zy-3 [5,6]. Components of the control rod are given in Table 2-1. The control rod and transient rod are the same with the only difference being the length of the rod. Rods are inserted from below the core. The control rods shown in Figure 2-5 represents the rod configuration used in the M2/M3CAL core loadings. Other historical control rod configurations and compositions are not provided, but it should be noted that other historical TREAT experiments had different control rods.

Table 2-1. Control Rod Components [1].

Quantity	Component	Material
3	Screw - Rework	18-8 Stainless Steel
1	Adapter Control Rod Grapple	STL AISI 1010-1020
1	Poison Section	Mild Steel, B_4C, Plating
1	Zirconium Follower	Zy-3, CP-2 Graphite
1	P1 Upper Follower (Transient Rods)	Mild Steel, CP-2 Graphite
1	P2 Upper Follower (Control Rods)	Mild Steel, CP-2 Graphite
1	Follower Control Rod #2	Mild Steel
1	Adapter - Control Rod	STL AISI 1015

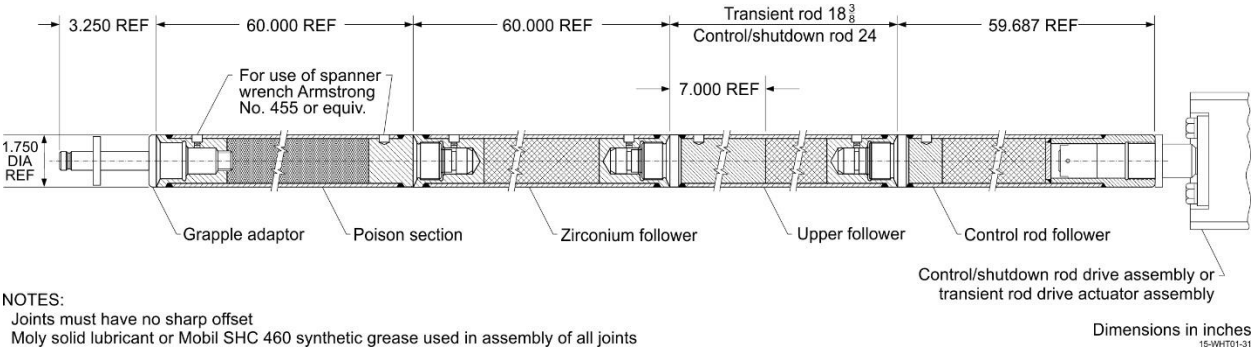

Figure 2-5. Control Rod Number II (DWG# ID-ID-13461) [1].

2.1.2.1.4 Coolant System

The TREAT system is air cooled using either natural convection or forced flow. Two turbocompressors, each rated for 3,250 cfm but reported to draw a total maximum of 6,000 cfm [1,5], circulate air through the reactor. The air is filtered and then enters through the top of the core, passing through the assemblies in the square channels formed by the chamfered edges of the assemblies and down to the lower plenum. The air is then filtered again as it is drawn from the lower plenum and discharged out a 60 feet stack. This system allows for steady state operations up to 100 kW, and it will also suffice to cool the core after transient operation [1]. For transient operation, the blowers would be started prior to the transient and maintained after shutdown to cool the system.

2.1.2.1.5 Instrumentation

In the north slot, a fast neutron hodoscope was installed. The fast neutron hodoscope allows for the detection and tracking of fuel within the experimental vehicle during a power transient. For the M-series experiments, an additional collimator was installed prior to the neutron hodoscope. This collimator was placed from the outside edge of permanent reflector through the concrete shielding to the north. To the west, a neutron radiography system was permanently installed, requiring the west gate to also remain permanently open. The majority of the instrumentation for these systems were installed outside the shielding.

Different detectors were used for the steady-state and transient operations. The exact (radial) position of each of the detectors was not recorded; however, it was documented that the transient chambers were only partially inserted [22]. All steady-state chambers and startup chambers were almost completely inserted [22]. Two holes directly above each other on the north, west, and south side penetrate the permanent reflector. They are spaced 24 inches apart, approximately 12 inches above and below the core midplane. Similarly, two holes penetrate the northwest, southwest, and southeast corners of the concrete shielding, again approximately 12 in. above and below the core midplane. These detector locations were filled with the following instruments given in Table 2-2. These positions were reported in December of 1980, and are

most likely those which were still in place during the M2/M3CAL experiments as the reported detector output in reference [23] corresponds with the detectors installed according to reference [22].

Table 2-2. TREAT Reactor Detectors in 1980 [22].

Location	Detector Reference Name	
NW Corner:	Upper - Transient Log 1, Transient Safety 1	Lower - Integral Power 1
West:	Upper - Start Up 2, Steady-State Safety 2	Lower - Steady-State Log Power 2
SW Corner:	Lower - Integral Power 2	
South:	Upper - Start Up 1, Linear	Lower - Steady-State Log Power 1, Steady-State Safety 1
SE Corner:	Upper - Transient Safety 2, Transient Log Power 2	Lower - Control Log, Control Power (Computer)

*2.1.2.2 **M2/M3 Calibration Experimental Components***

The M2/M3CAL experiment was comprised of test fuel pins placed within the neutronic equivalent of the Mark-IIIC test vehicle. This test vehicle was a simplified model of the full test vehicle. Parts were taken from the L03 and L04/L05 calibration vehicles, but a new spool piece was fabricated to replace the pump leg on the older L04/L05 calibration vehicle. In addition, a neutronic equivalent to the flowmeter magnet was added to the pump leg. The specific components can be seen in Figure 2-6 to Figure 2-17.

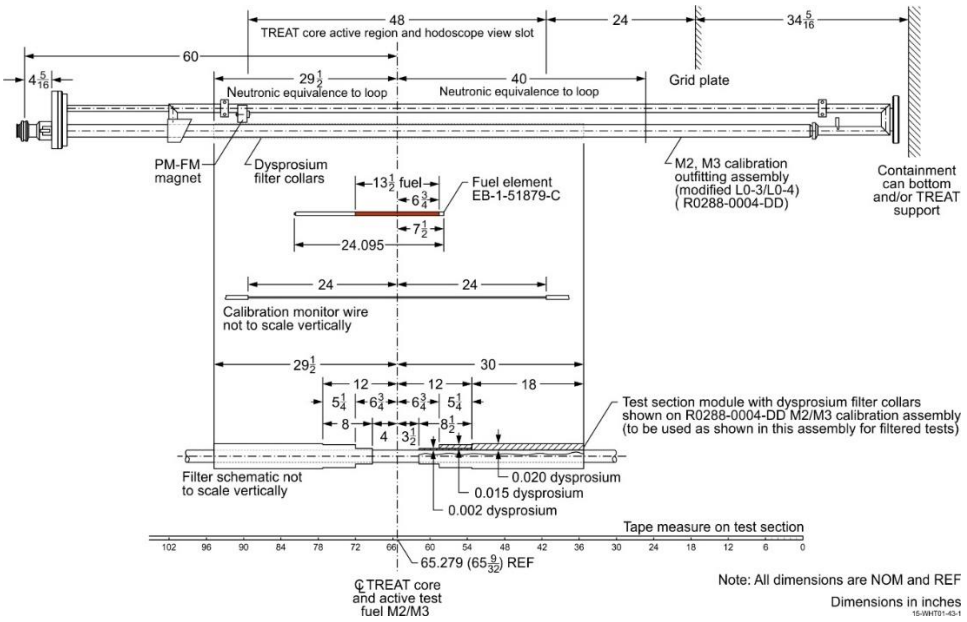

Figure 2-6. M2/M3CAL Test Train (DWG# R0288-0006) [1].

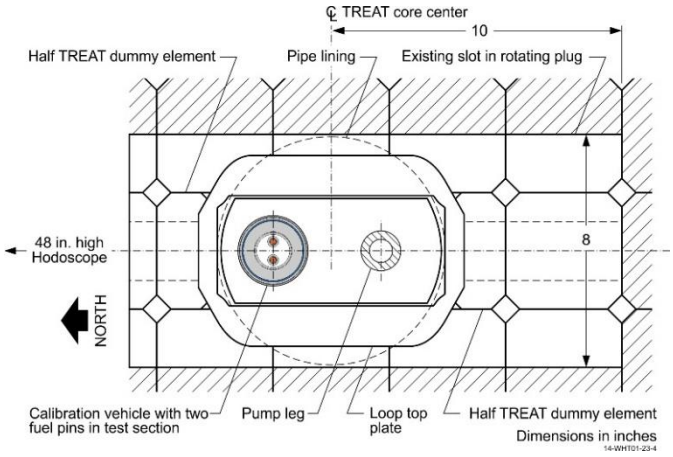

Figure 2-7. Top Down Cross Section of the Calibration Vehicle Location in the Core (based on [4]).[a]

[a] Note that the pin arrangement within the calibration vehicle is not representative of the M2/M3CAL pin configuration.

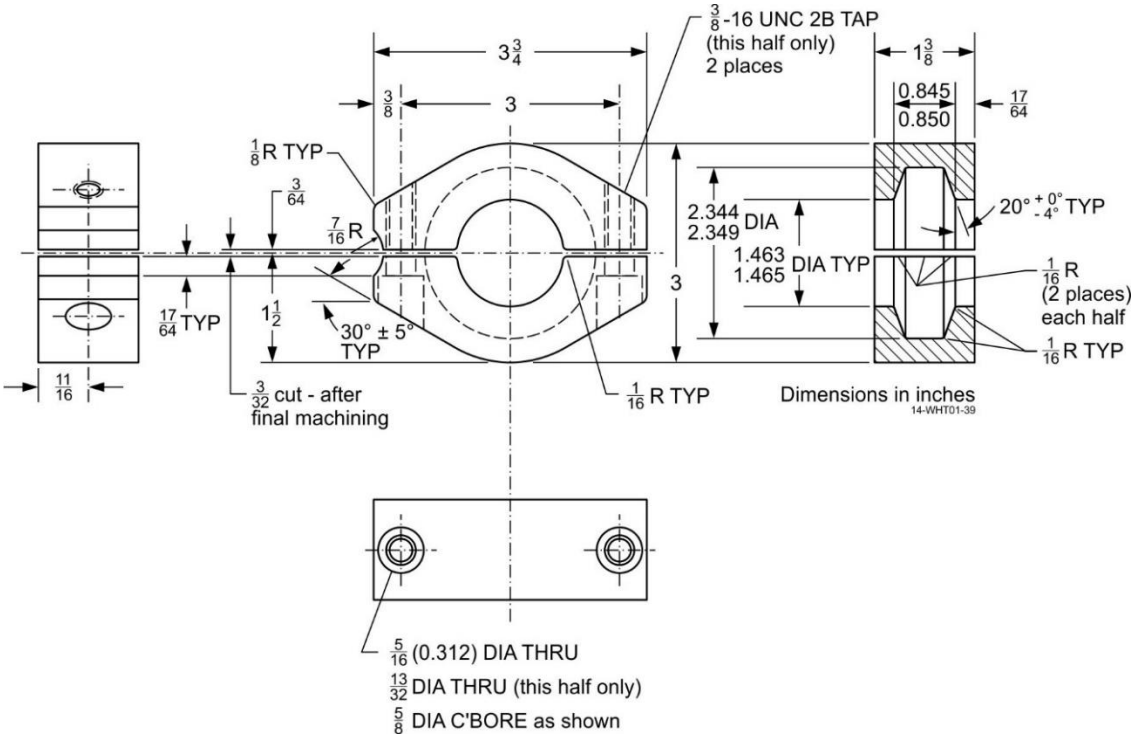

Figure 2-8. Clamp (top expansion tank tube) (DGW# R0225-0143) [1].

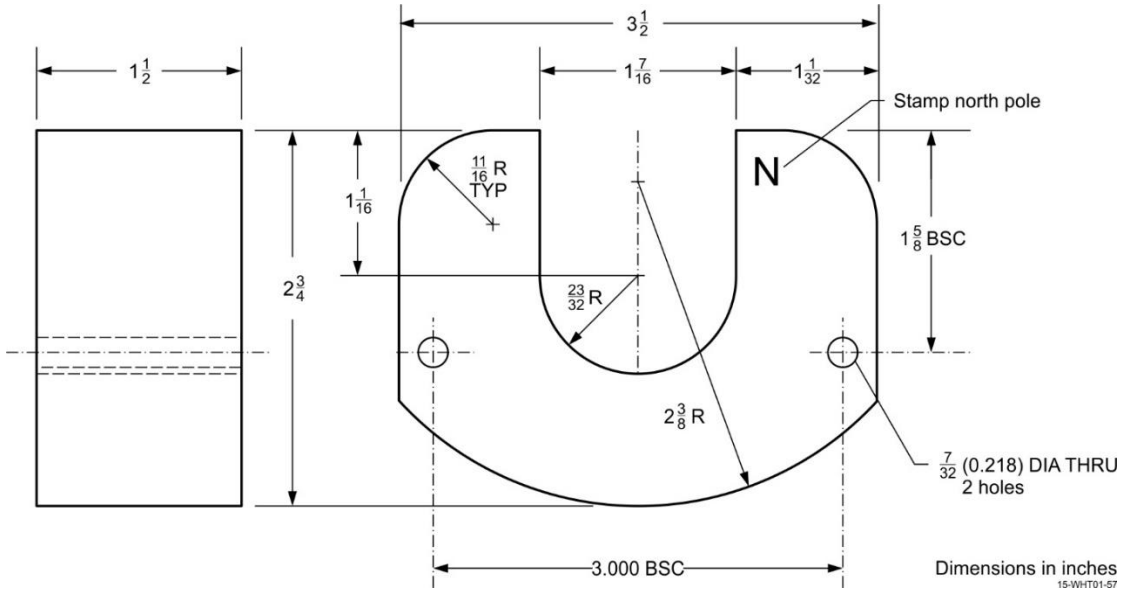

Figure 2-9. Pump Leg Flow Meter Magnet (DWG# R0253-0130) [1].

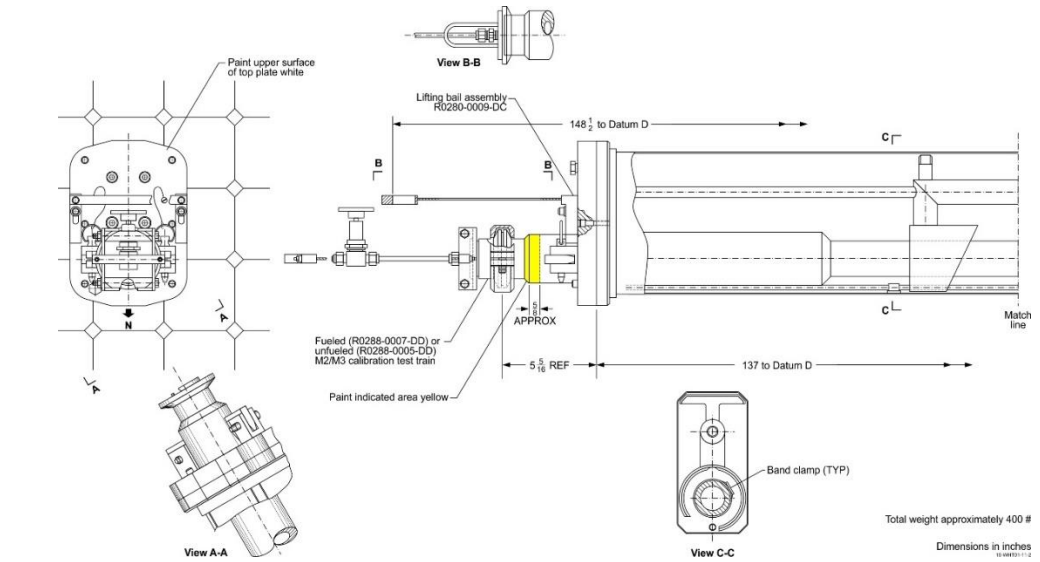

Figure 2-10. M2/M3CAL Assembly (Top) (DWG# R0288-0004) [1].

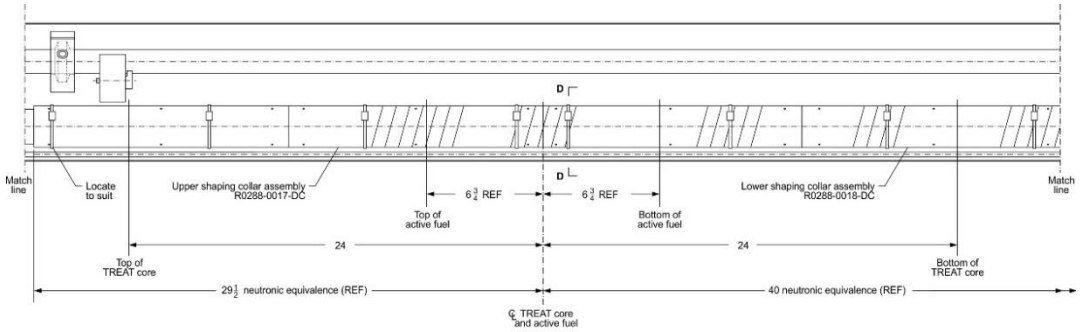

Figure 2-11. M2/M3CAL Assembly (Middle) (DWG# R0288-0004) [1].

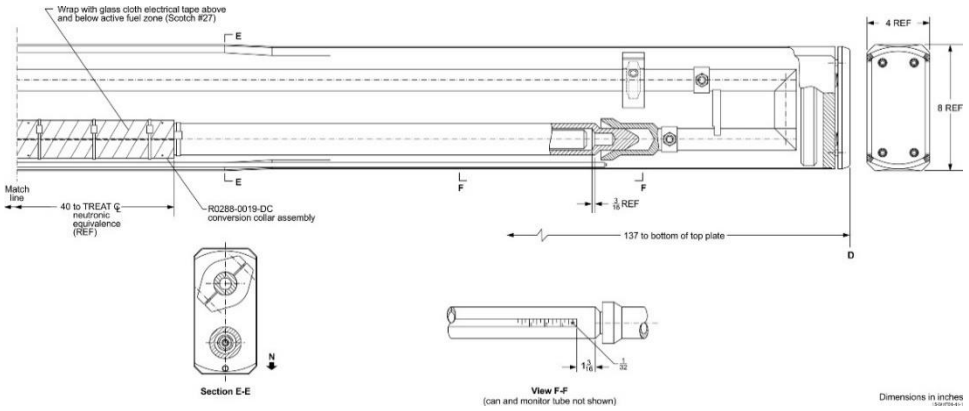

Figure 2-12. M2/M3CAL Assembly (Bottom) (DWG# R0288-0004) [1].

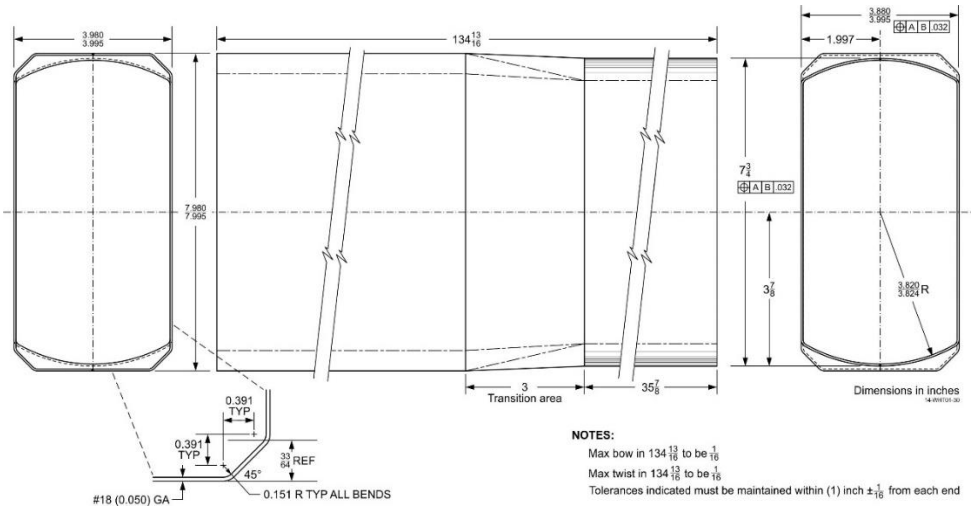

Figure 2-13. Mark III Can (DWG# R0230-0188) [1].

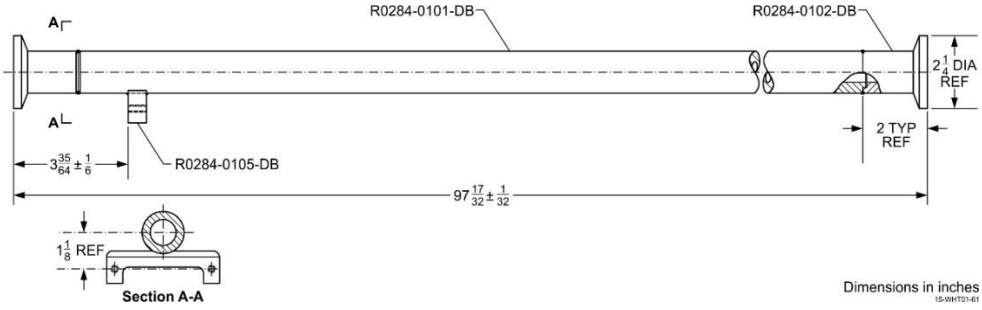

Figure 2-14. Spool Piece Assembly M2CAL (DWG# R0288-0002) [1].

The radial components of the calibration vehicle test section are given in Table 2-3 and in Figure 2-15. The geometry and the materials were designed to be representative of the Mark-IIIC M2/M3 test section. A

dysprosium collar with stainless steel forms along with dummy heaters were created and banded around the test section. The test pins are shown in Figure 2-16. The dysprosium shaping collar was intended to generate an axial power profile between that of the Integral Fast Reactor and EBR-II. A diagram of the shaping collar is given in Figure 2-17 which demonstrates the stair-step design.

For this calibration experiment, no sodium coolant was used in the system. Instead, the voids were filled with an inert plenum gas comprised of 25% argon and 75% helium gas [8]. The experiment was comprised of three fresh EBR-II Mark-II high enriched driver fuel pins. The pins have a 13.5-inch long fuel section. Around the fuel pins, flow tubes, shield tubes, and an outer tube surround each pin. These three pins are then grouped and placed in the test loop. Each pin was comprised of 95 wt% uranium and 5 wt% fissium. Fissium is the solid fission products that remain in the fuel after reprocessing. The fresh fuel pins used were fabricated without the usual sodium bonding such that the fuel sits loosely within the cladding. While the sodium bonding was not used for the fresh test pins in the M2/M3 calibration experiments, the details for the sodium bonding are still included in the table and figure below for consistency with the published experiment information. All other details regarding the pin geometry and materials in the tables and figures should be consistent with the M2/M3 calibration test pins.

The fuel section of the test pin was approximately centered with the midplane of the core. Neutron radiographs were taken of the test system (test fuel in the center of the calibration vehicle), and it was discovered that the fuel pins were actually placed 0.32 cm below the center of the core relative to the dysprosium shaping collar [4]. Details for the geometry of the test pins are given in Table 2-4.

The uranium-zirconium flux wires used in the transient coupling factor (TCF) measurements were 3.6 wt% uranium enriched to 93 wt% ^{235}U and are 48 inches long with a diameter of 0.030 inches [2]. A stainless steel sheath with inner diameter of 0.072 inches surrounded the wire and extends the length of the fuel pin region [2]. The flux wire holder (diameter 1 inch) was also surrounded with an extra dysprosium collar of

thickness 0.015 inches to prevent melting of the wire [2]. A diagram of a typical example flux wire is shown in Figure 2-18.

Table 2-3. Calibration Vehicle Radial Dimensions [2].

Test Loop	OD (in.)	ID (in.)	Thickness (in.)
Dummy Heaters	2.386	2.294	0.046
Dysprosium/Stainless Steel Filters/Shims			0.02
Stainless Steel Sleeve	2.254	2.130	0.062
Aluminum Sleeve	2.130	2.030	0.05
Loop Test Section	2.030	1.294	0.368

Test Train	OD (in.)	ID (in.)	Thickness (in.)
Outer Tube	1.25	1.12	0.065
Shield Tube	0.5	0.43	0.035
Flow tubes	0.31	0.28	0.015

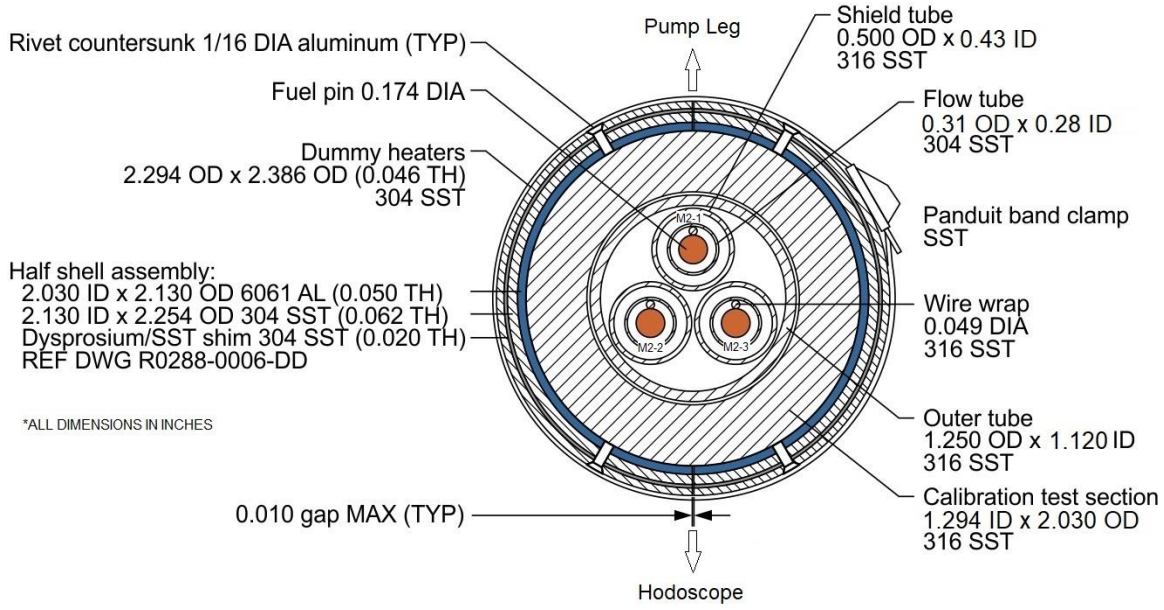

Figure 2-15. Cross-Sectional View of the M2/M3CAL Vehicle Test Section [1,2].

Table 2-4. Mark-II Fuel Pin Description [2].

Test Pin Fuel		
	Material	Uranium (95 wt%), Fissium (5 wt%)
	Density (g/cm^3)	17.6
	Length (in.)	13.500 ± 0.032 in.
	Diameter (in.)	0.130 +0.004/ -0.032
	Mass (g)	51.7 ± 1.0
Cladding		
	Material	316 Stainless Steel
	ID (in.)	0.1500 ± 0.0005
	Thickness (in.)	0.0120 ± 0.0005
	Fuel restrainer, dimple, distance above fuel (in.)	0.500
Fuel-Cladding Bond (Cold)		
	Material	Sodium
	Level, above fuel pin (max/min) (in.)	1.5/0.665
	Diametral gap (in.)	0.020
Plenum		
	Fill gas	Argon
	Volume, hot (max/min) (cm^3)	2.4/2.1
	Plenum volume/ fuel volume (max/min)	0.81/0.71
Fuel Pin Total Element		
	Mass (g)	80
	Length (in.)	24.095
Spacer Wire		
	Material	316 Stainless Steel
	Diameter (in.)	0.049
	Pitch, right hand (in.)	6

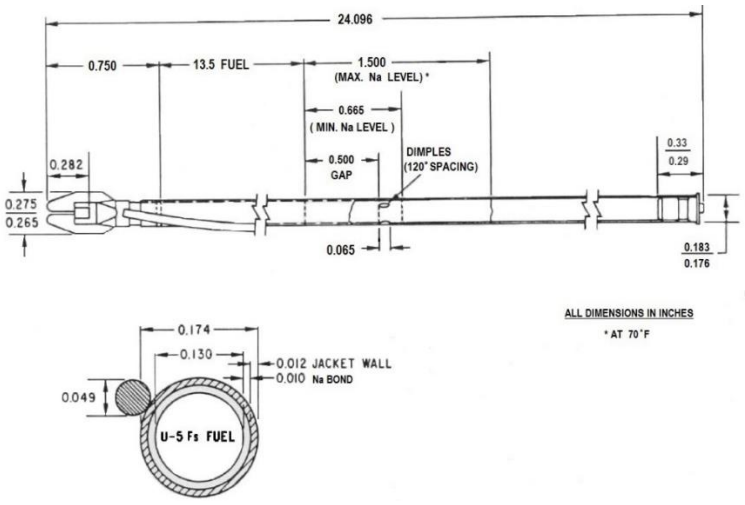

Figure 2-16. EBR-II Mark-II Driver Fuel Pin [2].

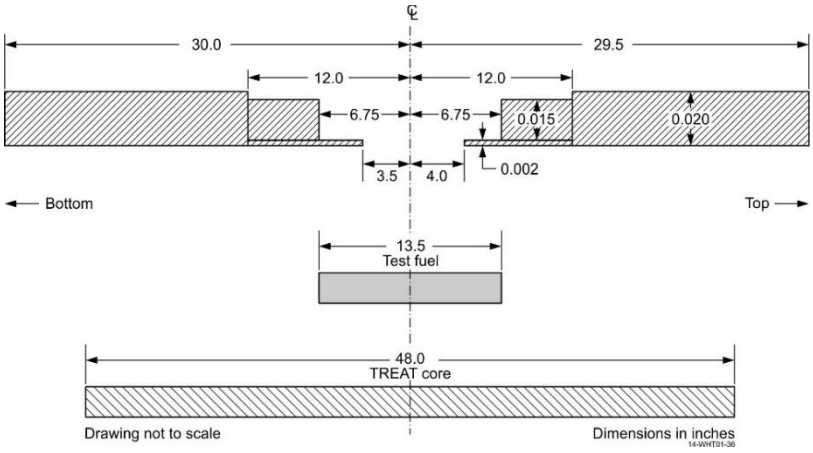

Figure 2-17. Dysprosium Shaping Collar [1].

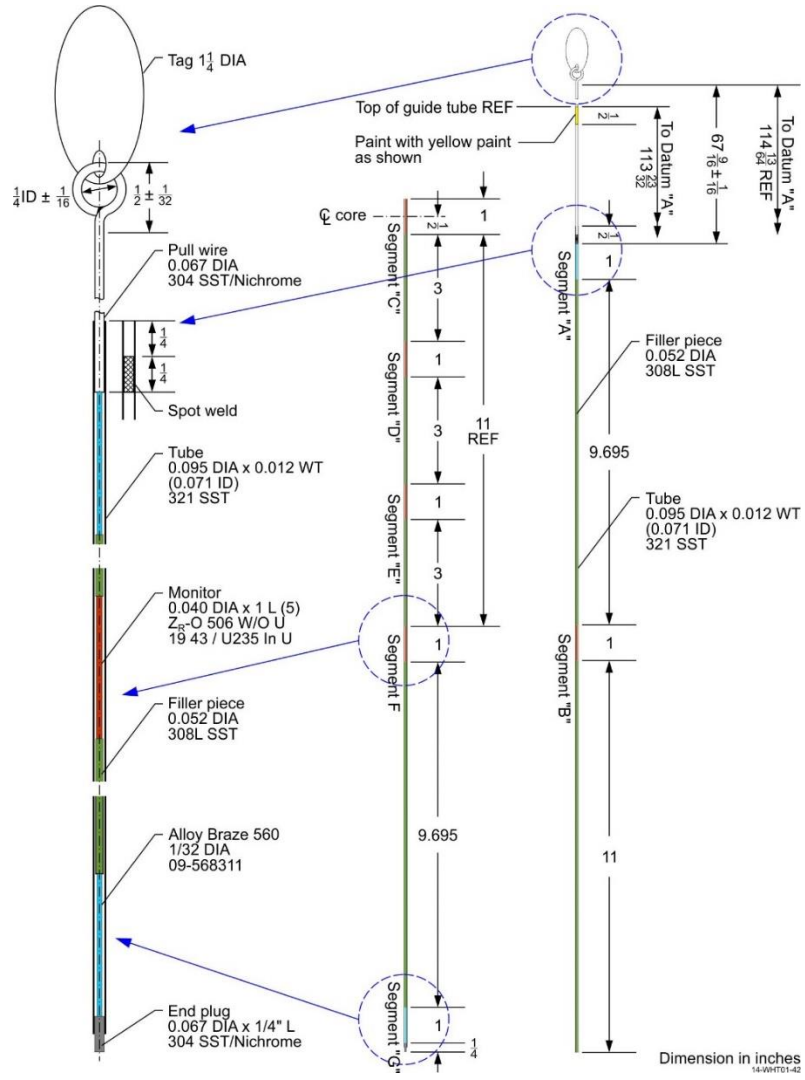

Figure 2-18. Example Monitor Wire (DWG# R0275-9910) [1].

*2.1.2.3 **Experimental Procedure***

As a part of the M2/M3CAL experiments, several partial and full transient wire irradiations were carried out. Prior to the transients, a low-level steady state test was performed on the core configuration 1370 to determine the power coupling between the core and the flux wire. The total energy produced by the core was reported to be 540 MJ [13]. The transient test 2580, a partial energy wire trial transient, was performed on September 21,1984 to determine the transient correction factor. The steady-state power of the core before the initiation of the transient was measured to be 50 W [13]. The transient followed a pre-programmed rod maneuver for approximately 10 s before scram. The total energy produced in the core was reported to be 206 MJ and the transient correction factor was calculated to be 0.87.

2.1.3 Material Data

Materials used in the TREAT components are noted previously in Section 2.1.2 as the components are introduced. These materials are summarized below.

2.1.3.1 Graphite Fuel

TREAT fuel is comprised of uranium (UO_2) dispersed in a graphite matrix. The average density of the fuel was reported to range between 1.71 to 1.76 g/cm^3 with an average of 1.73 g/cm^3 [9]. The uranium was mixed with the carbon to give a ratio of approximately 1 to 10,000 (U:C). The actual measured composition of uranium in the fabricated fuel was measured to range between 0.205 to 0.222 wt% with an average of 0.211 ± 0.004 wt% [9]. Another reference similarly reports the uranium concentration to be 0.2109 wt% [10]. The enrichment of the uranium was reported to be 93.1 wt% ^{235}U in the earliest reports [5,10], but more recent documents report the enrichment to be 93.24 wt% ^{235}U [6,7].

Impurities in the graphite fuel were measured both at the initial manufacturing and then later by Iskenderian when notable poisons were affecting reactor criticality. Iskenderian measured 50 samples (in 4 groups) to determine representative core impurities. Using spectrochemical analysis, these tests were conducted to

determine the boron, iron, cadmium, and rare earth contents within the fuel. The results shown in Table 2-5 determined the boron to have an average impurity of 7.6 ± 1.4 ppm (7.6E-4 ± 1.4E-4 wt%) [11]. Reanalysis of the data in Table 2-5 using a Chi-squared weighing method results in a boron impurity content of 7.53 ± 1.16 ppm (7.53E-4 ± 1.4E-4 wt%). The iron impurity was reported to be 0.0267 wt% [9], and the vanadium content of 30 ppm (3E-3 wt%) is assumed based on the data in Table 2-6. The cadmium composition was assumed to be only a local phenomenon with a very low actual average [11].

Hydrogen impurity content was not measured at the time of the actual manufacturing or initial post-criticality tests. In 2015, the TREAT fuel fabrication process was recreated by B&W. It was reported in Reference [1] that the hydrogen impurity in this recreated fuel was measured to be 0.097 wt%.

Table 2-5. Summary of Boron Impurity Measurements in Core Graphite (ppm[a]) [11].

Group No.	Number of Samples in Group	Average for Group	Average Deviation for Group	Average Deviation
1	8	6.4	22.7	0.95
2	10	5.1	1.3	0.4[b]
3	20	10.0	4.7	1.0
4	12	7.4	6.4	1.8
Total Number of Samples				50
Average Impurity for Four Groups				7.6
Average Deviation for Four Groups				1.4

Table 2-6. Typical Spectrochemical Analysis of Core Graphite Impurities (ppm[c]) [11].

Sample No.	B	Fe	V	Gd	Eu	Sm	Cd
1	13	300	30	< 0.2	< 0.2	< 1	--
2	4	400	30	< 0.2	< 0.2	< 1	--
3	10	400	30	< 0.2	< 0.2	< 1	--
4	5	500	30	< 0.2	< 0.2	< 1	--
5	7	1000	--	--	--	--	--
6	4	1000	--	--	--	--	15

[a] Impurities in ppm by weight.
[b] Incorrectly reported in original reference but correction reported in [1].
[c] Reported as "ppm" with no specification. Assumed to be ppm by weight.

2.1.3.2 Zircaloy-3

The density of zircaloy-3 (Zy-3) was reported to be 6.53 g/cm^3 [1]. Measurements of the Zy-3 were conducted by EAG in September of 2012 with the following results in Table 2-7 and

Table 2-8. For major elements measured using ICP, typical uncertainties range from 3 to 5% (at the 95% confidence level) [1].

Table 2-7. ICP-MS Measurement of Zircaloy-3 Composition [1].

Element	Concentration (ppm[a])	Element	Concentration (ppm[a])
Li	< 1	Pd	< 1
Be	< 1	Ag	150
B	< 1	Cd	< 1
C	--	In	7
N	--	Sn	3000
O	--	Sb	< 1
F	--	Te	< 1
Na	< 10	I	--
Mg	< 1	Cs	< 1
Al	5	Ba	< 1
Si	< 10	La	< 1
P	< 10	Ce	< 1
S	--	Pr	< 1
Cl	--	Nd	< 1
K	< 10	Sm	< 1
Ca	< 10	Eu	< 1
Sc	< 100 [b]	Gd	< 1
Ti	8	Tb	< 1
V	< 1	Dy	< 1
Cr	< 1	Ho	< 1
Mn	1	Er	< 1
Fe	2600	Tm	< 1
Co	< 1	Yb	< 1
Ni	< 1	Lu	< 1
Cu	< 1	Hf	79
Zn	< 1	Ta	< 1
Ga	< 1	W	< 1
Ge	< 1	Re	< 1
As	< 1	Os	< 1
Se	< 1	Ir	< 1

[a] Reported as ppm by weight

[b] Elevated limit due to polyatomic interference from zirconium [1].

Table 2-7. (continued).

Br	--		Pt	< 1
Rb	< 1		Au	< 1
Sr	< 1		Hg	< 1
Y	10		Tl	< 1
Zr	Matrix		Pb	6
Nb	10		Bi	< 1
Mo	< 1		Th	< 1
Ru	< 1		U	< 1
Rh	< 1			

Table 2-8. Other Measurements of Zircaloy-3 Composition [1].

Element	Concentration (ppm[a])
C [(a)]	120
N [(b)]	51
O [(c)]	920
S [(a)]	--
H [(b)]	22

(a) Determined by Combustion-IR.

(b) Determined by IGF-TC.

(c) Determined by IGF-NDIR.

2.1.3.3 Al-1100

The density of Al-1100 for TREAT is not given; however a standard density is reported to be 2.71 g/cm^3 [1]. The composition and impurity content for Al-1100 is not available for TREAT.

2.1.3.4 Al-6061

The density of Al-6061 for TREAT is not given; however a standard density is reported to be 2.70 g/cm^3 [1]. The composition and impurity content for Al-6061 is not available for TREAT.

[a] Reported as ppm by weight

2.1.3.5 Al-6063

The density of Al-6063 was not directly reported for TREAT. The reported density is 0.097 lb./in.^{3} (2.685 g/cm^3) [24]. The composition and impurity content for Al-6063 is not available for TREAT.

2.1.3.6 Mild, Low-Carbon Steel

No measurements or data are available for the steel alloys in TREAT. It would be expected however that the mild, low-carbon steels (also referenced as AISI 1010-1020 or ASTM A36) would have a composition similar to that of type 1018 or A36. The density of type 1018 mild low-carbon steel is 7.87 g/cm^3, and the density of type A36 low-carbon steel is 7.8 g/cm^3 [1].

2.1.3.7 SS-304 (SS-18-8)

The density of stainless steel 304 (SS-304) for TREAT is not given; however a standard density is reported to be 8 g/cm^3 [1]. Neither the grade of the TREAT SS-304 nor the direct measured composition is available.

2.1.3.8 SS-316

No material properties for the stainless steel 316 used in TREAT are available.

2.1.3.9 Lead Bricks

The density of lead for TREAT is not given; however a standard density is reported to be 11.34 g/cm^3 [1]. The composition and impurity content for the lead bricks is not available for TREAT.

2.1.3.10 Boron Carbide

Boron carbide (B_4C) was used in the poison section of the control rods. The third generation of control rods which were used in the M2/M3 experiments used packed B_4C powder (no added epoxy resin). The resulting

density is 1.8 g/cm^3 [1]. The composition and impurity content for the boron carbide is not available for TREAT.

2.1.3.11 Hematite/Magnetite Concrete

The concrete shielding and support for TREAT is made of a high-density concrete. Different references give this material to be heavy magnetite and/or hematite concrete with density between 200 and 220 lb./ft^3 depending on the reference [5-7,12]. The composition or impurity content of the TREAT concrete is not available.

2.1.3.12 Boral (50:50)

No material properties for the boral thermal shielding used at TREAT is available.

2.1.3.13 Chromel

The density of chromel ranges between 7.94 and 8.73 g/cm^3 but no specific properties were reported for the instrumentation components of TREAT [1]. The composition and impurity content for the chromel are not available for TREAT.

2.1.3.14 Alumel

The density of alumel ranges between 8.50 and 8.60 g/cm^3 but no specific properties were reported for the instrumentation components of TREAT [1]. The composition and impurity content for the alumel are not available for TREAT.

2.1.3.15 MgO Insulation

No material properties for the MgO insulation used in the instrumentation at TREAT are available.

2.1.3.16 Asbestos Insulation

The density of asbestos for TREAT is not given; however a standard density is 2.55 ± 0.02 g/cm^3[25]. The composition of the asbestos insulation for TREAT instrumentation is not available.

2.1.3.17 Argon Plenum Gas

Argon gas is used as the inert gas within the test vehicle. This gas was typically a mix of 25% argon and 75% helium [8]. No other specifications or details for this gas is available.

2.1.3.18 Graphitar

No material data for the graphitar used in TREAT is available. Graphitar was used for the bearings in TREAT and is made from carbon allotropes with a hydrocarbon binder. The composition and baking process are varied based on the desired application of the graphite piece. Typical bearing grades are 14, 18, 39, 67, 80, and 86 with grades 67 and 86 being the most likely ones used in TREAT specifically for the control rods [1]. Grade 67 is designed to be used in light duty, non-lubricated components; whereas grade 86 is designed to be used for high speed operation under heavy loads either dry or lubricated [1]. Grade 67 has a density of 1.72 g/cm^3, and grade 86 has a density of 1.90 g/cm^3 [26].

2.1.3.19 Air

The density of air at Idaho National Laboratory for TREAT is not given; however a standard density is reported to be 0.0012 g/cm^3 [1]. The basic composition of air is provided in Table 2-9 along with average fission products detected at TREAT in Table 2-10.

Table 2-9. Basic Composition of Air.[a]

Component	Volume (ppm[b])
Nitrogen (N_2)	780840
Oxygen (O_2)	209460
Argon (Ar)	9340
Carbon Dioxide (CO_2)	380
Neon (Ne)	18.18
Helium (He)	5.24
Methane (CH_4)	1.7
Krypton (Kr)	1.14
Hydrogen (H_2)	0.55
Water (H_2O)	10000

Table 2-10. TREAT Gaseous Fission Product Average Effluence at the Top of the Stack [1] [28] [29].[c]

Isotope	Measurement 1 (pCi/cc)	Measurement 2 (pCi/cc)
^{41}Ar	81.9 ± 1.5	66.4 ± 6.0
^{85m}Kr	3.5 ± 0.8	1.40 ± 0.15
^{87}Kr	10.5 ± 0.5	7.36 ± 0.80
^{88}Kr	8.7 ± 0.4	6.71 ± 0.75
^{135}Xe	0.66 ± 0.12	0.34 ± 0.15
^{135m}Xe	2.4 ± 0.7	0.41 ± 0.15
^{138}Xe	30.2 ± 3.9	10.7 ± 1.5

2.1.3.20 Start-Up Source

After the initial start-up, the source in the TREAT reactor was replaced with first a stronger polonium-beryllium source. Later an americium-beryllium source, commercially available, was used in TREAT. Based on the documentation, it is assumed that the Am-Be source would have been used during the timeframe of the M2/M3 tests. The exact composition of the Am-Be source is not known. It was documented to have been encased in a steel jacket and produced by the Monsanto Research Corporation in Dayton, Ohio. The source number was MRC-N-SS-W-AmBe-539. This 2.5-curie source has a ^{241}Am mass of 0.710 g with the americium in the form of AmO_2 [1]. The target mass is 2.3 g [1]. A stainless steel-304

[a] Reported as ppm by volume (not weight)

source container with an 0.7 inch outer diameter and 1.26 inches long holds the source [1]. The mass and thickness of the container were not reported nor were the dimensions of the source itself. The emission rate of the source was documented to be 4.89×10^6 n/sec, but the date of the measurement was not recorded [1].

2.1.3.21 Test Pin Fuel

Three EBR-II Mark-II driver fuel pins were used in the M2/M3 test experiment. The pins contain fresh fuel made with enriched uranium and fissium. Fissium is an alloy formulated to represent the equilibrium concentration of solid fission products accumulated during irradiation and not removed during fuel reprocessing. The density, mass, and composition of the fuel are given in Table 2-11.

Table 2-11. Mark-II Fuel Pin Composition [2].

Test Pin Fuel		51.7 g (typically) 17.6 g/cm^3
Uranium		95 ± 1 wt %
	^{235}U	66.72 ± 0.50 wt %
	^{234}U + ^{236}U + ^{238}U	33.28 ± 0.50 wt %
	^{234}U + ^{236}U	< 1.0 wt %
Fissium		5 ± 1 wt %
	Zirconium	0.2 wt %
	Molybdenum	2.4 wt %
	Ruthenium	1.9 wt %
	Rhodium	0.3 wt %
	Palladium	0.2 wt %

2.1.3.22 Flux Wire

High-enriched uranium-zirconium flux wires were used in the M2/M3 calibration experiment and the M2CAL 2580 Transient Test. The wire is composed of 3.6 wt% uranium enriched to 93% ^{235}U [2]. There was approximately 0.13 g of ^{235}U per wire [2]. Dimensions for the wire are given above in Section 2.1.2.2.

2.1.4 Temperature Information

No temperature data is available for the steady-state irradiations. A fuel temperature of 295.0 K was assumed based on temperature measurements taken for the critical configuration prior to the M2/M3 experimental transients [13]. The remaining core components were assumed to have a temperature 293.6 K.

2.2 Description of Reactivity Coefficient Measurements

2.2.1 Temperature Coefficient Measurement

The reactivity coefficients were measured on the Minimum Critical Mass Core configuration [15]. The behavior of the temperature coefficient is expected to not deviate significantly with different core loadings. The measurements were carried out for isothermal heating and for the case when the reactor had a temperature distribution characteristic of the power distribution [15].

2.2.1.1 Isothermal Coefficient

The criticality was calculated after the reactor had been cooled overnight by circulating cold outside air through the reactor. It was calculated again after it has been heated by circulating warm inside the air through the reactor. The thermocouples in the reactor and reflector indicate a uniform temperature distribution [15]. The temperature coefficient was obtained with both the short and long control rods. The results for the isothermal coefficient measurement are shown in Table 2-12.

Table 2-12 Isothermal Temperature Coefficient Measurement [15]

	Temperature			**Temperature Coefficient**	
	Hot (°C)	Cold (°C)	Δk (inhr)	(Inhr/°C)	(Δk/°C)
Short Rods	35.0	15.5	131	6.74	$-1.8 \pm 0.2 \times 10^{-4}$
Long Rods	37.5	22.0	104.5	6.76	$-1.8 \pm 0.2 \times 10^{-4}$

2.2.1.2 Temperature Coefficient with Normal Temperature Distribution

The loss in reactivity and the maximum core temperature were measured as a function of time during a constant-power heatup test and also during cooling with air flow after a transient [15]. The temperature coefficient was measured over a range of 170 °C and found to be -1.3 $\times 10^{-4}$ Δk/°C [15]. After applying the measured maximum-to-average flux ratio for the core, the temperature coefficient value was modified to be -2.2 $\times 10^{-4}$ Δk per average °C in the core [10].

2.3 Description of Kinetics Measurements

2.3.1 Description of the Prompt Neutron Lifetime Measurement

The prompt neutron lifetime was determined by the Rossi-α, transfer-function, and prompt critical transient measurement for different core loadings to be 9.0 $\pm 0.02 \times 10^{-4}$ sec [15].

2.3.2 Description of Delayed Neutron Parameters Measurement

The measurement of the delayed neutron parameters was also performed on Minimum Critical Mass Core configuration. The delayed neutron parameters were calculated using the Keepin delayed neutron data for U^{235} [11]. The published delayed neutron parameters for TREAT are presented in Table 2-13.

Table 2-13. Delayed Neutron Parameters for TREAT [10]

Delayed Group Index Number *i*	Decay Constant λ_i (sec^{-1})	Delayed Neutron Fraction β_i	Effective Delayed Neutron Fraction $\beta_{i,eff}$
1	0.0124	0.002111	0.000244
2	0.0305	0.001401	0.001567
3	0.111	0.001254	0.001411
4	0.301	0.002527	0.002828
5	1.13	0.000735	0.000826
6	3	0.000268	0.000302
		β_{eff} = 0.006845	β_{eff} = 0.007178

2.4 Description of Power Distribution Measurements

2.4.1 Description of Axial Power Distribution Measurement in the Flux Wire

The U-Zr flux monitor wire 48-1 was irradiated under low-level steady-state (LLSS) conditions prior to the transient operation on September 17, 1984 [17]. The control rod positions for this test are described in Table 2-14. The reported total energy produced by the core was measured to be 540 MJ from Integrator No. 1 instrument [17]. The LLSS irradiation lasted for 100 minutes and the power level was maintained at 90 KW [20]. Following the LLSS irradiation, the U-Zr monitor wire was cut into sections starting at the bottom. The first and last 16 in. of the wire was cut into 1 in long segments. The middle 16 in segment was cut into 0.5 in long segments. The segments were labeled, weighted and gamma counted for t relative activity [17]. The axial profile from gamma counting the relative fission product activity of the wire segments is shown in Figure 2-19.

Table 2-14. Rod Positions of LLSS Flux Monitor Wire Irradiation Test [18].

Rod No.	Position (in)
T-1	40.0
T-2	17.02
1	59.0
3	59.0
4	59.0
7	32.5
8	32.5
10	32.5

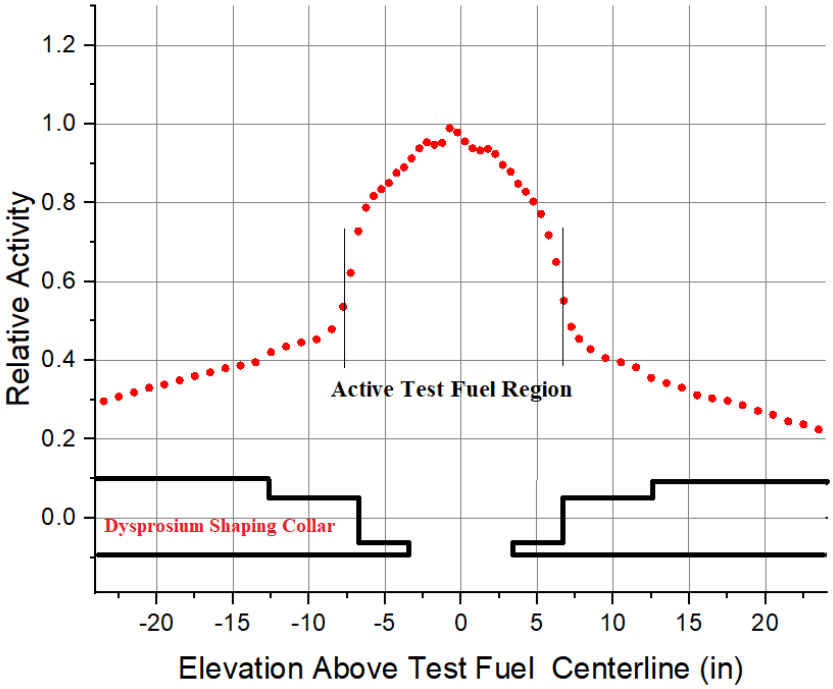

Figure 2-19. Measured Axial Power Profile for Monitor Wire 48-1 Irradiation Test [17].

In each of the wire activity distributions, one or two abnormally high points are observed just below the midplane of the distribution. Radiographs of the monitor wire holder within the calibration vehicle show an approximate 0.31 cm (0.13 in) gap in the 0.032 cm (0.015 in) thick dysprosium filter at about the same axial location. The gap caused a local increase in the neutron flux, hence also in the monitor wire activation [4].

2.5 Description of Transient Measurements

2.5.1 Overview of the Experiment

The M2CAL transient 2580 experiment (48-4 wire irradiation test) was conducted on September 21, 1984 at Idaho National Laboratory's TREAT Reactor as a part of partial energy wire trail transients. First, the experiment began with establishing the pre-transient (critical) conditions for M2CAL transient 2580 with an estimated power of 50 W [13]. The transient is then initiated by ejecting the transient rod T-2 following a pre-planned rod dynamic. The transient lasted approximately 10 seconds from initial rod withdrawal to

shutdown [13]. The rod ejection was equivalent to 1110 pcm of reactivity insertion. The average fuel temperature prior to the transient was measured to be 295 K, and the maximum fuel temperature during the transient, sampled from 11 thermocouples in the core, was measured to be 354K [13]. The power coupling factor PCF and the transient correction factor for the transient were measured to be 0.4262 and 0.87 respectively.

2.5.2 Geometry of the Experiment Configuration and Measurement Procedure

The steady-state geometry of the M2CAL experiment described in section 2.1.2 was used except for the replacement of the fuel pins by the flux wire inside the test vehicle [2-4]. Information regarding the dimensions and material composition of the flux wire are included in Section 2.1.3.22.

2.5.2.1 Transient Core Configuration

Initial Rod Positions

The pre-transient critical configuration for Transient 2580 is given in Table 2-15.

Table 2-15. Transient 2580 Pre-Transient Rod Positions - September 21, 1984 [13].

	Position (inches)
Inner Bank	59.0
Outer Bank	59.0
T-1	8.80
T-2	0.00

Transient Rod Dynamics

The transient experiment was initiated by a rapid withdrawal of the transient rods T-2 to establish a stable reactor period of 0.209 s [13]. The reactivity insertion due to the rod withdrawal was measured to be 1.11% (1110 pcm) [13]. After approximately 3 s, the exponential rise of power was then halted by T-2 partial insertion which allowed for the power to level off. This allowed the system to pre-heat before the

rods were further withdrawn to initiate the power ramp. When the power reached a pre-programmed setpoint, the rods were set to scram. For the entire time of the transient, the position of T-1 rods was held constant until the point at which the transient was terminated. The transient rod maneuver is plotted in Figure 2-20.

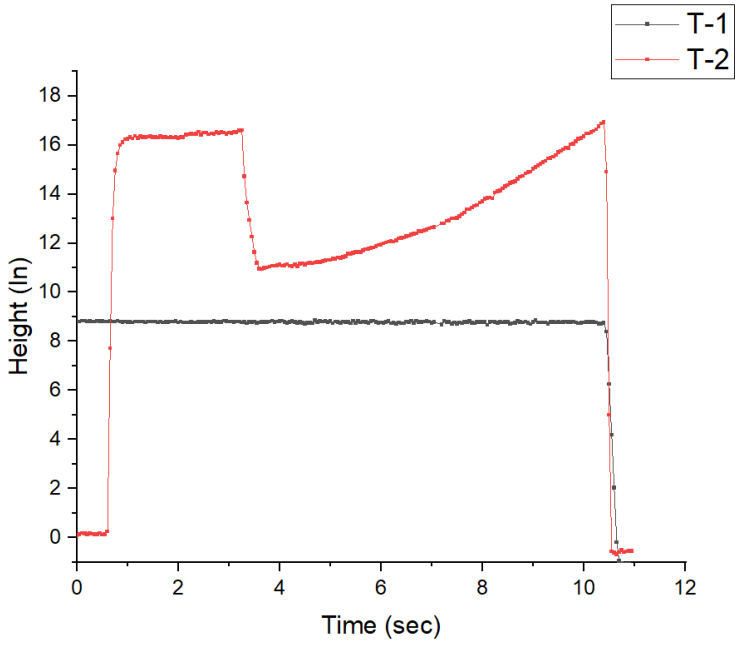

Figure 2-20. Rod Heights as a Function of Time for Transient 2580 [13].

2.5.2.2 Transient Experimental Power Measurements

Throughout the transient process, the core power was measured by the Transient Safety 1, 2 (Safety #1 and Safety #2) and Control Power (CP) detectors. The integral power was measured by Integral Power 1 and 2 (IP1 and IP2) detectors. The locations of these detectors are outlined in Table 1.1.2-11. The power trend plots for the transient are shown in Figure 2-21 and Figure 2-22.

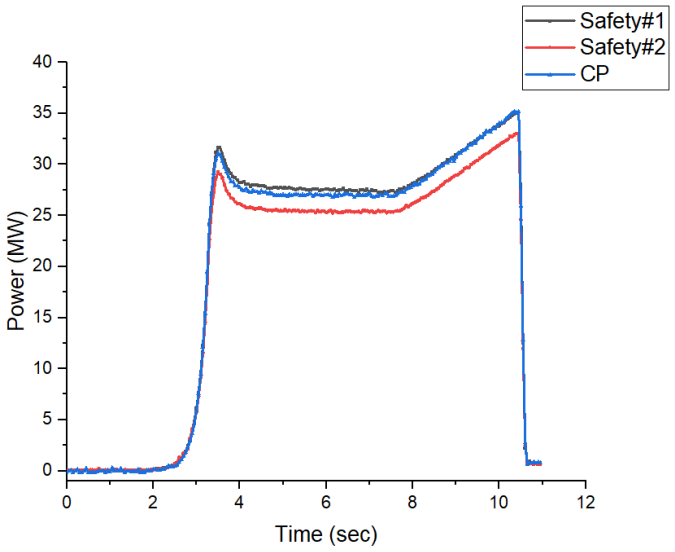

Figure 2-21. Power as a function of time for M2CAL transient 2580 plotted on a linear scale [13].

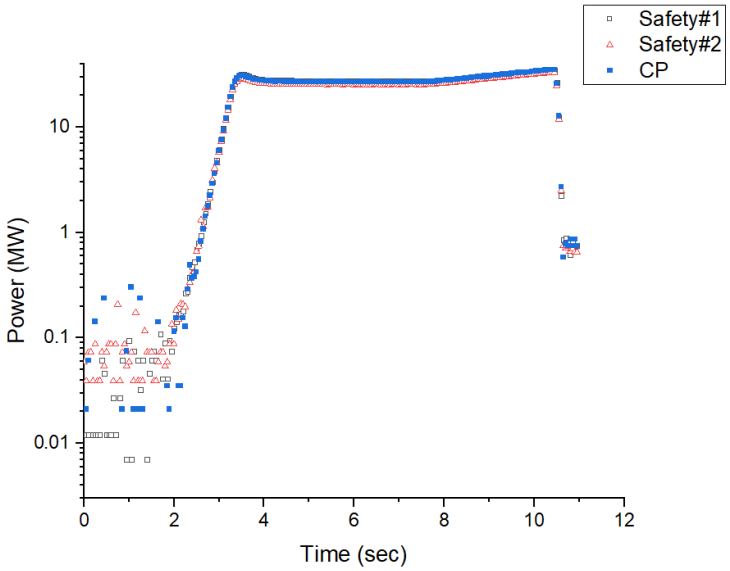

Figure 2-22. Power as a function of time for M2CAL transient 2580 plotted on a log scale [13].

All power detectors used in the experiment are uncompensated parallel-plated ^{10}B-coated ion chambers of the type ANL-IC25 [6]. The locations of these detectors are displayed in Figure 2-23, where the upper and lower levels are approximately 12 in. above and below the core midplane respectively [22].

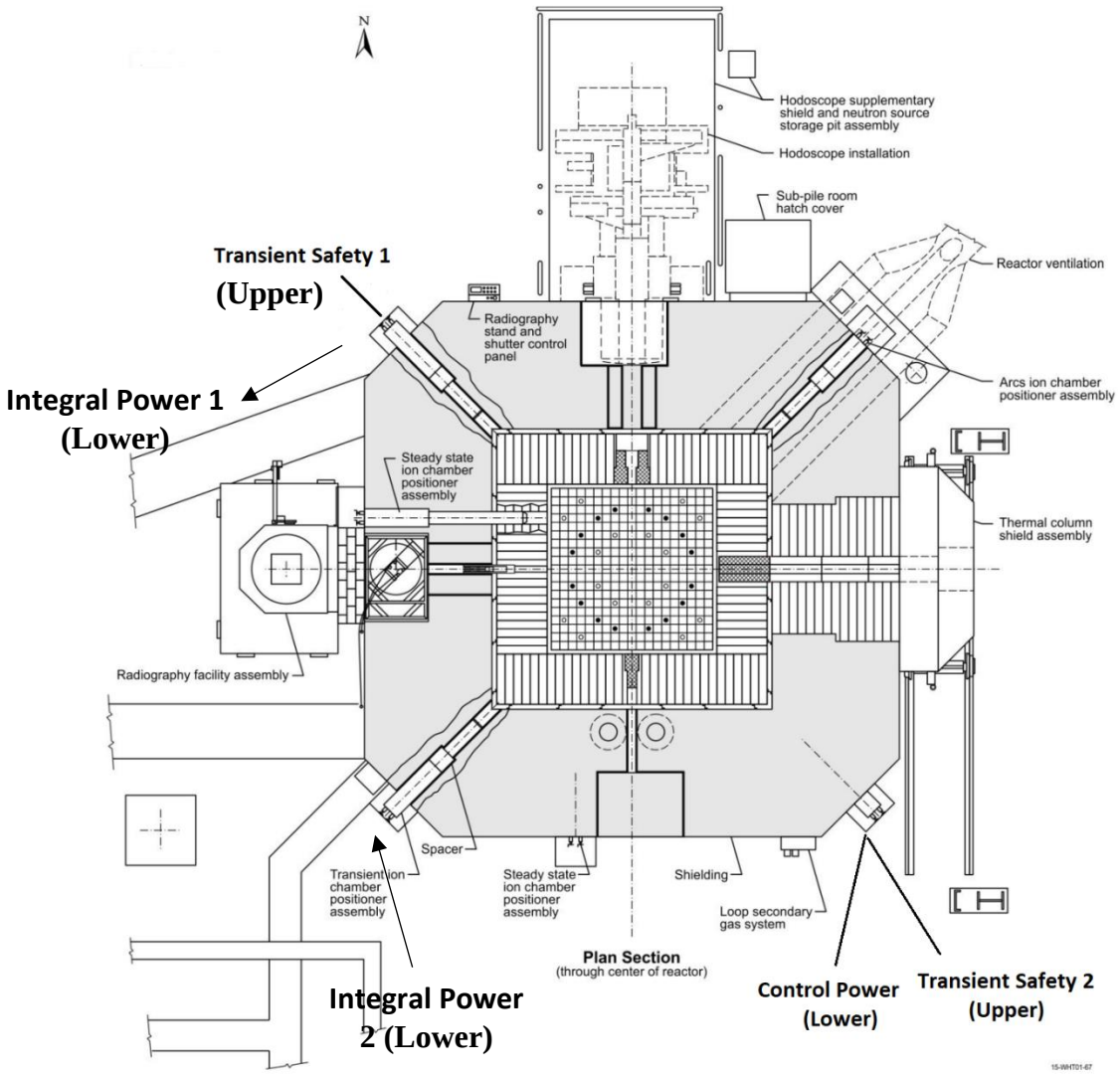

Figure 2-23. Positions of the Transient Detectors used in the Transient 2580 Test.

2.5.2.3 Transient Experimental Period Measurements

The reactor period for the first power ramp was measured indirectly by taking power readings at three different points in time, where the power increases by a factor of 10 [13]. Table 2-16 shows the time values at which the period was calculated. Equation (2-1) was used to calculate the period. The period was most likely measured by a period meter. No information on the measuring instrument was reported.

Table 2-16. Time Data Used for Period Calculation [13].

Decade Number	Time (ms)
Decade # 1	-
Decade #2	88
Decade #3	135
Decade # 4	184
Decade # 5	-

$$Period = \frac{Decade2 - Decade1}{\ln(10)} \qquad (2\text{-}1)$$

The period was calculated using the average of the difference between Decade #2 and Decade # 3 and the difference between Decade # 4 and Decade # 3. The period was reported to be 0.209 s [13].

2.5.2.4 Experimental Transient Rod Worth Measurement

The integral rod worth for the transient rods T-1 and T-2 was measured and plotted versus their positions in Figure 1.10.2.4-1 [14]. The worth was measured by incrementally increasing the rod position by 1 in and measuring the corresponding k_{eff} [14]. The total worth for T-1 and T-2 are 1.800 % and 2.778% respectively, amounting for a total transient rod worth of 4.578% [14].

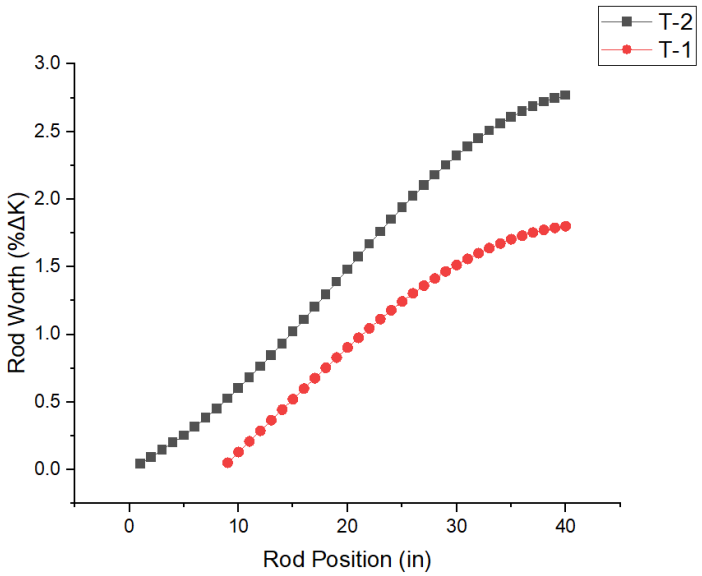

Figure 2-24. The Integral Rod Worth of Transient Rods T-1 and T-2 [14].

2.5.3 Material Data

Materials in the core were the same as those previously described in Section 2.1.3.

2.5.4 Temperature Data

The available reactor temperature date is limited to the beginning and the end of the transient. The temperature measurements were taken from a multipoint recorder sampled from 11 thermocouples in the core [14]. The initial and final temperature data points are presented in Table 1.10.4-1. The uncertainties associated with the data were not reported.

Table 2-17. Initial and Final Temperature Readings [14]

Point No.	Initial Reading	Final Reading	Point No.	Initial Reading	Final Reading
1	25 °C	28 °C	7	24 °C	78 °C
2	24 °C	29 °C	8	23 °C	75 °C
3	25 °C	26 °C	9	23 °C	75 °C
4	23 °C	77 °C	10	23 °C	72 °C
5	23 °C	74 °C	11	22 °C	81 °C
6	23 °C	72 °C			

The locations and types of the thermocouples used in the temperature measurements are displayed in Table 2-18 and also in Figure 2-2[16]. The locations of thermocouples # 1 and 2 were reported as inlet air to the exhaust filters and outlet air from reactor respectively [16].

Table 2-18. Reactor Core thermocouple Locations for Core Loading 1370 [16].

Thermocouple Number	Series Number	Location	Connector Terminal
3	520	H9	G-H
4	500	N12	C-D
5	500	N12	E-F
6	520	H9	C-D
7	501	N10	E-F
8	524	M10	C-D
9	501	N10	E-F
10	527	G10	C-D
11	503	M13	E-F

2.5.5 Additional Information Relevant to Transient Measurements

*2.5.5.1 **Description of Axial Power Distribution Measurement in the Flux Wire***

Flux wire 48-4 was irradiated during transient 2580, and the process of determining the axial power profile followed a similar approach to what is described in Section 2.4.1 [17]. It is worth noting that there is no difference in materials or dimensions between flux wire 48-1 and flux wire 48-4. The axial profile from gamma counting the relative fission product activity of the wire segments is shown in Figure 2-25.

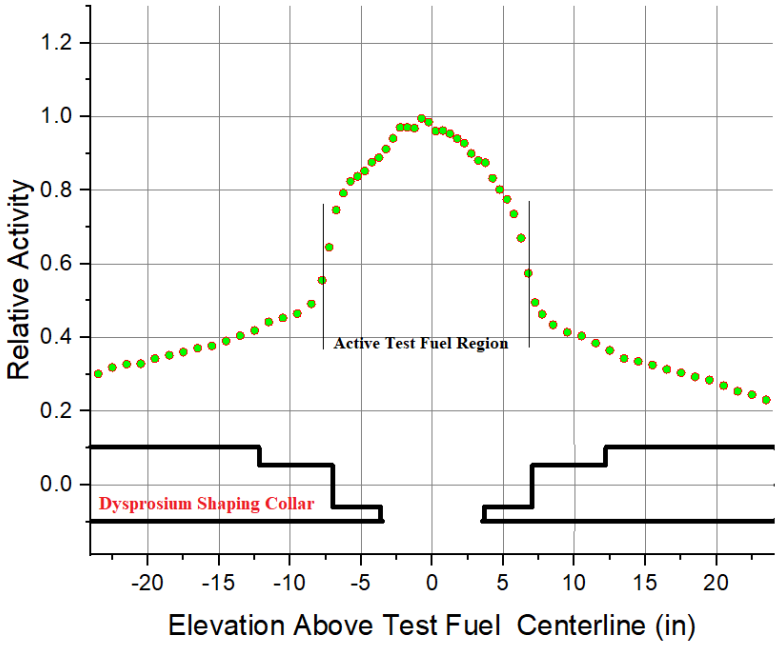

Figure 2-25. Measured Axial Power Profile for Monitor Wire 48-4 Transient Irradiation Test [17].

*2.5.5.2 **Description of the Transient Coupling Factors***

The transient correction factor (TCF) accounts for the difference between the power coupling during a reactor transient relative to that measured in low-level, steady-state (LLSS) power irradiations. The average TCF of the transient is used as a multiplicative factor to correct the LLSS measured value of test-fuel power coupling to obtain the final transient averaged power-coupling value [17]. The TCF is defined, in Equation (2-2), as the ratio of monitor-wire power coupling under transient conditions to the monitor-wire power coupling under LLSS conditions [17].

$$TCF = \frac{PCF_{Transient}}{PCF_{LLSS}} \qquad (2\text{-}2)$$

The power coupling is calculated experimentally by using Equation (2-3).

$$PCF = \frac{\frac{\#\,Fissions\,in\,Wire}{grams} \times 2.86 \times 10^{-11} \frac{J}{Fission}}{Total\,TREAT\,Energy\,(MJ)} \tag{2-3}$$

The absolute number of fissions per gram was determined for three 2.54 cm long segments formed by combining two segments together at approximately 53 cm (21 in.), 61 cm (24 in.), and 69 cm (27 in.) by dissolving the segments and counting for Ba^{140} La activity; the absolute fissions per gram values were divided by the associated relative fission activities to yield comparable midplane absolute values [18]. The number of the fissions in the wire is measured at the test fuel axial midplane after the LLSS test to be 9.29×10^{12} fissions/g with a TREAT energy of 540 MJ amounting for a PCF of 0.492 [17]. The absolute activity in the wire is measured to be 3.07×10^{12} fissions/g with a TREAT energy of 206 MJ during transient 2580 test. The TCF was calculated to be 0.87 [17]. In the steady-state wire irradiation, it was reported that during the irradiation the inner control rods were fully withdrawn and the outer rods banked and raised as needed [20]. The movements of the outer rods were not reported. It is worth noting that the power coupling depends on the rod positions and their movements [44].

2.5.5.3 ***Specific Heat Capacity Measurement***

The measurements for the Enthalpy of TREAT were carried out in 1960s [9]. A plot of the specific heat is shown in Figure 2-26.

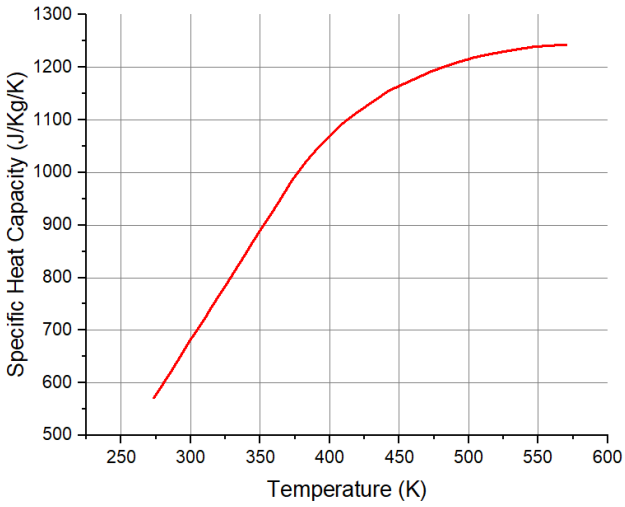

Figure 2-26. Instantaneous Specific Heats at Interpolated Temperatures of Graphite-Urania [9].

2.5.5.4 ***Evaluation of the Thermal Conductivity***

The results of thermal conductivity during a step-wise electric heating of a fuel sample in a helium atmosphere from 338.706 K to 1338.706 K are shown in Figure 2-27 [5].

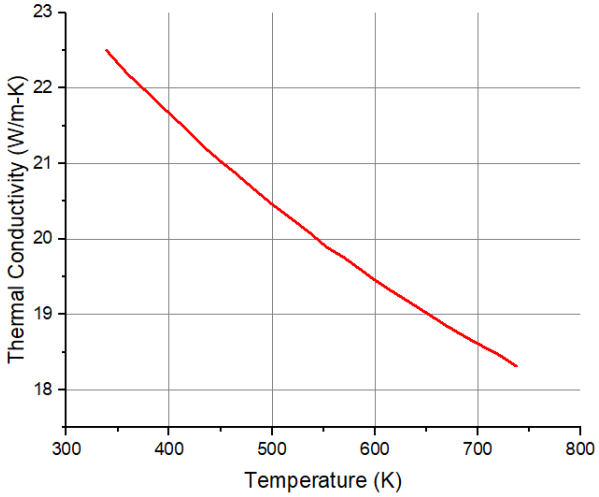

Figure 2-27. Measured Thermal Conductivity of Specimen Graphite-Urania Fuel during Step-Wise Electric Heating in Helium Atmosphere [5].

3 EVALUATION OF EXPERIMENTAL DATA AND UNCERTAINTIES

The M2 and M3 low-level steady state calibration test pin irradiations were previously analyzed and submitted as a benchmark to the International Reactor Physics Evaluation Project (IRPhEP) [45]. It has been evaluated and determined to be an acceptable benchmark experiment. The Serpent 2.1.29 reactor physics code was used to evaluate the estimated biases and uncertainty in k_{eff} [30]. Serpent is a three-dimensional, continuous energy Monte Carlo code capable of simulating neutron transport. A model of the reactor is described in Section 3, and that benchmark model was used to evaluate the uncertainty. The Evaluated Nuclear Data File, ENDF/B-VII.1, nuclear data cross section libraries were used in the model for all continuous libraries [31]. For the graphite thermal scattering cross sections, the ENDF/B-VIII.0 S(α,β) libraries were implemented [32]. Calculations used 100,000 particles per generation, 1500 active generations, and 100 skipped generations for a total of 150,000,000 neutron histories for each calculation. The 100 skipped cycles were determined to be sufficient to demonstrate fission source convergence in the Monte Carlo simulation. The resulting uncertainty in k_{eff} is ≤0.00007 and ≤0.00010 in Δk_{eff}.

To quantify the uncertainty in k_{eff}, a benchmark model was developed based on the information in Chapter 2 and described in Chapter 4. This model was perturbed one parameter at a time to estimate the uncertainties in k_{eff} due to uncertainties of the different core parameters. Simplifications from the detailed model to the benchmark model are given in Table 4-19 along with the resulting k_{eff} bias. This reactivity bias between the models was determined to be small. Therefore, it was assumed that the contribution to the k_{eff} uncertainty from the simplified components was negligible. The variation in k_{eff} due to a $\pm 1\sigma$ variation in the value of a given parameter was determined. The resulting change between the perturbed k_{eff} value and a reference k_{eff} value is then considered the uncertainty in k_{eff} due to the uncertainty in the given parameter [33]. The reference k_{eff} value is the k-eigenvalue calculated using the benchmark simplified model developed in Chapter 4.

Uncertainty values in this section correspond to the 1σ level unless otherwise stated. Each parameter was defined either with upper and lower bounds or with 1σ bounds based on experimental data, reported measurements, or convention with the measurements and data taking precedence. In the case where upper and lower bounds are the only defined limits, a conservative distribution was assumed. The distributions applied to different parameters, unless specifically noted, were as follows. In the case where the distribution was not symmetrical, a triangular distribution was applied. For dimensional tolerances, a triangular distribution was applied. All other parameters were assumed to have a flat distribution. Using the distributions to define then the 1σ values, each parameter was perturbed within the model by ±1σ to determine the corresponding reactivity impact. This then established a +1σ impact on k_{eff} and a -1σ impact on k_{eff} removing any assumption of symmetrical impact on k_{eff}. For parameters with a symmetrical impact on k_{eff}, the +1σ impact and -1σ impact were averaged [33]. Uncertainties were considered symmetrical if the absolute value impact from +1σ and -1σ deviations (including their statistical uncertainty) overlapped.

In evaluating the 1σ impacts, all components within the system are simultaneously perturbed. For example, in evaluating the impact of fuel dimensions, all the fuel blocks would be consistently adjusted by the 1σ value. This assumes a 100% systematic uncertainty. However, experimental system's uncertainty will be split between random and systematic components. Information for TREAT regarding the distribution of random and systematic uncertainty is not available, and for the TREAT reactor, the ability to quantify the systematic component for individual components is hampered by the age of the reactor and its components, most of which were manufactured over 50 years prior to this evaluation. While the manufacturing and measurements reported for this facility are believed to be of high quality, there are no records to support this assumption.

Other graphite reactors such as PROTEUS and HTTR similarly lack the needed information to individually define the systematic uncertainty ratios, and both systems also were believed to be high quality experimental systems. For these benchmarks, the systematic uncertainty is assumed to be 15% and 25% for

the PROTEUS and HTTR systems, respectively [34][35]. Following the precedent of these reactors, a systematic uncertainty of 25% is assumed for component dimensions and masses; other uncertainties are assumed to be 100% systematic, such as enrichment, material composition, impurities, etc. Because the total uncertainty of TREAT is dominated by the 100% systematic uncertainties of the boron and hydrogen impurities in the graphite fuel, the impact of the ratio of random-to-systematic uncertainty in most of the perturbed parameters is less significant. The random portion of the uncertainty was then divided by the square root of the number of elements [35]. The systematic and random portions were then added in quadrature to obtain the total uncertainty.

For some parameters, the statistical uncertainty is on the same order as the 1σ impact. For these parameters, an extended range of perturbation can be used and the results scaled to determine the 1σ impact with reduced statistical uncertainty. The scaling factor is determined as the standard uncertainty of the parameter divided by the variation of the parameter in the calculation.

For parameters with symmetrical impact on k_{eff}, the average of the +1σ and -1σ impact was used. For non-symmetrical components, the maximum of the absolute value of the +1σ or -1σ impacts was used. The total variation or impact on k_{eff} was then determined by adding in quadrature 1σ components. Variations in k_{eff} evaluated to be ≤0.00010 are considered negligible based on the statistical error from the Monte Carlo calculation and the large impact from a few dominate uncertainties for TREAT.

3.1 Evaluation of Critical Configuration Data

3.1.1 Total Experimental Uncertainty

The individual impacts determined above are compiled below in Table 3-1. Within this table, only the non-negligible values (> 0.00010 Δk_{eff}) are included. Some negligible quantities (neg.) were included in the

benchmark biasing or in the calculation of other uncertainties, and some were assumed or calculated to be negligible. The largest uncertainty arises from the boron and hydrogen impurity in the fuel content. These two impurities contribute more than 90% of the total uncertainty in k_{eff}. It is assumed that all the parameters are uncorrelated, and that the total uncertainty on k_{eff} is calculated by combining the individual components within Table 3-1 as the root-sum squared. A conservative approach was used to determine the total uncertainty by including the greater of the absolute value of the $+1\sigma$ or -1σ for non-symmetric components in the quadrature sum. The total uncertainty is then $\pm 0.01296\ \Delta k_{eff}$. Contributions with a Δk_{eff} greater than 0.00100 are highlighted below. The M2CAL uncertainties have been evaluated and determined to be acceptable benchmark experiment.

Table 3-1. Summary of Evaluated Impacts from the $\pm 1\sigma$ Variation of Parameters within TREAT M2/M3CAL. These impacts include both total of the systematic and random components.

Perturbed Parameter	Parameter Value	$\pm 1\sigma$ Uncertainty	Δkeff ($\pm 1\sigma$)
Fuel Block Flat-to-Flat (inches)	3.800	0.0054	neg.
Fuel Height (inches)	47-5/8	0.013	neg.
CP-2 Graphite Plug Flat-to-Flat (inches)	3.780	0.0064	neg.
CP-2 Graphite Upper Height (inches)	24-11/16	0.0064	neg.
CP-2 Graphite Lower Height (inches)	23-1/16	0.0064	neg.
Al-1100 Top Fuel Fitting			neg.
Al-6063 Can Thickness (inches)	0.050	0.002	neg.
Zy-3 Can Thickness (inches)	0.025	0.002	-0.00075
Zy-3 Can Flat-to-Flat (inches)	3.960	0.010	neg.
Zy-3 End Cap Thickness (inches)	3/32	0.006	neg.
Zy-3 Assembly Tab Thickness (inches)	3/32	0.006	neg.
Zy-3 Spacer Thickness (inches)	1/8	0.006	neg.
Zy-3 Outgas Tube Thickness (inches)	3/8	0.015	neg.
Zy-3 Other Fuel Assembly Components			neg.
Control Rod Hole through Fuel (inches)	2.330	0.0095	neg.
Control Rod Tube Thickness (inches)	2.25	0.02	-0.00029
Control Rod Assembly Other Components			neg.
Source Assembly Components			neg.
Thermocouple Fuel Assembly Components			neg.
Slotted Assembly Components			neg.
Reflector Thickness			neg.

Table 3-1. (continued).

Reflector Detector Holes			neg.
North Gate Height (inches)	28	1.1	-0.00022
West Gate Slot Height (inches)	4	0.4	neg.
Shielding Height			neg.
Shielding Thickness			neg.
Shielding Instrument Holes			neg.
Shielding/Thermal Column			neg.
Fuel ^{234}U Content (wt%)	0.90864	0.01	neg.
Fuel ^{235}U Content (wt%)	93.1	0.05	0.00017
Fuel ^{236}U Content (wt%)	0.42736	0.01	neg.
Fuel ^{238}U Content (wt%)			neg.
Fuel O:U Ratio	2.0	0.2	neg.
Fuel U-mass Content (wt%)	0.211	0.004	0.00161
Fuel Density (g/cm^3)	1.73	0.01	0.00092
Fuel Fe Content (wt%)	0.0267	0.0077	-0.00045
Fuel V Content (ppm)	30	9	neg.
Fuel B Content (ppm)	7.53	1.16	-0.00988
Fuel H Content (ppm)	510	266	0.00795
Al-6063 Composition	Max/Min Al		0.00021
Al-6063 Density (g/cm^3)	2.685	0.01	neg.
Al-6061 Composition	Max/Min Al		neg.
Al-6061 Density (g/cm^3)	2.70	0.01	neg.
Al-1100 Composition	Max/Min Al		0.00023
Al-1100 Density (g/cm^3)	2.71	0.01	neg.
Zy-3 Composition*			0.00054
Zy-3 Density (g/cm^3)	6.53	0.01	neg.
CP-2 Graphite Composition	Max/Min C		0.00033
CP-2 Graphite Density (g/cm^3)	1.67	0.0255	0.00140
Air Composition			neg.
Air Density (g/cm^3)	0.0012	6.9E-5	-0.00013
SS-304 Composition	Max/Min Fe		0.00020
SS-304 Density (g/cm^3)	8	0.01	neg.
SS-316 Composition	Max/Min Fe		neg.
SS-316 Density (g/cm^3)	8	0.01	neg.
Mild, Low Carbon Steel Composition	Max/Min Fe		neg.
Mild, Low Carbon Steel Density (g/cm^3)	7.87	0.01	neg.
Concrete Composition*	---		0.00014
Concrete Density (g/cm^3)	3.364	0.065	neg.
B_4C Composition	Max/Min B_4C		neg.

Table 3-1. (continued).

B_4C Density (g/cm^3)	1.8	0.01	neg.
Lead Composition			neg.
Lead Density (g/cm^3)	11.34	0.01	neg.
Graphitar Composition / Density			neg.
Rod Insertion Position (inches)	---	0.02	neg.
Control Rod Absolute Position (inches)	---	0.12	0.00044
Experiment Can Thickness (inches)	0.050	0.003	neg.
Dummy Heater Thickness (inches)	0.046	0.003	neg.
Pump Leg Thickness (inches)	0.3	0.02	neg.
Flow Tube Thickness (inches)	0.015	0.001	neg.
Shield Tube Thickness (inches)	0.035	0.002	neg.
Outer Tube Thickness (inches)	0.065	0.004	neg.
Loop Tube Thickness (inches)	0.368	0.016	neg.
Dy/Steel Collar Thickness (inches)	0.02	0.002	neg.
Al Sleeve Thickness (inches)	0.05	0.002	neg.
Experimental Material Composition			neg.
Total (Computed as a quadrature of the above components**)**			**0.01296**

* 1σ given as absolute value.

The three top contributing parameters to k_{eff} will be considered in the transient benchmark uncertainty analysis, where their contribution calculated in quadrature amounts to 98.7% of the uncertainty in k_{eff} . However, their concentrations and uncertainties will be adjusted to fall within a range that lead to a critical core. This analysis is detailed in Section 5.4.3.1. In the next sections, the new values for these parameters will be used to determine the benchmark uncertainty.

3.2 Evaluation of Reactivity Coefficient Data

3.2.1 Temperature Coefficient Measurement

The temperature coefficient of reactivity measurements were performed on the Minimum Critical Mass Core configuration in two different techniques as discussed in Section 2.2.1. Given that the reactivity coefficient calculation performed on the benchmark model will follow an isothermal approach, the isothermal coefficient measurement will be chosen to be compared to the calculations. The effect of the top

three parameters on the reactivity coefficient of temperature that have the highest impact on reactivity in Table 3-1 was investigated and displayed in Table 3-2.

Table 3-2. Impact of Core Parameters Perturbation on the Temperature Coefficient of Reactivity.

Perturbed Parameter	Parameter Value	±1σ Uncertainty	Δ Temperature Coefficient (±1σ) (Δk/°C)
Fuel U-mass Content (wt%)	0.211	0.004	-2.8084E-6
Fuel B Content (ppm)	8.095	0.3435	-8.0379E-7
Fuel H Content (ppm)	137.5	79.385	-5.1266E-6

The benchmark uncertainty for the temperature coefficient of reactivity amounts for 3.2% where the uncertainties in Table 3-3 are added in quadrature. Therefore the temperature coefficient of reactivity will be taken to be $-(1.8 \pm 0.25) \times 10^{-4}$ Δk/°C.

3.3 Evaluation of Kinetics Measurements Data

3.3.1 Prompt Neutron Lifetime Measurement

The prompt neutron lifetime was measured using Rossi alpha, transfer function and superprompt-critical period methods. The best value for the transfer function method was taken as 9.0×10^{-4} sec while it was $8.8 \pm 0.5 \times 10^{-4}$ sec for the Rossi alpha method. It is reasonable to choose a value of 9.0×10^{-4} sec and uncertainty of 0.3×10^{-4} sec based on the spread of the results. The effect of the boron, hydrogen and fuel content on the prompt neutron lifetime is highlighted in Table 3-3.

Table 3-3. The Impact of Core Parameters on the Prompt Neutron Lifetime.

Perturbed Parameter	Parameter Value	±1σ Uncertainty	Δl_p (±1σ) (%)
Fuel U-mass Content (wt%)	0.211	0.004	1.04%
Fuel B Content (ppm)	8.095	0.3435	neg.
Fuel H Content (ppm)	137.5	79.385	neg.

3.3.2 Delayed Neutron Parameters Measurement

β_{eff} was used in the measurement of the prompt neutron lifetime in both Rossi-alpha and transfer function methods, which gave the same result within about 2% [10]. This implies that β_{eff} used was correct. However, the stated uncertainty in these measurements ± 5% and ± 2%, respectively, would allow for an uncertainty in β_{eff} of about ± 7% [10]. Assuming that the uncertainty is the same for each effective delayed neutron fraction $\beta_{i,eff}$, the uncertainty would be about ± 1.5%. For the decay constants, the uncertainties in the measurement were given by Keepin et al [27].Table 3-4 highlights the measurement and their uncertainties. The benchmark uncertainty for β_{eff} amounts for 1%. The impact of perturbed core parameters on β_{eff} and each individual group is tabulated in Table 3-6, Table 3-7, Table 3-8, Table 3-9, Table 3-10, and Table 3-11.

Table 3-4. Delayed Neutron Data for U-235.

Group Index *i*	Half-Life T_i (s)	Decay Constant λ_i (sec^{-1})
1	55.72 ±1.28	0.0124 ±0.0003
2	22.72 ±0.71	0.0305 ± 0.0010
3	6.22 ± 0.23	0.1114 ± 0.0041
4	2.3 ± 0.09	0.3014 ± 0.0118
5	0.61± 0.083	1.1363 ± 0.1546
6	0.23 ± 0.025	3.0137 ± 0.3276

Table 3-5. Impact of Core Parameters Perturbation on β_{eff}.

Perturbed Parameter	Parameter Value	±1σ Uncertainty	$\Delta\beta_{eff}$ (±1σ)
Fuel U-mass Content (wt%)	0.211	0.004	2.368E-5
Fuel B Content (ppm)	8.095	0.3435	-2.791E-5
Fuel H Content (ppm)	137.5	79.385	2.091E-5

Table 3-6. Impact of Core Parameters Perturbation on $\beta_{1,eff}$.

Perturbed Parameter	Parameter Value	±1σ Uncertainty	$\Delta\beta_{1,eff}$ (±1σ) (%)
Fuel U-mass Content (wt%)	0.211	0.004	-1.96
Fuel B Content (ppm)	8.095	0.3435	4.28
Fuel H Content (ppm)	137.5	79.385	1.28

Table 3-7. Impact of Core Parameters Perturbation on $\beta_{2,eff}$.

Perturbed Parameter	Parameter Value	±1σ Uncertainty	$\Delta\beta_{2,eff}$ (±1σ) (%)
Fuel U-mass Content (wt%)	0.211	0.004	neg.
Fuel B Content (ppm)	8.095	0.3435	1.33
Fuel H Content (ppm)	137.5	79.385	1.34

Table 3-8. Impact of Core Parameters Perturbation on $\beta_{3,eff}$.

Perturbed Parameter	Parameter Value	±1σ Uncertainty	$\Delta\beta_{3,eff}$ (±1σ) (%)
Fuel U-mass Content (wt%)	0.211	0.004	-1.12
Fuel B Content (ppm)	8.095	0.3435	-1.59
Fuel H Content (ppm)	137.5	79.385	neg.

Table 3-9. Impact of Core Parameters Perturbation on $\beta_{4,eff}$.

Perturbed Parameter	Parameter Value	±1σ Uncertainty	$\Delta\beta_{4,eff}$ (±1σ) (%)
Fuel U-mass Content (wt%)	0.211	0.004	neg.
Fuel B Content (ppm)	8.095	0.3435	neg.
Fuel H Content (ppm)	137.5	79.385	neg.

Table 3-10. Impact of Core Parameters Perturbation on $\beta_{5,eff}$.

Perturbed Parameter	Parameter Value	±1σ Uncertainty	$\Delta\beta_{5,eff}$ (±1σ) (%)
Fuel U-mass Content (wt%)	0.211	0.004	neg.
Fuel B Content (ppm)	8.095	0.3435	-1.97
Fuel H Content (ppm)	137.5	79.385	neg.

Table 3-11. Impact of Core Parameters Perturbation on $\beta_{6,eff}$.

Perturbed Parameter	Parameter Value	±1σ Uncertainty	$\Delta\beta_{6,eff}$ (±1σ) (%)
Fuel U-mass Content (wt%)	0.211	0.004	-3.43
Fuel B Content (ppm)	8.095	0.3435	3.16
Fuel H Content (ppm)	137.5	79.385	-3.05

3.4 Evaluation of Power Distribution Data

3.4.1 Axial Power Distribution Measurement in the Flux Wire

The segments were weighted, and gamma counted for relative activity after the 48-1 wire irradiation test. The uncertainty of the measurement was not reported or highlighted on the axial power plot. The benchmark uncertainty for the axial power distribution was measured and displayed in Table 3-12. The total uncertainty is calculated in quadrature to be 13.15%- 5.295%.

Table 3-12. Impact of Core Parameters Perturbation on the Axial Power Distribution.

Perturbed Parameter	Parameter Value	±1σ Uncertainty	Δ Axial Power (±1σ) (%)*
Fuel U-mass Content (wt%)	0.211	0.004	6.50 –2.95
Fuel B Content (ppm)	8.095	0.3435	5.47 – 2.93
Fuel H Content (ppm)	137.5	79.385	10.05 – 3.28

* The upper and lower percent change in the fission rate for the wire segments.

3.5 Evaluation of Transient Measurements

3.5.1 Evaluation of Transient Configuration and Measurements

3.5.1.1 Evaluation of Transient Core Configuration

Initial Rod Positions

The fully withdrawn inner and outer banks would be 6.6 ± 0.3 in. from the active fuel region. The fully inserted control rod T-2 would be 9.6 ± 0.3 in. above the bottom of the of the active fuel region. The uncertainty in transient rod T-1 location, however, is probably between ±0.02 and ±0.002 inches.

Transient Rod Dynamics

The uncertainty in transient rod T-1 and T-2 height is probably between ±0.02 and ±0.002 inches.

3.5.1.2 Evaluation of Transient Experimental Power Measurements

No uncertainty in the power measurement was reported in any TREAT document. However, the published measurements can be used to determine the uncertainty. Transient Safety # 1 and Control Power detectors seem to produce comparable power readings in spite of the difference in location and level. This suggests that the core power is biased towards the readings of Transient Safety # 1 and Control Power. A mean power trace can be calculated by assuming that the difference between Safety # 1 and Safety # 2 measurements represents a 4σ of a flat distribution.

The integral power was measured by Integral Power # 1 and 2, where the difference in the final measurement between the two detectors amounts to 14%. The total TREAT energy measured by combining

the power readings of the power detectors (Transient Safety # 1, Transient Safety # 2 and Control Power) is always higher than 200 MJ. This suggests that Integral Power # 1 is more accurate than Integral Power # 2. The final integral power most likely has an uncertainty no less than 2%.

3.5.1.3 Evaluation of Experimental Period Measurements

The uncertainty in the period or the measuring device was not reported in any TREAT document. The difference between the period measured from decade # 2 and decade # 3 and the period measured from decade #3 and decade # 4 is 4%. An additional 2% uncertainty in the period was assumed given that the uncertainty in power would probably be no less than 2%.

3.5.1.4 Evaluation of Experimental Transient Rod Worth Measurement

The uncertainty in the experimental differential worth is calculated by taking into account a reactivity control accurate to ±0.02 inch. The impact of core parameters perturbation on the integral rod worth at 17 in. is shown in Table 3-13.

Table 3-13. Impact of Core Parameters Perturbation on the Integral Rod Worth at 17 in..

Perturbed Parameter	Parameter Value	±1σ Uncertainty	Δ Integral Worth (±1σ) (pcm)
Fuel U-mass Content (wt%)	0.211	0.004	neg.
Fuel B Content (ppm)	8.095	0.3435	neg.
Fuel H Content (ppm)	137.5	79.385	21

3.5.2 Evaluation of Temperature Measurement

The uncertainty in the temperature measurement was not reported. Modern Alumel-Chromel thermocouples have an uncertainty of ±0.75%- ±0.5%. 40 Years ago, when the M2CAL tests were performed, the uncertainty would be no less than ±1%.

3.5.3 Evaluation of Additional Information Relative to Transient Measurements

3.5.3.1 Evaluation of Axial Power Distribution Measurement in the Flux W*ire*

The process of evaluation follows the same procedure discussed in Section 3.4.1.

3.5.3.2 Evaluation of the Transient Coupling Factors

The absolute number of fissions per gram were calculated for the three segments using radiochemical analysis as discussed in Section 2.5.5.2 . Comparable absolute values for the highest point in the axial power distribution of the wire were obtained by dividing the absolute fissions per gram values by the associated relative fission activities. It was reported that that the three comparable values used in calculating the PCF agreed with each other to within 2%. This suggests an uncertainty in the PCF no less than 2%. Another reference reports an uncertainty of 10% for the PCF calculations performed on the fuel pins in M2 and M3 Calibration Experiments [21]. It is reasonable to assume that the PCF calculation in the wire would have the same uncertainty since the cutting of the segments and the radiochemical analysis in both the pin and wire irradiation are similar. However, no evidence of such large uncertainty was found in the TREAT literature. Based on the finding in Section 3.4.1, the benchmark uncertainty for the PCF in both steady-state and transient is 13.1%. The total uncertainty in the PCF is calculated in quadrature to be 13.25%.

A reanalysis of the TCF calculations for M2 and M3 test determined that several analysis shortcuts were introduced to the preliminary results in Reference 2 [18]. These shortcuts are:

1. Only three segments of the flux wire were used in the TCF calculation.
2. The axial midplane of the distribution was taken as the peak value of a statistically fluctuating measured distribution instead of a fitted curve.

Due to these shortcuts, one or two abnormally high data points were observed below the axial midplane of the relative distribution. Reference 18 reanalyze the distribution by omitting the anomalous points, and introducing a smoothed curve in the active fuel region [18].

4 BENCHMARK SPECIFICATIONS & SIMPLIFICATIONS

4.1 Benchmark-Model Specifications for Critical and / or Subcritical Measurements

The M2 and M3 low-level steady state calibration experiment was evaluated. The critical configuration irradiated three test pins. The core features a full slot from north to south with the experimental vehicle with the test pins was placed in the center of the core.

4.1.1 Description of the Benchmark Model Simplifications

A detailed model and benchmark model were created for the M2/M3 core configuration for the TREAT reactor. The benchmark model which was derived from the detailed model reduces the evaluated area of the system to include significant reactivity contributors. This introduces a bias to k_{eff} which is approximated using Monte Carlo calculations in Serpent. Impacts on $k_{eff} \leq 0.00100$ were considered small, and impacts $\leq$ 0.00010 were considered negligible.

The core was modeled according to the description given in Section 2. This full detailed model attempts to capture all key factors in the TREAT core. Using this model, the reactivity bias due to different core components was approximated. Simplifications included in the bias consist of the removal of the top and bottom shielding, simplification of the source and slotted assemblies, removal of the thermocouple assemblies, removal of the tie bolts, removal of the hodoscope instrumentation, removal of the radiography voids, and removal of the top assemblies' fittings and top of the control rods.

Impurities and material considerations were included in the uncertainty evaluation in Section 3. The impurities have been modeled explicitly and are therefore not included in the biasing here since they were not removed from the model. For materials where the impurities were reported as less than the detector

limit, it was assumed the impurity was not present. Therefore, in the fuel, CP-2 graphite, and Zy-3 modeling, these isotopes were not included.

Some possible biases introduced in the model were not evaluated. These included the following components which were assumed to have negligible contributions to k_{eff}. Justifications for these assumptions are also noted below.

- Control Rod Assembly
    - Subpile support structure of the control rods was approximated using the bearing tube with an additional 3.5 inches of mild steel structure surrounding the actual control rod. These dimensions are based on the detailed support for which all dimensions were not reported. This support structure is only included in the detailed modeled and used for determining the benchmark biasing.
- Thermocouple Assemblies
    - These assemblies were used only in the biasing quantification and not the benchmark model.
    - Approximations were made to the top fitting. This includes neglecting the wires within the top fitting and approximating the plug holder with no outlet for the wire. In addition, the top conic sections were reduced to step sections. Since the mass of the top fitting was not known, the mass was not conserved for the top fitting. Instead, the step changes best attempt to replicate the given geometry.
    - None of the tapering of the holes at the fuel block edge were modeled. The small change in fuel mass is assumed to result in a mass change well within the uncertainty in the fuel density already included in the analysis in Section3.
    - Explicit drawings for the thermocouple assemblies do not include all the necessary dimensions for the holes through the spacers. Within the model these are approximated as straight holes with the same diameter as the holes through the upper endcap.

    - The thermocouple wires were modeled as Alumel-Chromel wire with insulation in the assemblies known to have been used during the M2/M3CAL LLSS irradiations. Some other assemblies were not modeled with thermocouple wires.

- Slotted Assembly
    - The stiffeners were approximated with no rounded corners but with straight edges. This change is many orders of magnitude smaller than the dimensions of the stiffener and should have negligible impact. The stiffeners are removed from the benchmark model and are only used to estimate reactivity impacts.
    - Slotted assembly H-19B is located on the southernmost side of the core. This assembly was approximated with dimensions for the can to be equal to the other slotted assemblies. The relatively small change to the one assembly is expected to have negligible impact.
- Assemblies were modeled without the expansion slots in the can. Given the small change from the increase or decrease of the can thickness shown in Section3, the removal of the slot should have negligible impact.
- Stainless steels AISI 1010-1020 and AISI 1015 were noted for different components throughout the core. These materials have similar compositions to the mild, low carbon steel. It was approximated that the 1010 and 1015 stainless steels could be modeled as mild, low carbon steel and that the impact would be negligible.
- Components made of 18-8 stainless steel were modeled as stainless steel-304 which has the same basic composition. This small change is assumed to have negligible impact.
- The chamfered transition to square in the graphite reflector blocks is approximated with a straight change to conserve the volume of the block. This change is expected to have negligible impact as the volume and therefore mass is conserved.
- Core Reflector

- Thermocouples were present within the core's permanent graphite reflector. These minor penetrations were assumed to have negligible impact on the core model given the small impact of all the tie bolts.

- Radiography Instrumentation
  - The radiography instrumentation was largely comprised of borated materials. The exact instrumentation was not modeled, and instead, the cavities were represented as void in the benchmark model. This approximation was used to determine the approximate impact of neglecting the radiography instrumentation for the simplified model, and it was found to be small.

- Experiment
  - No magnet, experiment vehicle cap, or joining pieces are modeled. For those which have drawings, no dimensions are given to be able to accurately represent them. Due to the small amount of material that would be used for these components and the location of these components well within the axial graphite reflector or even outside the core, the expected impact is negligible.
  - Similarly, the exact dimensions of the top and bottom of the experimental vehicle are not given. For the purpose of biasing, they are approximated in the full detailed model.

To quantify the bias for the benchmark model, the full detailed model was modified to determine the reactivity values of components both within the core and out in the exterior.

The top shielding including the boral steel plates, the upper concrete, and parts of the withdrawn graphite reflector blocks were removed from the model. The benchmark model then only extends up to the bottom of the concrete shelf.

Below the core, the concrete shielding and the support structure were removed. This included the gridplate and everything below such as the control rod supports, the assembly supports and guides, and the plenum beneath the core.

The control rod assembly has a stationary Zy-2 tube between the control rod and the assembly, and some of the slotted assemblies have Zy-4 components. Both the Zy-2 and Zy-4 throughout the core were replaced with Zy-3 in the benchmark model.

The slotted assemblies which were placed from north to south between the experiment and the hodoscope contained Zy-3 and Zy-4 stiffener pieces for support. These pieces were removed from the benchmark model and replaced with air. The source assembly located in the northeast corner of the core was reduced in the benchmark model to simplify the geometry. The source can which penetrated from the top was removed and the hole within the graphite reflector, spacers, and endcap were filled with the associated material corresponding to those components. Within the central graphite region, the source and surrounding air were removed and replaced with graphite.

Thermocouple assemblies were placed throughout the core configuration. Not all were used to collect data during the M2/M3CAL LLSS experiment, but the modifications to the assemblies and to the fuel were explicitly modeled in the detailed model. These assemblies were replaced with standard fuel assemblies in the benchmark model with the fuel density scaled with the ratio based on the relative mass of the fuel in the thermocouple assembly and the standard fuel assembly. To the north, the hodoscope would have had an inner collimator installed. This steel device along with the extra concrete blocks were removed from the benchmark model and included into the biasing.

To the west, the radiography instrumentation would have been comprised of borated materials. These cavities in the reflector and shielding were approximated using void. This void was removed and replaced

with concrete in the shielding and air within the reflector in the simplified model. The graphite reflector supports were held with tie bolts which were removed and replaced with graphite in the simplified model. The tops of the assemblies are fitted with aluminum fittings. These fittings along with the portion of the control rod above the axial reflector were removed from the benchmark model with only small reactivity impacts which were included in the biasing. The results from the removal or simplification of these components are given in Table 4-1 where each of the individual components is shown to have a small impact of k_{eff}. The subcore structure has the largest impact of 0.00102 ± 0.00010 Δk_{eff} which including the uncertainty is assumed to still have a small impact on the total reactivity. The total reactivity bias was determined by comparing the original detailed model to the final benchmark model. Due to compensating effects, the bias is less than that which would result from the summing in quadrature of the individual components. However, comparing the detailed model and benchmark model results in the bias which is representative of the differences that would be expected between calculations conducted with one versus the other.

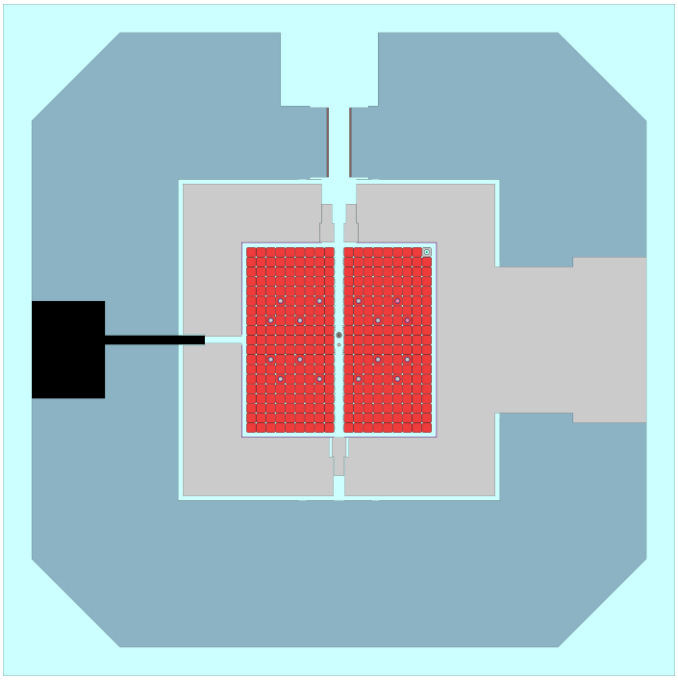

Figure 4-1. M2/M3CAL detailed Serpent model cross section of the core from the top down at the core midplane.

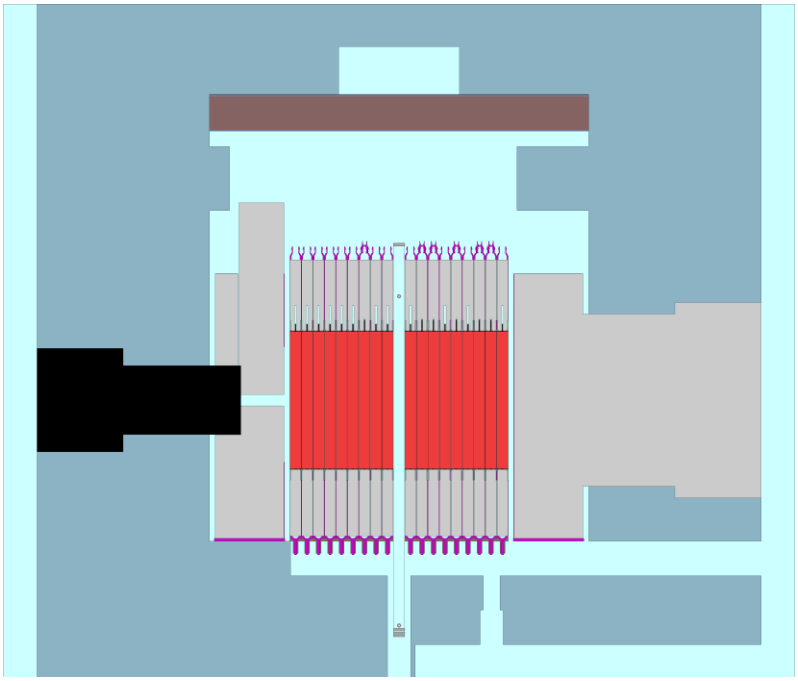

Figure 4-2. Cross section of the TREAT detailed model from east to west.

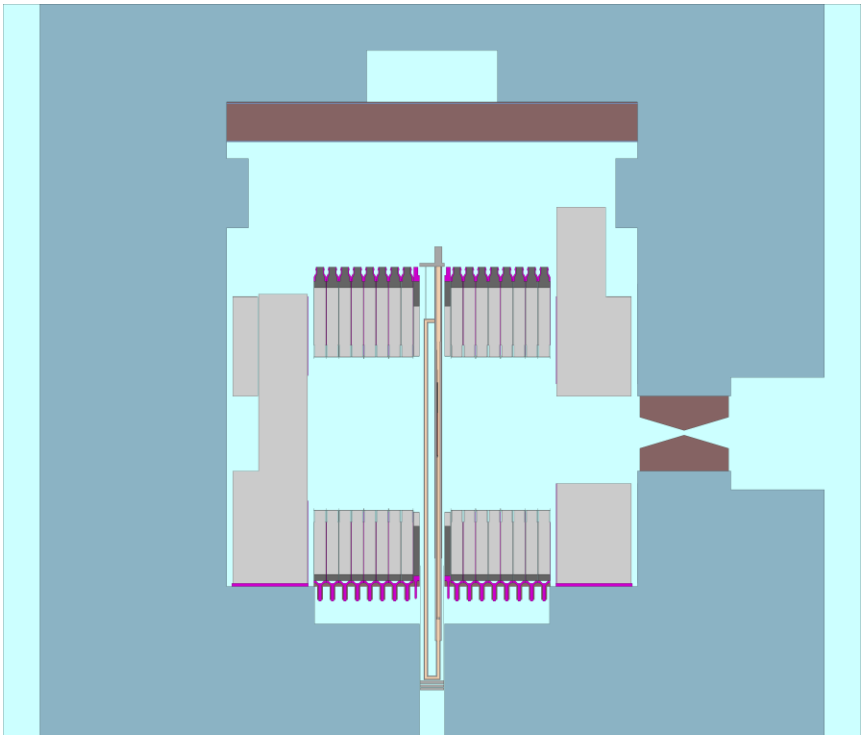

Figure 4-3. Cross section of the TREAT detailed model from north to south.

Table 4-1. Benchmark Model Calculated Simplification Bias.

Simplification	**$\Delta k_{eff} \pm 1\sigma$**
Removal of top concrete shielding, top boral steel plate, and top of graphite removable blocks	-0.00017 ± 0.00010
Removal of lower concrete shielding, lower plenum, grid plate, assembly supports, and control rod assembly supports	-0.00102 ± 0.00010
Removal of slotted assembly stiffeners	0.00060 ± 0.00010
Removal of all thermocouple assemblies and replacing them with standard fuel assemblies	-0.00001 ± 0.00010
Removal of hodoscope steel collimator in concrete shielding	-0.00047 ± 0.00010
Removal of radiography void and replacing with concrete and air	0.00025 ± 0.00010
Removal of tie bolts and replacing with graphite	0.00040 ± 0.00010
Remove Zy-2 and Zy-4 and replace with Zy-3	0.00046 ± 0.00010
Total Benchmark Model Simplification Bias	-0.00070 ± 0.00010

4.1.2 Material Data

The material compositions used in the model are provided below.

4.1.2.1 Standard Fuel Assembly

The standard fuel assembly is comprised of graphite fuel enriched to 93.1 wt% U^{235} (Table 4-2) in a Zy-3 can (Table 4-5). Above and below, CP-2 graphite (Table 4-6) has end tubes made from Al-6063 (Table 4-4). The upper fixture and bottom fuel fitting are made from Al-6061 (Table 4-3).

Table 4-2. Graphite Fuel Composition.

Element	Atom Density (atoms/b-cm)
^{234}U	8.5345E-08
^{235}U	8.7072E-06
^{236}U	3.9799E-08
^{238}U	5.1380E-07
O	1.8692E-05
C	8.6462E-02
B-10	1.4440E-02
B-11	5.8124E-02
Fe	4.9810E-06
V	6.1354E-07
H	5.2714E-04
Total	8.7024E-02
Mass Density (g/cm^3)	1.73

Table 4-3. Al-6061 Composition.

Element	Atom Density (atoms/b-cm)
Si	3.4736E-04
Fe	1.0191E-04
Cu	7.0365E-05
Mn	2.2197E-05
Mg	6.6899E-04
Cr	6.0979E-05
Zn	3.1088E-05
Ti	2.5477E-05
Co	6.8975E-06
Ni	6.9257E-06
Sn	3.4243E-06
Al	5.8593E-02
Total	5.9939E-02
Mass Density (g/cm^3)	2.70

Table 4-4. Al-6063 Composition.

Element	Atom Density (atoms/b-cm)
Si	2.3029E-04
Fe	5.0670E-05
Cu	1.2723E-05
Mn	1.4716E-05
Mg	4.4906E-04
Cr	1.5549E-05
Zn	1.2366E-05
Ti	1.6890E-05
Co	6.8592E-06
Ni	6.8873E-06
Sn	3.4052E-06
Al	5.8984E-02
Total	5.9803E-02
Mass Density (g/cm^3)	2.685

Table 4-5. Zy-3 Composition.

Element	Atom Density (atoms/b-cm)
Al	7.2873E-07
Ti	6.5723E-07
Mn	7.1579E-08
Fe	1.8308E-04
Y	4.4231E-07
Nb	4.2327E-07
Ag	5.4684E-06
In	2.3974E-07
Sn	9.9379E-05
Hf	1.7406E-06
Pb	1.1386E-07
C	3.9289E-05
N	1.4318E-05
O	2.2618E-04
H	8.5832E-05
Zr	4.2804E-02
Total	4.3462E-02
Mass Density (g/cm3)	6.530

Table 4-6. CP-2 Graphite Composition.

Element	Atom Density (atoms/b-cm)
Li	9.7091E-08
B-10	1.6987E-08
B-11	6.8373E-08
C	8.3681E-02
Mg	2.4827E-09
Al	8.2001E-08
Si	2.5066E-06
P	2.1105E-08
Si	1.4114E-06
Cl	1.2765E-08
Ca	4.0149E-06
Ti	2.5212E-07
V	2.3691E-06
Mn	3.6612E-10
Fe	1.1165E-07
Ni	2.3989E-08
Cu	2.3739E-09
Sr	1.3774E-08
Y	5.6559E-10
Zr	3.7483E-09
H	7.4449E-06
O	3.7225E-06
Total	8.3703E-02
Mass Density (g/cm^3)	1.67

4.1.2.2 Control Rod Assembly

The materials which comprise the basics for the control rod assembly are given above in Table 4-2 to Table 4-6. The control rods themselves are comprised of boron carbide (B_4C) (Table 4-8). Joiners for the control rods are made of the mild low carbon steel (Table 4-9). The bushing was made of graphitar (Table 4-7), and the bearing tube and bushing retainer of Al-1100 (Table 4-10). The control rod tube, tabs, fuel can, and spacer were modelled using Zy-3 (Table 4-5).

Table 4-7. Graphitar Composition.

Element	Atom Density (atoms/b-cm)
C	8.6240E-02
Total	8.6240E-02
Mass Density (g/cm^3)	1.72

Table 4-8. Boron Carbide Composition.

Element	Atom Density (atoms/b-cm)
B-10	1.5567E-02
B-11	6.2660E-02
C	1.9557E-02
Ti	2.2575E-05
Mn	1.9670E-07
Na	4.7004E-07
Al	4.0050E-05
Si	3.8476E-05
Ca	2.6963E-06
Total	9.7889E-02
Mass Density (g/cm^3)	1.8

Table 4-9. Mild Low Carbon Steel (STL-1018).

Element	Atom Density (atoms/b-cm)
C	7.8920E-04
P	4.5904E-05
S	5.1733E-05
Ti	2.4753E-06
Cr	1.3672E-04
Mn	7.7642E-04
Fe	8.3345E-02
Ni	1.6150E-04
Cu	1.4917E-04
Mo	2.9634E-05
Total	8.5499E-02
Mass Density (g/cm^3)	7.87

Table 4-10. Al-1100 Composition.

Element	Atom Density (atoms/b-cm)
Si	1.3801E-04
Fe	6.9406E-05
Cu	3.2102E-05
Mn	7.4265E-06
Zn	1.2481E-05
Co	6.9230E-06
Ni	6.9513E-06
Sn	3.4369E-06
Al	6.0032E-02
Total	6.0308E-02
Mass Density (g/cm^3)	2.71

4.1.2.3 Source Assembly

The materials which comprise the source assembly are given above in Table 4-4 to Table 4-6 and Table 4-10.

4.1.2.4 Slotted Assembly

The materials which comprise the slotted assembly are primarily given above in Table 4-5, Table 4-6, and Table 4-10. In addition, the components of the lead bricks are given in Table 4-11.

Table 4-11. Lead Composition.

Element	Atom Density (atoms/b-cm)
Fe	6.1143E-07
Ni	2.9088E-07
Cu	8.0600E-07
As	4.5575E-07
Pb	3.2945E-02
Ag	3.1655E-06
Bi	8.1696E-06
Zn	5.2228E-07
Sn	2.8764E-07
Sb	2.8043E-07
Total	3.2960E-02
Mass Density (g/cm^3)	11.34

4.1.2.5 Experiment

The experimental vehicle was made from stainless steel-304 (SS-304) (Table 4-15). The test pins (Table 4-12) have a stainless steel-316 cladding (Table 4-16) with a dysprosium (Table 4-14) shaping collar with Al-6061 (Table 4-3) and SS-304 sleeves. Argon/helium gas (Table 4-13) fills the test loop.

Table 4-12. Test Pin Fuel Composition.

Element	Atom Density (atoms/b-cm)
^{234}U	1.0756E-04
^{235}U	2.8582E-02
^{236}U	1.0664E-04
^{238}U	1.3865E-02
Zr	1.1619E-04
Nb	1.1408E-05
Mo	2.7171E-03
Ru	2.0555E-03
Rh	2.8839E-04
Pd	1.8924E-04
Total	4.8039E-02
Mass Density (g/cm^3)	17.6

Table 4-13. Argon Gas Composition.

Element	Atom Density (atoms/b-cm)
Ar	1.2232E-05
He	3.6696E-05
Total	4.8928E-05
Mass Density (g/cm^3)	1.0553E-03

Table 4-14. Dysprosium Composition.

Element	Atom Density (atoms/b-cm)
^{156}Dy	1.7744E-05
^{158}Dy	3.0101E-05
^{160}Dy	7.3796E-04
^{161}Dy	5.9851E-03
^{162}Dy	8.0719E-03
^{163}Dy	7.8884E-03
^{164}Dy	8.9543E-03
Total	3.1686E-02
Mass Density (g/cm^3)	8.55

Table 4-15. Stainless Steel - 304 Composition.

Element	Atom Density (atoms/b-cm)
C	1.4039E-04
N	1.7198E-04
Si	6.4327E-04
P	3.4997E-05
S	2.2537E-05
Cr	1.7141E-02
Mn	8.7694E-04
Fe	6.1038E-02
Ni	7.5927E-03
Total	8.7662E-02
Mass Density (g/cm^3)	8.00

Table 4-16. Stainless Steel - 316 Composition.

Element	Atom Density (atoms/b-cm)
C	1.6045E-04
N	1.7198E-04
Si	6.4327E-04
Cr	1.5751E-02
Mn	8.7694E-04
Fe	5.7798E-02
Ni	9.8499E-03
Mo	1.2551E-03
Total	8.6565E-02
Mass Density (g/cm^3)	8.00

4.1.2.6 Reflector

The reflector is comprised of CP-2 graphite the composition which is given in Table 4-6 and aluminum plates (Table 4-10).

4.1.2.7 Shielding

Concrete shielding surrounds the core. The composition is given in Table 4-17.

Table 4-17. Concrete Composition.

Element	Atom Density (atoms/b-cm)
Ca	2.6703E-03
Si	1.6504E-03
Al	1.1909E-03
Fe	1.7705E-02
Mg	1.2050E-03
S	5.0554E-05
K	2.1482E-05
Na	3.2649E-05
Mn	2.8526E-05
V	1.6202E-05
Cr	2.6628E-06
Ti	7.3481E-04
O	4.7215E-02
H	2.3615E-02
Total	9.6138E-02
Mass Density (g/cm^3)	3.36

4.1.2.8 Coolant

The reactor is air cooled with the composition in Table 4-18.

Table 4-18. Air Composition.

Element	Atom Density (atoms/b-cm)
N	3.8722E-05
O	1.0654E-05
Ar	2.3159E-07
C	9.4644E-09
He	1.2993E-10
H	4.9610E-07
Kr	2.8267E-11
Total	5.0114E-05
Mass Density (g/cm^3)	0.0012

4.1.3 Temperature Data

The benchmark model temperature is 293.6 K for all materials except the fuel which is 295 K.

4.1.4 Experimental and Benchmark-Model k_{eff} and / or Subcritical Parameters

The experimental k_{eff} was approximately unity with the critical position determined by the rod height. The 1σ standard deviation is derived and summarized in Section 3 for the experimental value. The bias and uncertainty were determined and summarized in Section 3.1.1 and Section 4.1.1. The benchmark k_{eff} value then shown in Table 4-19 with the total benchmark uncertainty is the uncertainty from the experiment with the bias uncertainty summed under quadrature.

Table 4-19. Experimental and Benchmark Eigenvalue, Bias, and Uncertainty.

Experimental			Bias			Benchmark		
k_{eff}	±	σ	Δk_{eff}	±	σ	k_{eff}	±	σ
1.00000	±	0.01296	-0.00070	±	0.00010	0.9993	±	0.0130

4.2 Benchmark-Model Specifications for Transient Measurements

4.2.1 Overview of the Experiment

The M2CAL transient 2580 experiment was conducted on September 21, 1984 at Idaho National Laboratory's TREAT Reactor as a part of partial energy wire trail transients. The experiment began with establishing the pre-transient (critical) conditions for M2CAL transient 2580 with an estimated power of 50W . The transient is then initiated by ejecting the transient rod T-2 following a pre-planned rod dynamic. The transient lasted approximately 10 seconds from initial rod withdrawal to shutdown. The rod ejection was equivalent to 1110 pcm of reactivity insertion. After the transient, the flux wire was cut into segments and measured for the fission rates per gram in each segment.

4.2.2 Geometry of the Experiment Configuration and Measurement Procedure

The steady-state geometry of the M2CAL experiment was used except for the replacement of the fuel pins by the flux wire inside the test vehicle. Information regarding the dimensions and material composition of the flux wire are included in Sections 4.2.4 and 4.2.5.

4.2.3 Description of the Benchmark Model Simplifications

The LLSS and the transient tests follow the same benchmark specifications outlined in Section 4.1.1. Other specifications and simplifications that pertain to the pre-transient and transient tests are noted below

- No heights were given for the top of wire, monitor wire holder or the dysprosium extra collar. These components except for the dysprosium extra collar were assumed to go to the top of the inside of the can and bottom of the neutronically equivalent section. The dysprosium extra collar goes to the top and bottom of the dysprosium sections outlined in Table 4-20.

- Initial Temperature Distribution

  The initial temperature distribution in the fuel was assumed to be homogenous, and has a constant value of 295 K. The reported initial temperature readings from the thermocouples outlined in Table 1.10.4-1 have only a difference of 2 K.

- The Fuel Density

  The density of the fuel was assumed to be constant throughout the transient process. Since the transient test is short, this assumption is reasonable.

- Boundary Conditions for the Heat Conduction Equation

The heat conduction equation is solved with Neumann boundary condition, where the temperature gradient at the core edge is set to zero. This assumption is reasonable since the temperature readings in the graphite reflector region near the periphery of the core (Thermocouples 1, 2, 3) experience a very small increase during the transient test.

- Heat Transfer Parameters

  Reference 19 provides a 4th order least squares fit for the specific heat capacity that spans a temperature range from 0 to 982 °C. However, this fit is not good at lower temperatures. A first order fit of the heat capacity is used for the range of temperatures relevant to Transient 2580. The linear fit spans a temperature range from 0 to 126.7 °C. Equation (4.2.3-1) is used to calculate the specific heat in J/(Kg K), where T is in Kelvins. The equation is derived from the fitting of digitized data from Figure 2-26.

$$C_p = -528.99369 + 4.03815 \times T \qquad (4.2.3\text{-}1)$$

  The equation is implemented such that the specific heat capacity of a certain mesh is dependent on the temperature of this mesh. The measured thermal conductivity of the Graphite-Urania Fuel in Figure 2-27 starts from 65 °C. No data on the thermal conductivity that covers the entire temperature range of Transient 2580 was found in any TREAT document. To represent the thermal conductivity of lower temperatures, the thermal conductivity was assumed to follow a 2nd order polynomial function. Temperatures starting from 22 °C were assumed to follow the same 2nd polynomial. This assumption is reasonable since the thermal conductivity at 22 °C is only 2.5% higher than that of 65 °C. The 2nd polynomial was implemented in a similar manner to that of the specific heat capacity. Equation (4.2.3-2) was derived from the fitting of digitized values from Figure 2-27, where K is in W/m-K and T is in Kelvins.

$$K = 28.20519 - 0.01988 \times T + 8.82446 \times 10^{-6} \times T^2 \qquad (4.2.3\text{-}2)$$

It is worth noting that the thermal properties of the reflector meshes were assumed to be the same as the fuel [36].

4.2.4 Dimensions

The dimensions of M2CAL 2580 Transient test are the same dimensions outlined in Section 4.1.2 except for the removal of fuel pins and the insertion of the flux wire in the experimental vehicle.

4.2.4.1 Experimental Components and Test Vehicle

The experiment is located in the middle of the core with the middle of the flux wire approximately located at the fuel centerline. The flux wire is 121.92 cm long and 0.076 cm in diameter. The wire is surrounded by a stainless steel sheath which was concentric with and ran the fuel region. The sheath is enclosed from the bottom by an end plug. The sheath had an inner diameter of 0.183 cm. The flux wire holder (diameter 1 inch) was surrounded with an extra dysprosium collar of thickness 0.0381 cm to prevent melting of the wire. No heights were given for the top of wire, monitor wire holder or the dysprosium extra collar. These components except for the dysprosium extra collar were assumed to go to the top of the inside of the can and bottom of the neutronically equivalent section. The dysprosium extra collar goes to the top and bottom of the dysprosium sections outlined in Figure 4-4 and Figure 4-5.

Dimensions for the flux wire setup are given below in Table 4-20. The dimensions of the flux wire setup are displayed below in Table 4-20. The setup of the experimental vehicle of the M2CAL irradiation transient 2580 is shown in Figure 4-4 and

Figure 4-5.

Table 4-20. Flux Wire and Surrounding Components Dimensions.

	OD (cm)	ID (cm)	Z-Location Bottom (cm)	Z-Location Top (cm)
Flux Wire	0.0762	---	-60.96	60.96
Stainless Steel Sheath	0.18288	0.24384	-61.595	62.23
Stainless Steel Wire Top	0.17018	---	60.96	136.04875
Endplug	0.17018	---	-60.69	-60.595
Monitor Wire Holder	2.54	2.2098	-101.6	136.04875
Dysprosium Collar	2.6162	2.54	-76.2	74.93

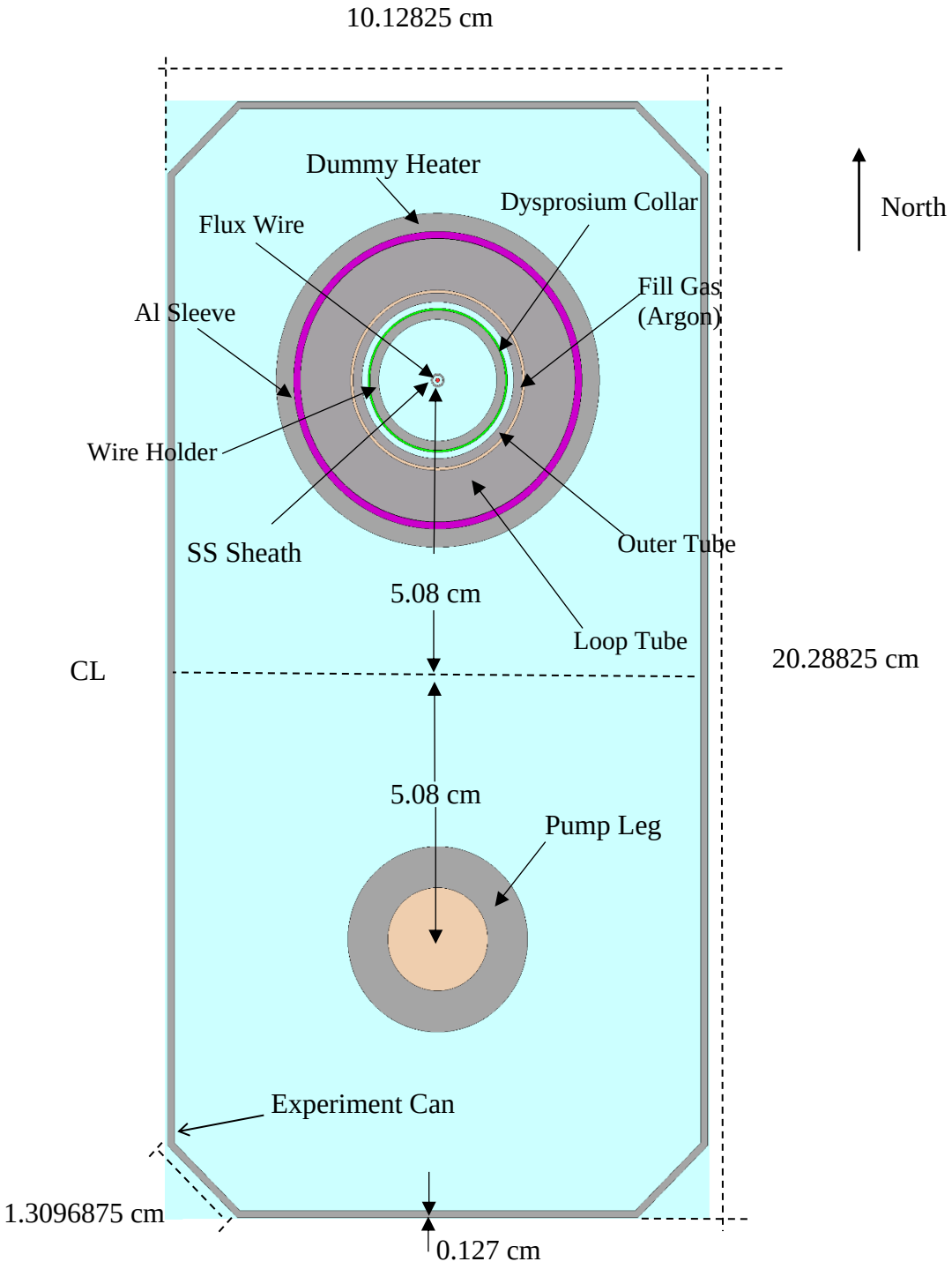

Figure 4-4. Experiment Cross Section with Experiment Can Dimensions.

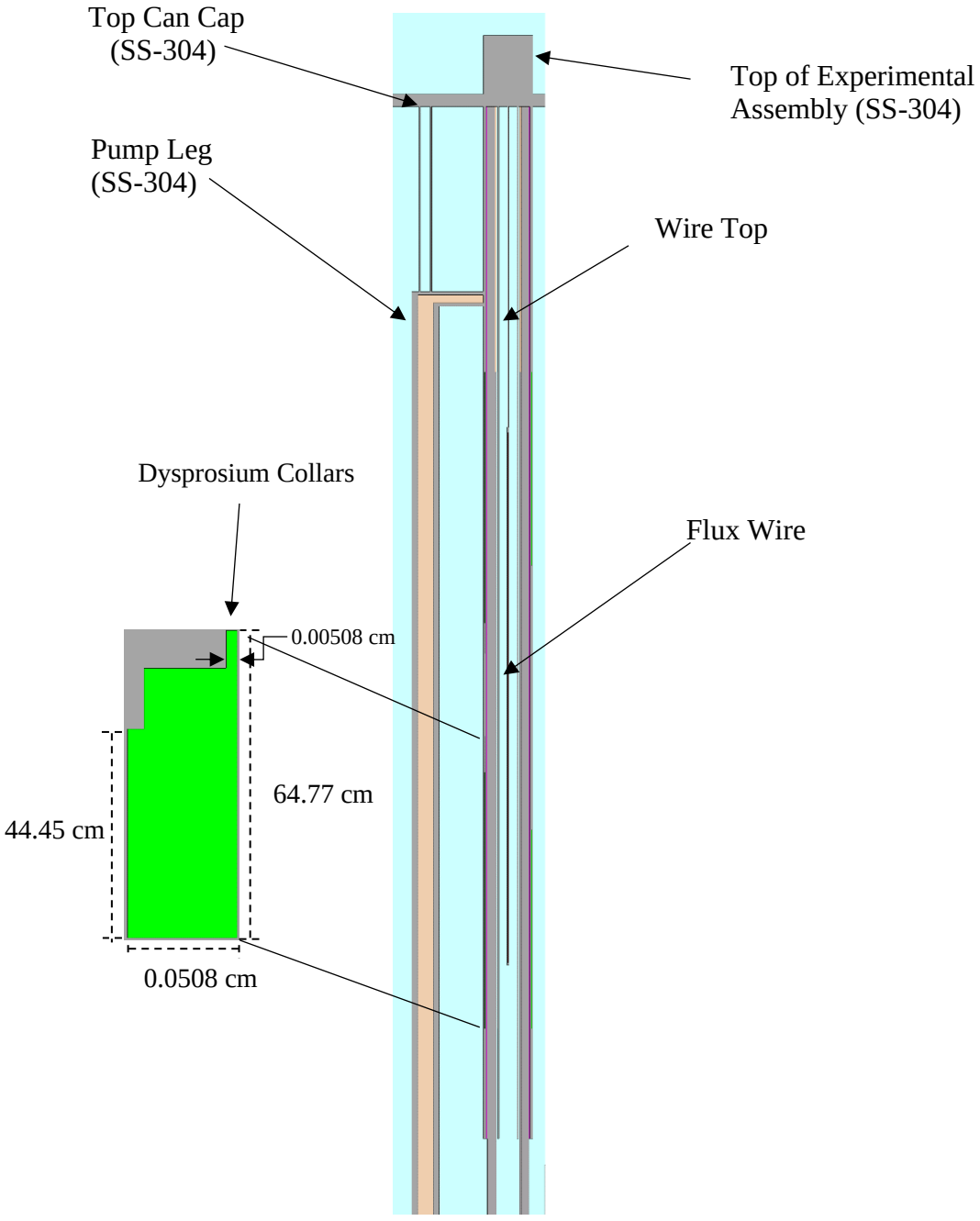

Figure 4-5. Experiment Cross Section.

4.2.5 Material Data

The material compositions used in the M2CAL transient 2580 test are similar to the compositions described in Section 4.1.2 except for the test pins. Additional Material information for the flux wire setup is included down below.

4.2.5.1 Experiment

The center of the 48 in. flux wire is located at the fuel centerline. The wire was made of a uranium-zirconium alloy (Table 4-21) , where the uranium is 3.6 wt% enriched to 93 wt% ^{235}U. The wire is enclosed in a stainless steel-316 sheath (Table 4-15), and is also connected to the experiment can by a stainless steel-316 pole. The opening of the sheath from the bottom is closed by a stainless steel-316 plug. This setup was enclosed in a stainless steel-316 wire holder (1 inch in diameter). The holder was surrounded by a dysprosium collar (Table 4-14) of thickness 0.0381 cm.

Table 4-21. Flux Wire Composition.

Element	Atom Density (atoms/b-cm)
^{234}U	2.46174E-9
^{235}U	5.98738E-4
^{238}U	4.44945E-5
Zr	4.44190E-02
Total	4.50622E-02
Mass Density (g/cm^3)	6.98

5 RESULTS

5.1.1 Results of Calculations of the Critical or Subcritical Configurations

Criticality calculations for the TREAT M2/M3CAL configuration were completed using the Serpent 2.1.29 Monte Carlo code. The benchmark model described in Section 4 was implemented in the code. This model used the ENDF/B-VII.1 neutron cross section data for all materials except for the graphite thermal scattering law, where the ENDF/B-VIII.0 S(α,β) was used [31] [32] [37]. In ENDF/B-VIII.0, graphite thermal scattering libraries are available for crystalline graphite, 10% porous reactor graphite, and 30% porous reactor graphite. Given the density of the TREAT graphite, the 30% porous reactor graphite library (tsl-reactor-graphite-30P.endf) was implemented.

Historically, calculated k_{eff} values for graphite moderated systems have generally been lower than experimental values when using the ENDF/B-VII.1 libraries. Examples include the HTR-PROTEUS configurations and the associated benchmarks [34]. The benchmark eigenvalues are consistently biased below the experimental values when calculated using the ENDF/B-VII.1 neutron cross sections. This benchmark also specifically cites the representation of the graphite as a possible contributor to the low eigenvalues. ENDF/B-VIII.0 addressed the graphite cross section by introducing new "reactor graphite" thermal scattering libraries. Reactor graphite exhibits a microstructure with a lower density than that of ideal graphite. In ENDF/B-VIII.0, the microstructural difference (and lower density) between reactor graphite and ideal graphite is represented as distributed porosity. Reactor graphite with a density less than 1.8 g/cm^3 is represented using the 30% porous graphite library.

Comparing the ENDF/B-VII.1 and ENDF/B-VIII.0 total graphite cross sections in Figure 5-1, significant improvement is seen in the ENDF/B-VIII.0 cross section when compared with experimental data. The introduction of the porosity increases the cross section, resulting in improved agreement with total cross

section measurements below the Bragg cutoff (incoming neutron energy less than 0.002 eV). Implementing these cross sections in the HTR-PROTEUS benchmark, showed marked improvement in the comparison of the calculated and benchmark eigenvalues as seen in Figure 5-2 [34].

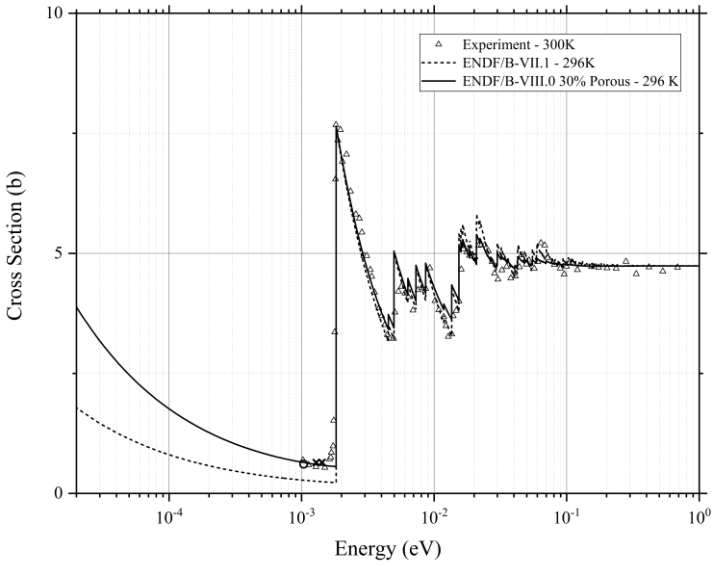

Figure 5-1. Graphite total thermal cross sections compared with experimental data [38]. The ENDF/B-VIII.0 30% porous graphite achieves best agreement with the experimental data as can be clearly seen in the region below 2 meV.

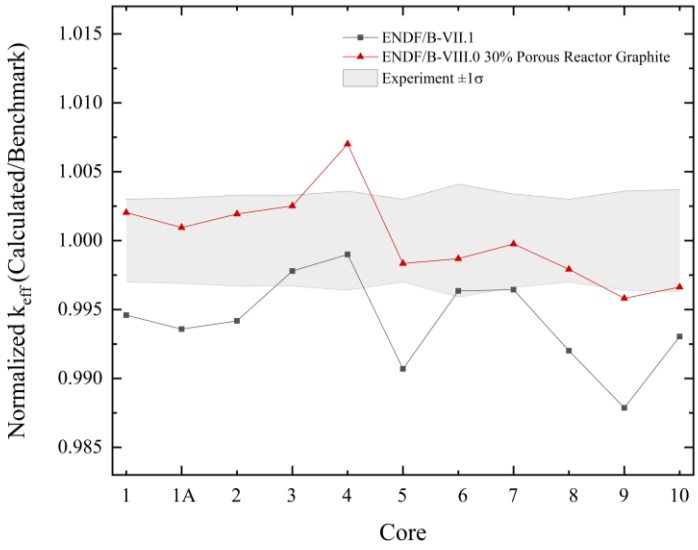

Figure 5-2. HTR-PROTEUS benchmark core configurations evaluated using the ENDF/B-VII.1 carbon and ENDF/B-VIII.0 30% porous "reactor graphite" thermal scattering cross sections. The ENDF/B-VII.1 libraries were used for the remaining materials. The average deviation of the calculated k_{eff} from the

benchmark value is ±300pcm when the ENDF/B-VIII.0 30% porosity library is used. For ENDF/B-VII.1, the average deviation is -660 pcm.

Based on the above, the 30% porous reactor graphite library was used in the modeling of TREAT. This corresponds to the best representation of the nuclear reactor graphite used in both the reflector and fuel regions of the core.

Monte Carlo calculations in Serpent were completed using 100,000 particle histories per cycle, 1500 active cycles, and 100 skipped cycles for a total of 150,000,000 neutron histories in the k_{eff} calculation. These run parameters resulted in converged source entropy. The calculated k-eigenvalue is given in Table 5-1. The calculated value for the TREAT reactor k_{eff} value is greater than the experiment by 2.49% when using the 30% porous graphite cross sections, but it is still within the 2σ limit of the benchmark.

Table 5-1. Benchmark Eigenvalues. The analysis is performed using a hydrogen content of 510 ppm and boron content of 7.53 ppm in TREAT fuel. The uncertainty in the benchmark k_{eff} was calculated as shown in Table 3-1.

Neutron Cross Section Libraries	Calculated* $k_{eff} \pm \sigma$	Benchmark $k_{eff} \pm \sigma$	(C-E)/E %	Difference (pcm)
ENDF/B-VII.1 with ENDF/B-VIII.0 30% porous graphite	1.02414 ± 0.00007	0.9993 ± 0.0130	2.49	2427

* Calculated k_{eff} standard deviation from Monte Carlo statistical error.

Possible sources of bias in TREAT simulations include the large uncertainty in the hydrogen content and the boron concentration. Regardless of the graphite thermal scattering library, these quantities result in calculated k_{eff} values that significantly deviate from the benchmark.

5.1.2 Temperature Coefficient Calculation

The temperature coefficient of reactivity was determined by calculating the eigen value at different core temperatures in the pre-transient settings. The reflector was assumed to have a constant temperature regardless of the core temperature. The calculated eigen values and their associated temperature are displayed in Table 5-2. A least squares fit was performed on the data in Table 5-2 to determine the temperature coefficient of reactivity. The uncertainty of the eigen values were propagated to determine the uncertainty in the temperature coefficient of reactivity. Figure 5-3 shows the trend line and the values calculated by the model.

Table 5-2. Core Eigen Values at Different Temperatures.

T (K)	$k_{eff} \pm \sigma$		
295	0.999998	±	0.000021
310	0.997274	±	0.000045
325	0.994378	±	0.000045
355	0.988427	±	0.000045
370	0.985209	±	0.000045
385	0.982972	±	0.000046

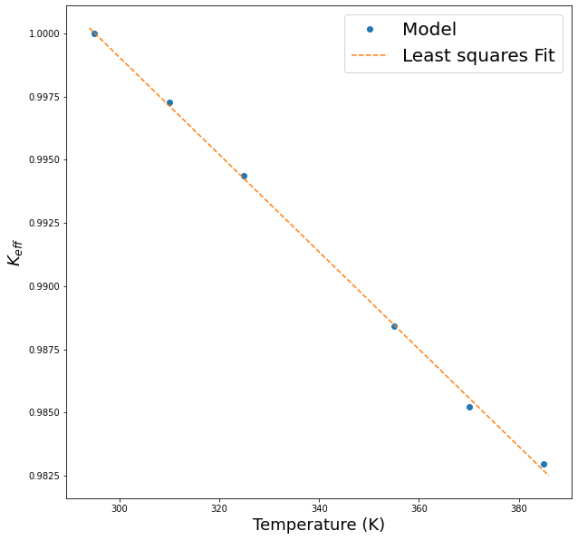

Figure 5-3. Core Eigen Values at Different Temperatures.

The parameters of the fit equation $k_{eff} = a \times T + b$ are displayed in Table 5-3. The calculated and the measured average temperature coefficient of reactivity are tabulated in Table 5-4.

Table 5-3. Least Squares Fit Parameters.

Parameter	Value± σ		
a	0.0001926	±	4.353E-7
b	1.0568	±	7.822E-6

Table 5-4. Average Temperature Coefficient of Reactivity for Model and Experiment.

Calculated α_T± σ δk/k per °C	Benchmark α_T± σ δk/k per °C	(C-E)/E %
-(1.926±0.004) ×10^{-4}	-(1.8±0.25) ×10^{-4}	6.66

5.2 Results of Kinetics Parameter Calculations

5.2.1 Prompt Neutron Lifetime Calculation

The benchmark model was executed in steady-state to determine the prompt neutron lifetime. Using the Iterated Fission Probability method (IFP) implemented in Serpent, the Adjoint weighted prompt neutron lifetime was calculated. The results are shown in Table 5-5.

Table 5-5. Experiment and Model Results for the Prompt Neutron Lifetime.

Calculated (s) l_p± σ	Experiment (s) l_p± σ	(C-E)/E %	Difference (s)
$9.58759 \times 10^{-4} \pm 3.3 \times 10^{-7}$	$(9.0 \pm 0.39) \times 10^{-4}$	6.528	0.587×10^{-4}

5.2.2 Delayed Neutron Parameters Calculations

The effective delayed neutron fraction and decay constants of the benchmark model were calculated using the Meulekamp's method implemented in Serpent at steady state and are shown in Table 5-6 and Table 5-7.

Table 5-6. Experiment and Model Results for the Effective Delayed Neutron Fraction.

Precursor	Calculated $\beta_{i,eff} \pm \sigma$	Experiment $\beta_{i,eff} \pm \sigma$	(C-E)/E %
1	$0.000241 \pm 1.27 \times 10^{-6}$	$0.000244 \pm 1.19 \times 10^{-5}$	-1.230
2	$0.00124 \pm 1.71 \times 10^{-6}$	$0.001567 \pm 2.95 \times 10^{-5}$	-20.868
3	$0.00119 \pm 2.89 \times 10^{-6}$	$0.001411 \pm 2.74 \times 10^{-5}$	-15.663
4	$0.00265 \pm 2.81 \times 10^{-6}$	$0.002828 \pm 1.41 \times 10^{-4}$	-6.294
5	$0.00109 \pm 2.67 \times 10^{-6}$	$0.000826 \pm 2.10 \times 10^{-5}$	31.961
6	$0.000451 \pm 1.73 \times 10^{-6}$	$0.000302\ 1.68 \times 10^{-5}$	49.338
β_{eff}	$0.006867 \pm 6.71 \times 10^{-6}$	$0.007178 \pm 4.21 \times 10^{-4}$	-4.333

Table 5-7. Experiment and Model Results for the Decay Constants.

Precursor	Calculated (sec^{-1}) $\lambda_i \pm \sigma$	Experiment (sec^{-1}) $\lambda_i \pm \sigma$	(C-E)/E %
1	$0.0133 \pm 4.79 \times 10^{-9}$	$0.0124 \pm 4.86 \times 10^{-4}$	7.25
2	$0.0327 \pm 1.54 \times 10^{-8}$	$0.0305 \pm 1.45 \times 10^{-4}$	7.21
3	$0.121 \pm 3.39 \times 10^{-8}$	$0.1118 \pm 5.77 \times 10^{-4}$	8.22
4	$0.3027 \pm 1.51 \times 10^{-7}$	0.301 ± 0.016	0.564
5	$0.8494 \pm 1.19 \times 10^{-6}$	1.13 ± 0.17	-24.83
6	$2.8530 \pm 2.74 \times 10^{-6}$	3 ± 0.37	-4.9

5.3 Results of Power Distribution Calculations

5.3.1 Flux Wire Axial Power Distribution Calculation

The power profile of the flux wire was calculated in Serpent at steady state conditions, following the power and control rod settings described in Section 2.4.1. The fission rates inside the wire segments were calculated using Super-imposed track-length detectors (dtl) in Serpent. The wire was divided into cylindrical surfaces following the experimental cuts described in Section 2.4.1. The fission rates per gram were then normalized relative to the highest fission rate per gram value. The axial relative activity profile for the flux wire is plotted in Figure 5-4.

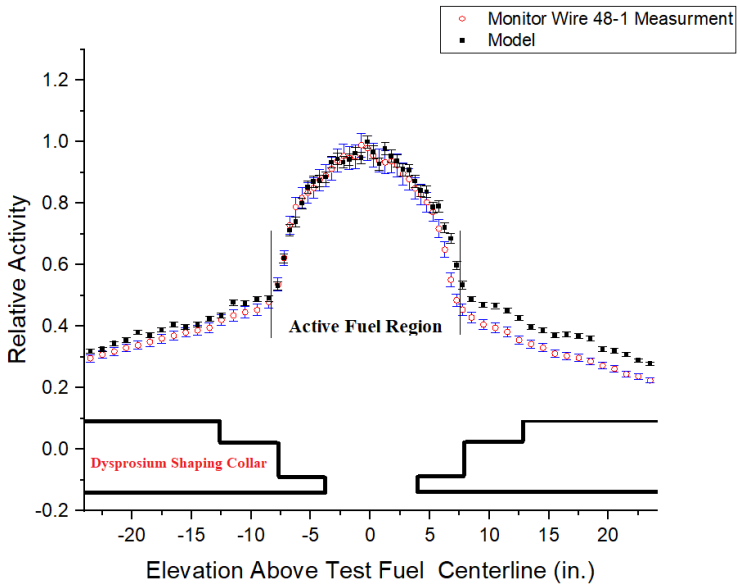

Figure 5-4. Axial Relative Activity for the Model and the Experiment along the Flux Wire.

The axial power profile for the model in the upper section appears to be overestimated. This could be explained by the wrong normalization process discussed in Section 3.5.3.2.

5.4 Results of Calculations for Transient Measurements

5.4.1 Steps of Transient Modeling

The transient simulation in Serpent starts by acquiring live neutron and delayed neutron precursor distributions, determined in a criticality source simulation. The dynamic simulation tracks these distributions through space and time. The transient simulation is divided into time steps, where population control is applied to the neutron and precursor populations at the end of each interval. To determine the live neutron source for the next transient calculation, Serpent saves neutrons at tentative collision sites with a user-defined probability, where their locations, direction cosines, energy and weight are stored. Geometry transformation in the dynamic mode (e.g. control rod ejection) is allowed and updated at the end of each time interval based on the defined kinematics [39].

In order to accurately capture temperature feedback in TREAT, Serpent was coupled with the finite volume, open source computational fluid dynamic code OpenFOAM [40]. The transient simulation starts in Serpent by generating source neutrons and precursors distribution and tracking the evolution of the neutron population at each step of 0.05 sec. The neutron distribution in the core is normalized to a volumetric power distribution which is sent to OpenFOAM to calculate the temperature distribution by solving the heat conduction equation. In OpenFOAM, the reactor core is divided into fine volumetric meshes.

The time dependent simulation process begins with determining the source neutron and precursor distributions through a critical k-eigenvalue calculation in Serpent. The neutron and precursor distributions files are the time zero input for the time dependent simulation. The dynamic simulation mode in Serpent allows for running external source simulations in sub- and super critical systems over extended period of times, while keeping the neutron population within reasonable limits. This method is based on a sequential population control [41]. The dynamic simulation is divided into time intervals of 0.05 s to capture the reported experimental power measurements. At the end of each time step, Serpent calculates the integral fission power for each mesh volume, where it is transferred by a file sharing system and a python script to OpenFOAM. The temperature gradient for each time step is calculated in OpenFOAM using the "laplacianfoam" solver, which was modified to include a source term. The laplacianfoam solver solves Equation (5-1) to determine the temperature distribution across the core. The time scheme implemented in OpenFOAM is the Euler implicit time scheme with a Δt of 0.005 s. In this scheme, OpenFOAM receives the power distribution at the end of the time step and uses it to calculate the temperature distributions from the beginning to the end of the time step.

$$\frac{\partial T}{\partial t} - \frac{1}{\rho C_p}\nabla(K\nabla T) = \frac{q}{\rho C_p} \tag{5-1}$$

Where T is temperature [K], k is the thermal conductivity [W/m/K], ρ is the density [Kg/m^3], C_p is specific heat [J/kg/K] and q is the power output from Serpent [W/m^3]. The workflow of the coupled Serpent/OpenFOAM is shown in Figure 5-5.

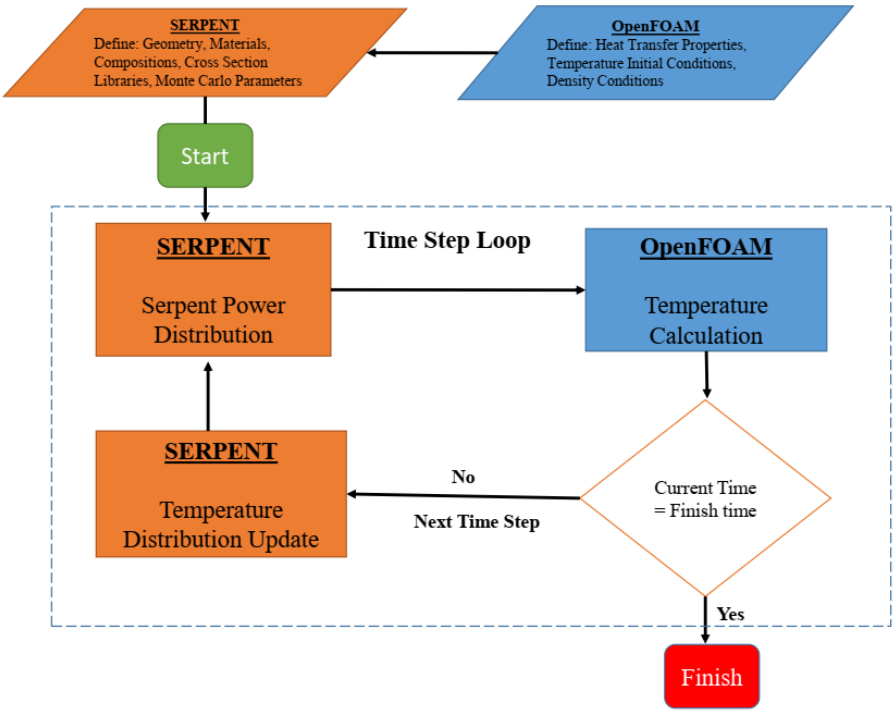

Figure 5-5. Flow chart of coupled Serpent-OpenFOAM system [42].

5.4.2 Description of Modeling Assumptions and Simplifications

- Control Rod Movement

  The control rod movement in Serpent is not continuous within a time step. However, the step insertion or ejection is realized at the end of the time step. This simplification is justified, since the time increment for the rod movement is 0.05 s. Moreover, the reported control rod movements follow the same time increments.

- Transient Rod T-1 Movement

For most of the transient, the rod kinematics of T-1 was not changed in Serpent. During most of the transient, T-1 is effectively constant, where the highest deviation is around 0.027 inch. The reactivity increase from 8 inch to 9 inch was calculated to be 90 pcm. The fluctuation of T-1 would account for only a fluctuation in reactivity by less than 2.5 pcm.

- Thermal Scattering Interpolation

  The temperature effects in Serpent are treated using an interpolation scheme for thermal bound scattering and on-the-fly target motion sampling for the free atom cross sections. Target motion sampling introduces Doppler broadening effects in the cross section by determining the thermal motion of the target nucleus by sampling a temperature-dependent Maxwell-Boltzmann velocity distribution.

- Meshing in OpenFOAM

  The temperature distribution was calculated in OpenFOAM for a 6174 cubic mesh, whose size is approximately 10×10×10 cm. An additional 10.16 cm of the reflector graphite on the top, bottom and sides was added in the mesh. In the early stages of establishing the coupling scheme between OpenFOAM and Serpent, the mesh size was tested for convergence and was shown to converge.

- Cooling Channels

  The cooling channels were not included in the meshing process within OpenFOAM. Due to the small volume of these channels, the number of meshes would increase several orders of magnitude to reliably include them in the model. Since transient 2580 is a short test, the heating in the core was assumed to follow an adiabatic process. The OpenFOAM representation of the core is considered a solid cube with the core elements coarsely meshed.

- Flux Wire Activity Measurement

  The cutting of the flux wire segments in the LLSS wire irradiation followed the reported experimental procedures outlined in Section 2.4.1. However, the same approach for the transient would require excessive computation cost to attain an uncertainty lower than 2% for the number of

fissions in each segment. To reduce transient runtime while attaining good statistics, the flux wire was divided into 16 segments, where the first and last 16 in of the wire was cut into 4 in long segments. The middle 16 in segment was cut into 2 in long segments. This simplification was tested in steady-state, and found to be a reasonable assumption as can be seen in Figure 5-6. The experimental power profile of 48-1 wire was collapsed into 16 segments and compared to a collapsed 64 segments measurement in LLSS and a 16 segments measurement in LLSS. Based on Figure 5-6, no significant difference between the collapsed segments of the model and the 16 calculated segments by the model.

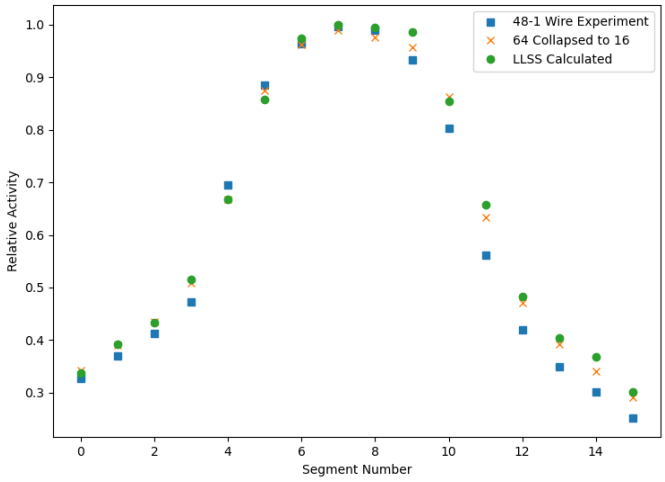

Figure 5-6. Collapse of 64 Segments to 16 segments (LLSS) After Renormalization.

5.4.3 Transient Observable Calculations

5.4.3.1 Pre-Transient Core Composition Determination

Prior to the start of the transient process, the core must be critical to ensure the stability of the power trace. To this end, the core composition is set such that the core becomes critical, and the control rod worth is comparable to the experimental worth. Based on the steady-state benchmark analysis of the M2-CAL experiment, the parameters that have a significant impact on criticality are only considered. It is evident

from Table 5-8 that the boron and hydrogen impurities and the uranium content have the largest uncertainties. They contribute, alone, more than 98.7% of the total uncertainty in k_{eff}. The total uncertainty in k_{eff} was estimated to be 0.01296.

Table 5-8. Summary of Evaluated Impacts from the ±1σ Variation of Parameters within TREAT M2/M3-CAL.

Perturbed Parameter	Parameter Value	±1σ Uncertainty	Δk_{eff} (±1σ)
Fuel B Content (ppm)	7.53	1.16	-0.00988
Fuel H Content (ppm)	510	266	0.00795
CP-2 Graphite Density (g/cm^3)	1.6700	0.0255	0.00140
Fuel Eu Content (ppm)	0.10	0.06	-0.00023
Fuel Gd Content (ppm)	0.10	0.06	-0.00162
Fuel Sm Content (ppm)	0.50	0.29	-0.00228
Fuel U-mass Content (wt%)	0.211	0.004	0.00161

The next step is to put constraints on the ranges of core compositions that lead to a near-critical core. Firstly, the poison traces (Eu, Gd, Sm) will not be considered in this analysis since their content is below the limit of detection. Several steady state cases were executed to determine the ranges of boron, hydrogen and uranium that could lead to a near-critical state. The k_{eff} values of a 3D grid that represents the parameters was constructed and shown in Figure 5-7. The new ranges for hydrogen and boron were determined and displayed in Table 5-9 . The uranium content was found to be close to the range prescribed in Table 5-8. The mean and standard deviation values in Table 5-9 were determined by assuming a flat distribution.

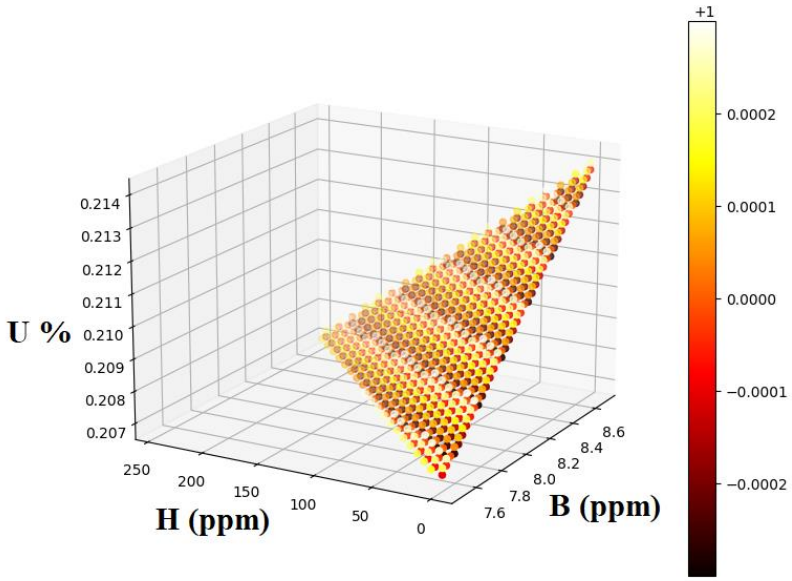

Figure 5-7. Near-Critical Surface Plot for Boron, Hydrogen and Uranium Ranges. The legend represents k_{eff}.

Table 5-9. New Constraints on the Concentrations of Hydrogen and Boron.

Parameter	Lower Value	Upper Value	Mean	±1σ Uncertainty
Fuel B Content (ppm)	7.5	8.69	8.095	0.3435
Fuel H Content (ppm)	0	275	137.5	79.3856

The optimal core composition of boron, hydrogen and uranium was determined by calculating the centroid of the triangle in Figure 5-7. The centroid coordinates were found to be B = 8.293 pp, H = 91.66 ppm, and U = 0.2093%. Based on these values, the core is not exactly critical. Minor adjustment had to be made to reach criticality. The core becomes critical at B = 8.313 ppm, H = 73 ppm, and U= 0.2096%. The integral rod worth at 16 in. was calculated and was found to be only 18 pcm higher than the reported experimental value. The eigen value at steady state was calculated using 450,000 neutrons over 4000 cycle with 350 skipped cycles to ensure the convergence of the fission source. The eigenvalue of the core was found to be $1.00004 \pm 2.1 \times 10^{-5}$.

5.4.3.2 Transient Power Calculation

The total power of the TREAT core was calculated at each 0.05 s throughout the dynamic simulation. The power was calculated in Serpent using 9,100,000 neutrons distributed on 60 batch, where the number of histories per batch was 50,555. A mean experimental power trace was calculated by calculating an average value under the assumption that the difference between Safety # 1 and Safety # 2 measurements represents a 4σ of a flat distribution. The evolution of the experimental power and calculated power traces is shown in Figure 5-8, Figure 5-9 and Figure 5-10. The energy produced by the core throughout the transient for the model and the experiment are compared in Figure 5-11. The final energy measured by the Integral Power # 1 was 205.7 MJ compared to 176.97 MJ measured by the Integral Power # 2. The final core energy of the model was compared to the experimental measurement in Table 5-10.

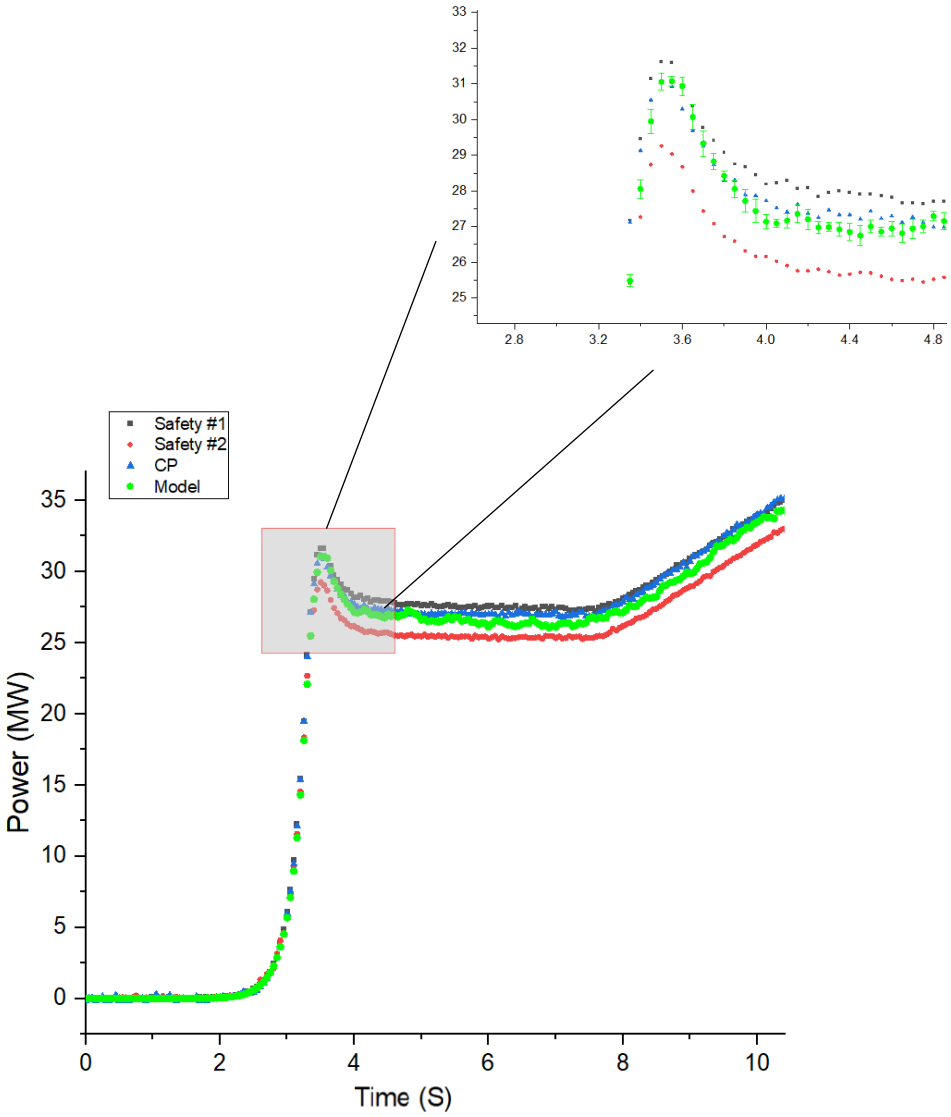

Figure 5-8. Experimental and Model Linear Power

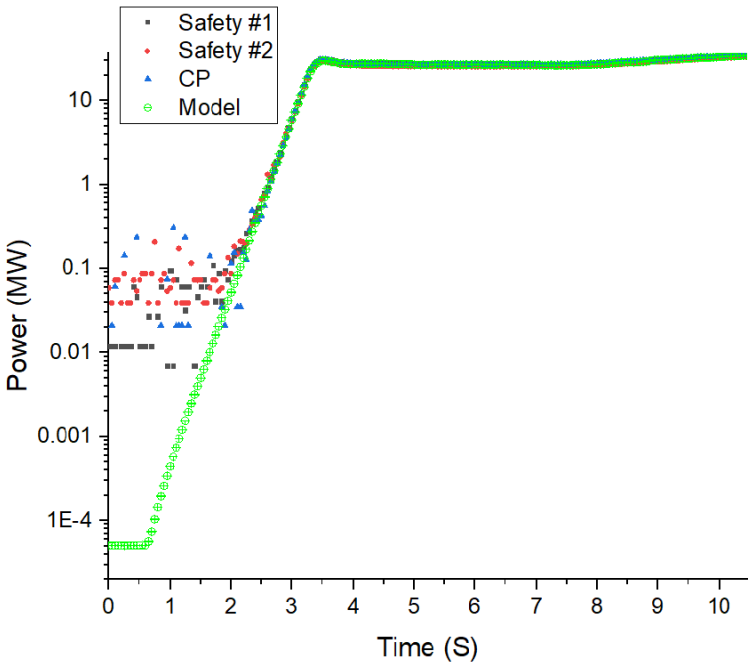

Figure 5-9. Experimental and Model Logarithmic Power.

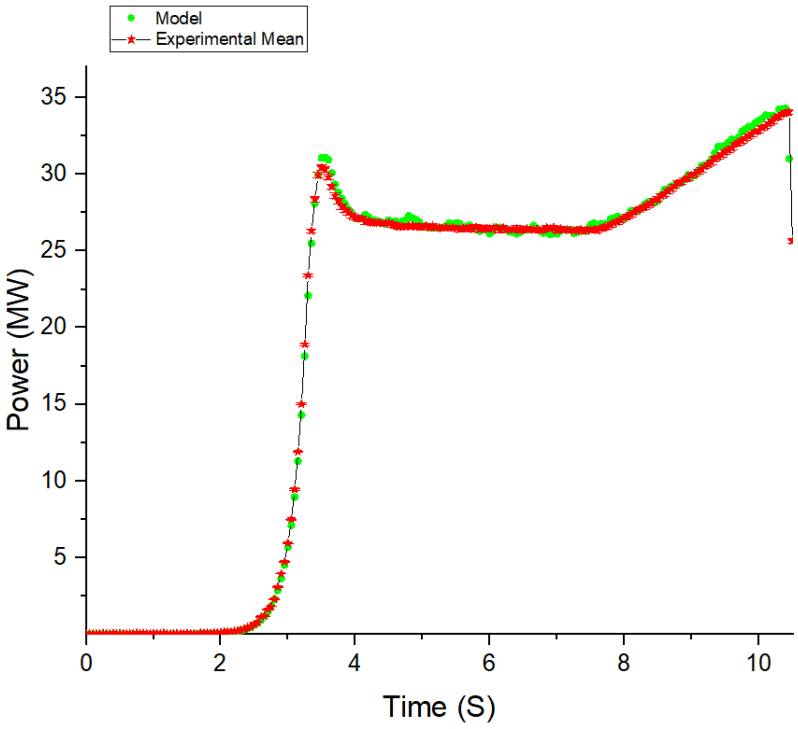

Figure 5-10. Experimental Mean Trace versus the Calculated Trace.

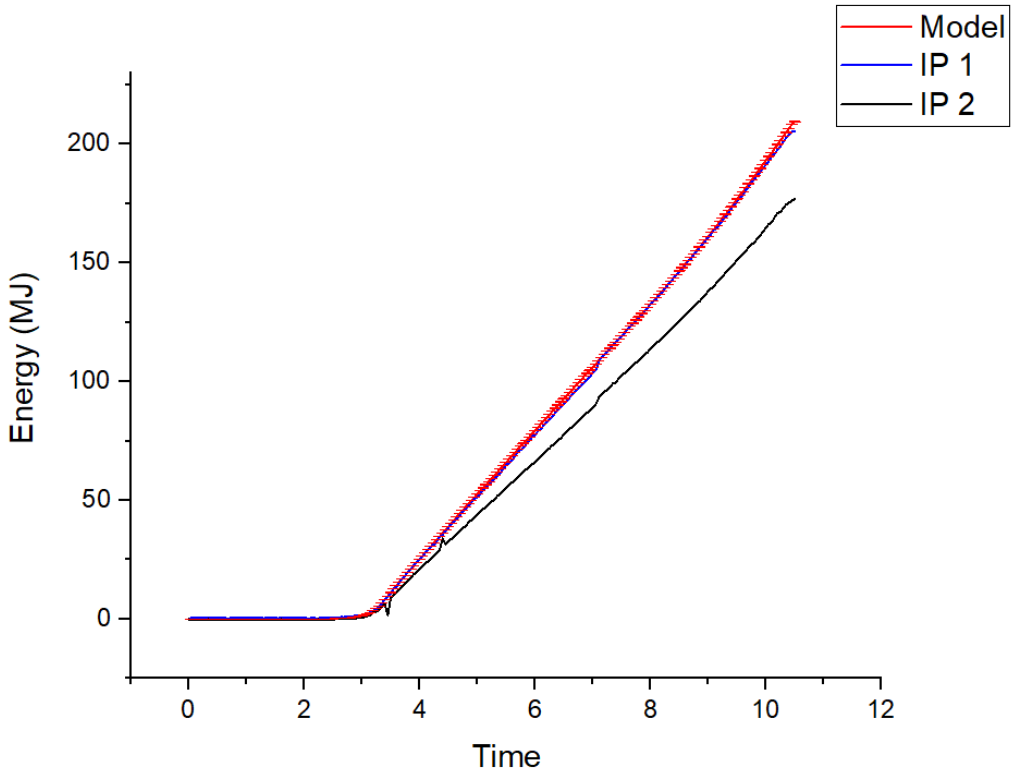

Figure 5-11. Core Energy as a Function of Time for the Model and the Experiment.

Table 5-10. Benchmark and Model Final Core Energy.

Calculated Energy ± σ (MJ)	Benchmark Energy± σ (MJ)	(C-E)/E %
209.542 ± 0.07	205.7 ± 4.1	1.8

Power Ramp

The power ramp, starting after 7.8 seconds, was simulated 4 times with different random seeds. The traces of the 4 runs are shown in Figure 5-12 along with the experimental and the benchmark traces. A weighted average trace (Figure 5-13) was computed taking into consideration the uncertainties of data points, where more weight is assigned to lower uncertainty values. The uncertainties of the mean trace were calculated using the weighted standard deviation formula. The mean trace was calculated to investigate the deviation

of transient runs with different random seeds and compare them to the benchmark trace as can be seen in Table 5-11. The ramp rate for the experimental traces were calculated in displayed in Table 5-12. The Experimental power ramp rate is compared to the model power ramp rate in Table 5-13.

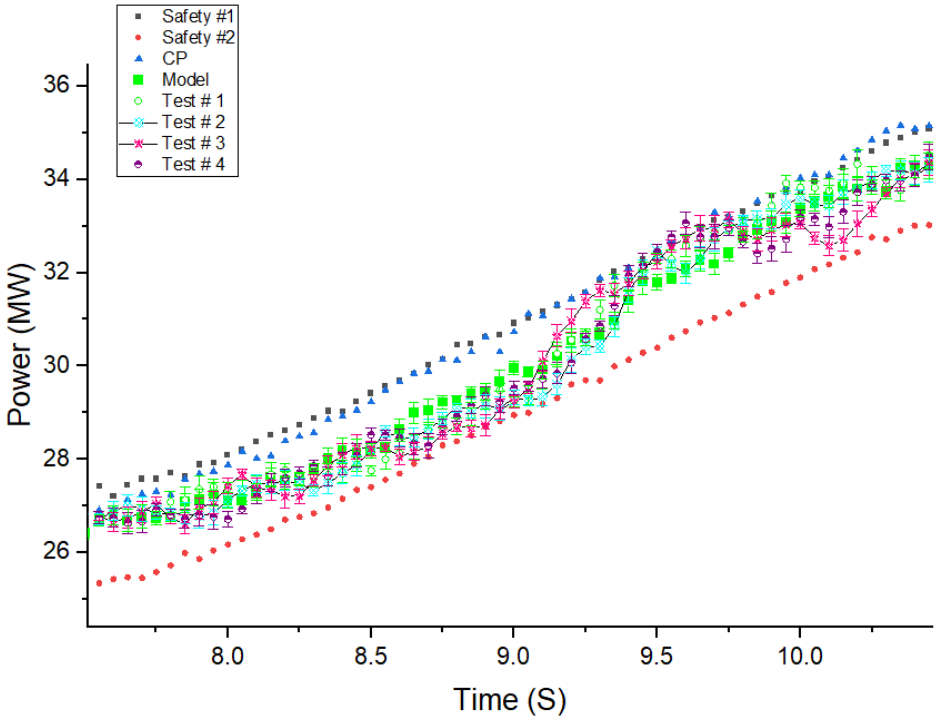

Figure 5-12. The Traces of the Power Ramp using Different Random Number Seeds.

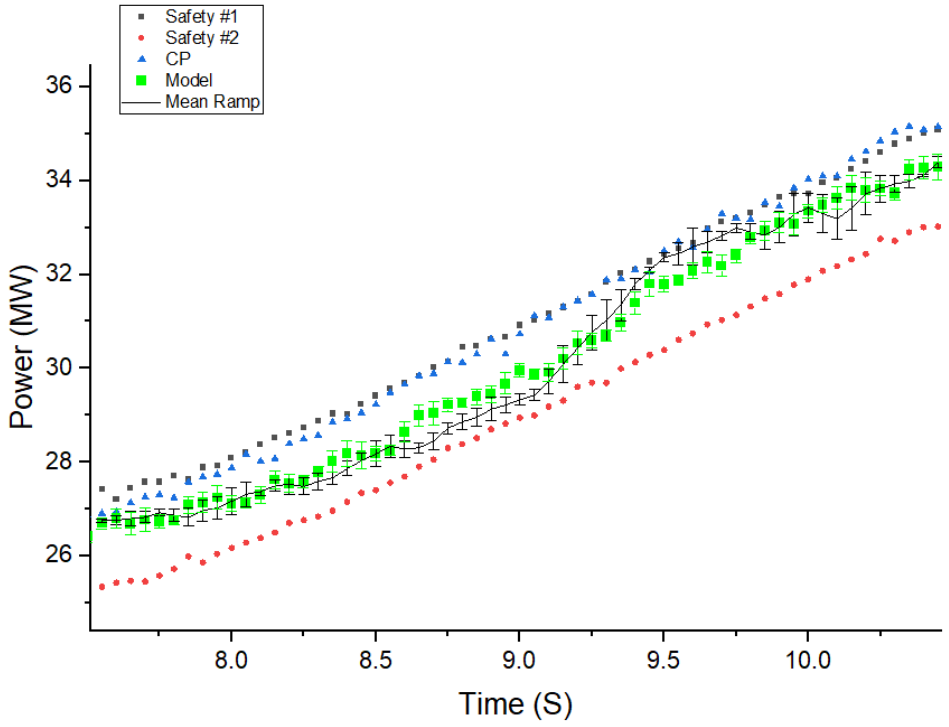

Figure 5-13. The Mean Trace Compared to the Model and the Experimental Traces

Table 5-11. Power Ramp Rates at Different Random Number Seeds.

Test Name	Run 1 (MW/s)	Run 2 (MW/s)	Run 3 (MW/s)	Run 4 (MW/s)	Mean Trace (MW/s)	Model (MW/s)
Ramp Rate	3.234±0.03	3.023±0.02	2.865±0.02	2.989±0.02	3.004 ± 0.02	2.917± 0.025

Table 5-12. Power Ramp Rates for the Experimental Traces.

Detector	Safety # 1 (MW/s)	Safety # 2 (MW/s)	CP (MW/s)	Experimental Mean (MW/s)
Ramp Rate	2.968	2.958	3.145	3.024 ± 0.086

Table 5-13. Comparison between the Experimental and Benchmark Power Ramp Rates.

Calculated Ramp Rate± σ (MW/s)	Benchmark Ramp Rate ± σ (MW/s)	(C-E)/E %
2.917 ± 0.025	3.024 ± 0.086	-3.53

5.4.3.3 Reactor Period Calculation

The stable period in the first 2 s was calculated by taking the average period between 3 power readings in time shown in Table 5-14. These readings were chosen to be as close as possible to the time intervals of the experimental procedure. Though, the power is not increasing by exactly a factor of 10. Equation (5-2) was slightly modified to include the power readings. The values of the period for the experiment and the model are compared in Table 5-16.

Table 5-14. Power Readings for Period Calculation.

Time (s)	Power ± σ (MW)
0.9	2.5907E-4 ±1.5285E-6
1.35	2.4800E-3 ± 1.4432E-5
1.85	2.5880E-2 ±1.5217E-4

$$Period = \frac{t_2 - t_1}{\ln(\frac{Power_2}{Power_1})} \tag{5-2}$$

Table 5-15. Reactor Period Calculations.

Time Range (s)	Period ± σ (s)
0.9 – 1.35	0.1992 ± 0.0092
1.35 – 1.85	0.2132 ± 0.0057
Average Period	0.2062 ± 0.00541

Table 5-16. Reactor Period for the Benchmark and the Model.

Calculated Period ± σ (s)	Benchmark Period (s)	(C-E)/E %
0.2062 ± 0.00541	0.209 ± 0.012	-1.34

5.4.3.4 *Transient Rod Worth Calculation*

The worth of transient rod T-2 was measured by incrementally pulling out the rod by 1 inch and measuring the change in k_{eff}. The experimental and calculated differential worth of the T-2 within transient 2580 rod movement is in Figure 5-14. The integral worth for T-2 was also calculated and compared to the experimental measurement in in Figure 5-15. The value of the integral worth reported at 16 inch is 1.111%, contrasted with 1.128% calculated by the model.

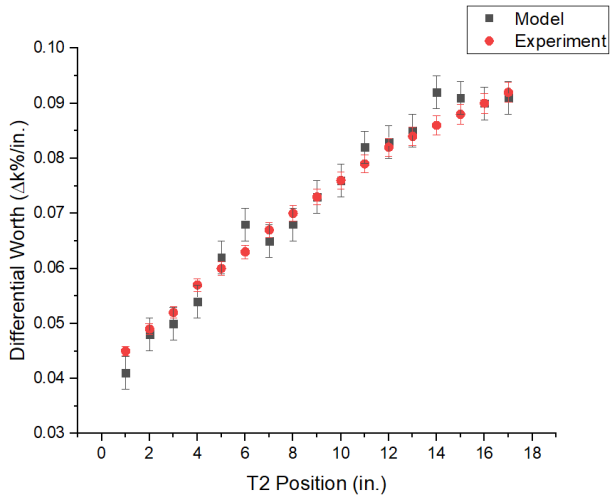

Figure 5-14. The Experimental and Calculated Differential Worth of T-2.

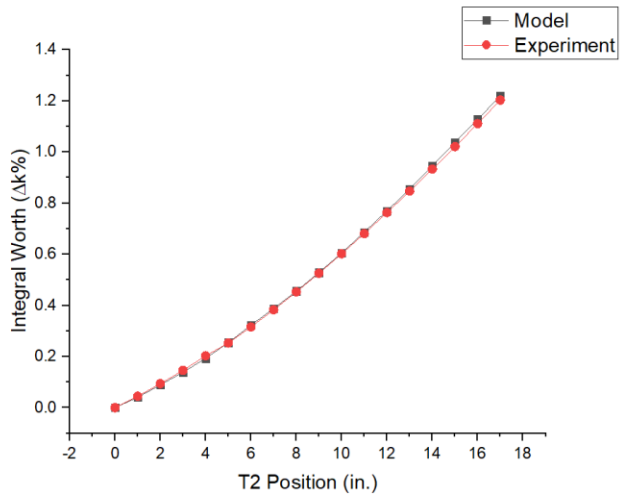

Figure 5-15. Experimental and Calculated Integral Worth of T-2.

5.4.4 Temperature Calculations

The temperature distribution throughout time was calculated by solving the heat equation in OpenFOAM. The average and maximum temperatures throughout the transient are shown in Figure 5-16. The evolution of the temperature field at the midplane of the x-y projection of the core is shown in Figure 5-17. The maximum temperature at the end of the transient for the model and the experiment are compared in Table 5-17.

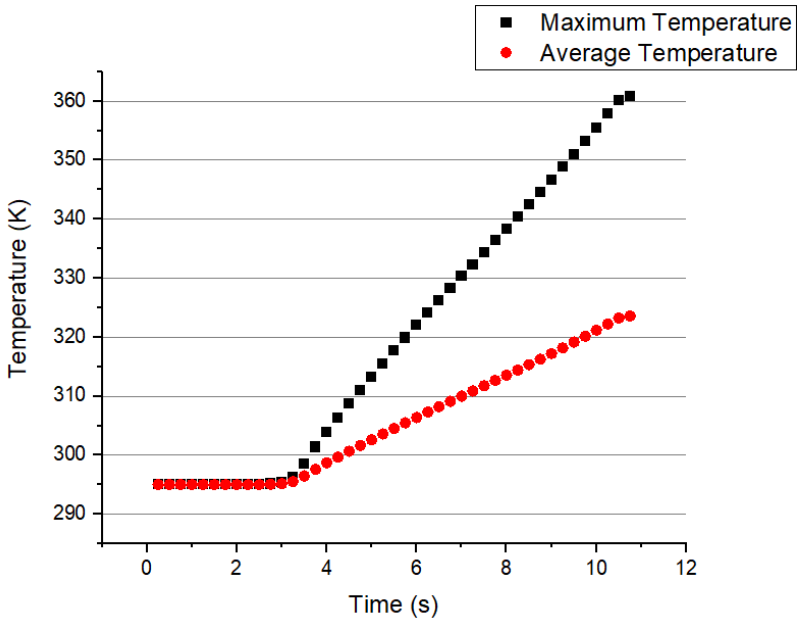

Figure 5-16. Calculated Average and Maximum Temperatures throughout the Transient.

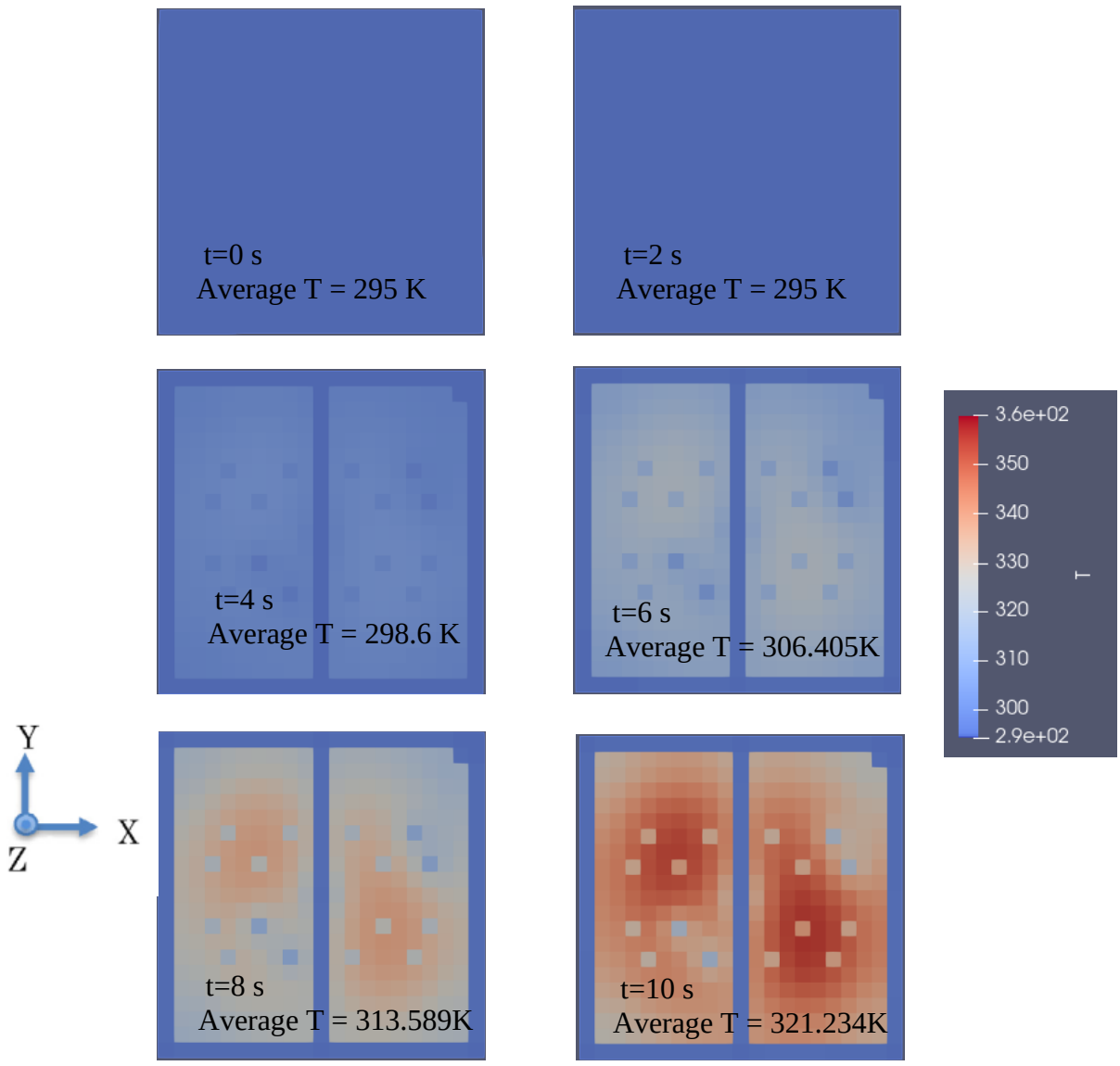

Figure 5-17. Evolution of Temperature Fields during the Transient.

Table 5-17. Comparison between the Maximum Temperatures of the Model and the Experiment at the End of the Transient.

Calculated T (K)	Benchmark T (K)	Difference T (K)	(C-E)/E %
360.79	354 ± 3.5	6.79	1.9

5.4.5 Additional Calculations Relevant to the Transient

5.4.5.1 Axial Power Distribution Calculation in the Flux Wire

The number of segments in the wire was reduced to 16, where the right and left 16 in. segments have 4 segments each. The middle 16 in. segment was cut into 2 in. long segments. The experimental wire irradiation measurement in transient 2580 test was also reduced to 16 segments. The fission rates within the segments were aggregated throughout the transient, and the total fission per gram in each segment was determined. The axial fission rate profile was normalized according to its maximum point and compared to the measured relative activity of the reduced segments and plotted in Figure 5-18. This calculation was performed with core composition of 0.211% of uranium, 50 ppm of hydrogen and 8.445 ppm of boron.

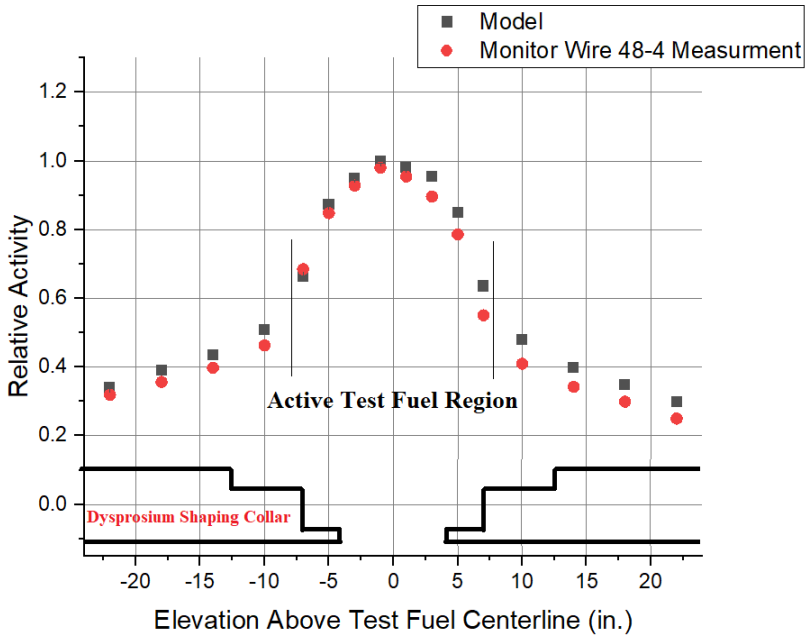

Figure 5-18. Experimental and Calculated Relative Activity of the 48-4 Wire.

5.4.5.2 Transient Coupling Factors Calculation

The power coupling factor PCF in LLSS was calculated using Equation (5-3) and substituting by the fission rate per gram of one of the segments close to the center of the wire where the fission rate per gram is

maximum. The PCF is 0.412 ± 0.0088 at a power level of 90 KW. The calculated and Experimental PCFs are compared in Table 5-18.

$$PCF = \frac{\frac{\#\,Fissions\,in\,Wire}{grams} \times 2.86 \times 10^{-11} \frac{J}{Fission}}{Total\,TREAT\,Energy\,(MJ)} \tag{5-3}$$

Table 5-18. Calculated and Experimental PCF for 48-1 Wire Irradiation.

Calculated PCF± σ	Benchmark PCF ± σ	(C-E)/E %
0.412 ± 0.008	0.492 ± 0.065	-16

The PCF was also calculated in transient by assigning a super-imposed track-length detector that covers approximately 7 inches, 3.5 inches in both the upper and lower sections of the flux wire measured from the center of the wire. A comparison between the experimental and calculated transient PCFs is highlighted in Table 5-19.

Table 5-19. Experimental and Calculated PCF for 48-4 Wire Irradiation.

Calculated PCF± σ	Benchmark PCF ± σ	(C-E)/E %
0.379 ± 0.001	0.4262 ± 0.0564	-10.9

The TCF was calculated according to Equation (5-4) to be 0.903 ± 0.024. The calculated and experimental TCFs are compared in Table 5-20.

$$TCF = \frac{PCF_{Transient}}{PCF_{LLSS}} \tag{5-4}$$

Table 5-20. Calculated and Experimental TCF for Transient 2580.

Calculated TCF± σ	Benchmark TCF ± σ	(C-E)/E %
0.921 ± 0.017	0.87 ± 0.16	5.8

The power coupling factors for the steady-state and transient irradiations deviate from the experimental values. One reason is the large uncertainty in the hydrogen content. The fission rates in the active fuel region were calculated at nominal core and ± σ_H concentrations in Figure 5-19. The difference in fission rates in the segments ranges from 3-10% in the active fuel region where the PCF is determined. It is evident that a decreasing hydrogen concentration leads to an asymmetric and skewed axial power profile. The effects of other core parameters were previously highlighted in Table 3-12. The change in fission rates inside the segments could be caused by a spectral shift in the neutron spectrum streaming from the core to the flux wire or an increase in flux magnitude due to the decrease in the moderator-to -fuel ratio in the core. The neutron spectrum inside the active fuel segments was investigated at the nominal and ± σ_H concentrations. Figure 5-20 shows an increase in flux magnitude in the thermal region as the hydrogen concentration increases. No noticeable spectral shift can be concluded from Figure 5-20. The average neutron energy in the thermal region was calculated for each case and were found to be the same within 1%.

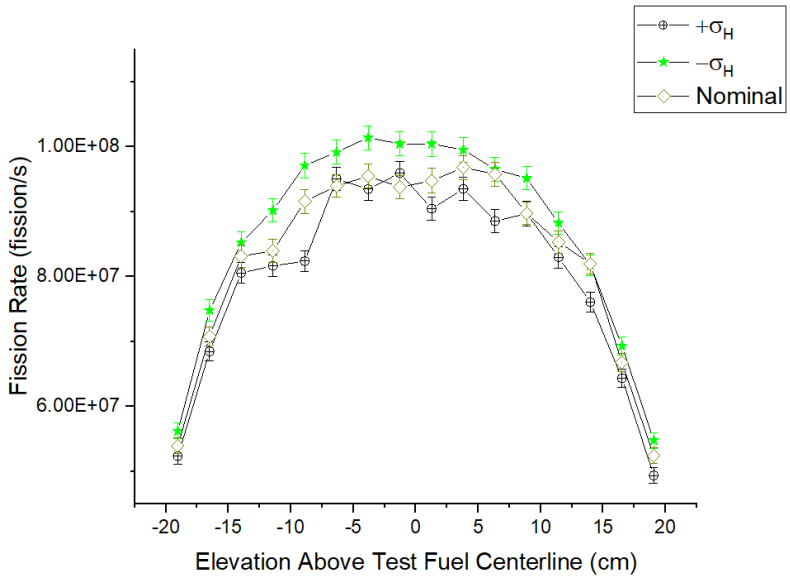

Figure 5-19. Effect of Changing Hydrogen Concentration on the Axial Power Profile.

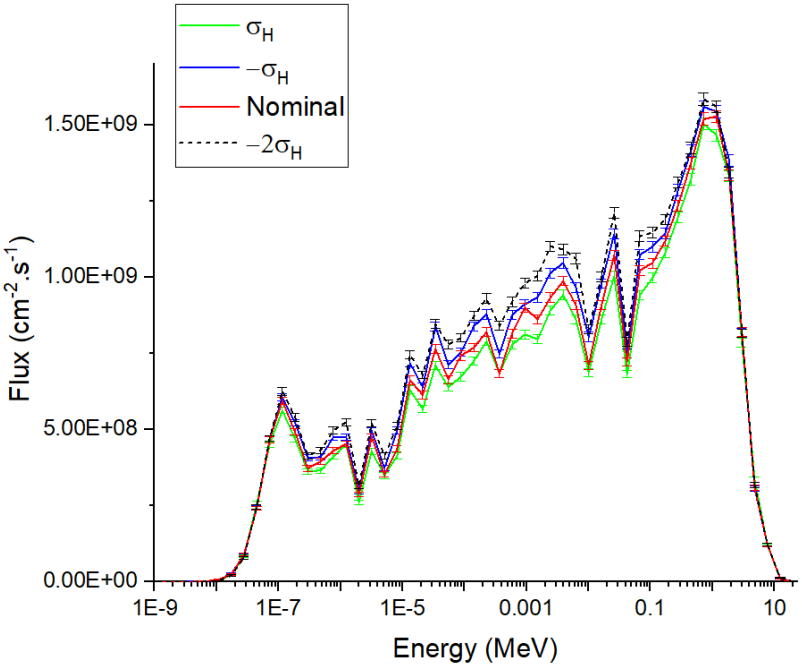

Figure 5-20. Effect of Changing Hydrogen Concentrations on the Neutron Spectrum at the Active Region of the Flux Wire.

5.4.5.3 **Inverse Point Kinetic Calculations**

In order to analyze the reactivity behavior of the core in the power ramp region, the inverse equation of point kinetics [43], given by Equation (5-5), was solved for the power traces of the model and the experiment, and the results are displayed in Figure 5-21.

$$\rho(t) = \beta + l\frac{d}{dt}(\ln P(t)) - \frac{1}{P(t)}\sum_{i=1}^{6}\beta_i(P_0 e^{-\lambda_i t} + \lambda_i \int_0^t P(t')e^{-\lambda_i(t-t')}) \qquad (5\text{-}5)$$

Where:

$\rho(t)$ Represents the reactivity as a function of time.

$P(t)$ Represent the power.

β Represents the delayed neutron fraction.

λ_i Represents the decay constants for the delayed neutron of family i.

l Represents the prompt neutron lifetime.

β_i Represents the effective delayed neutron fraction for family i.

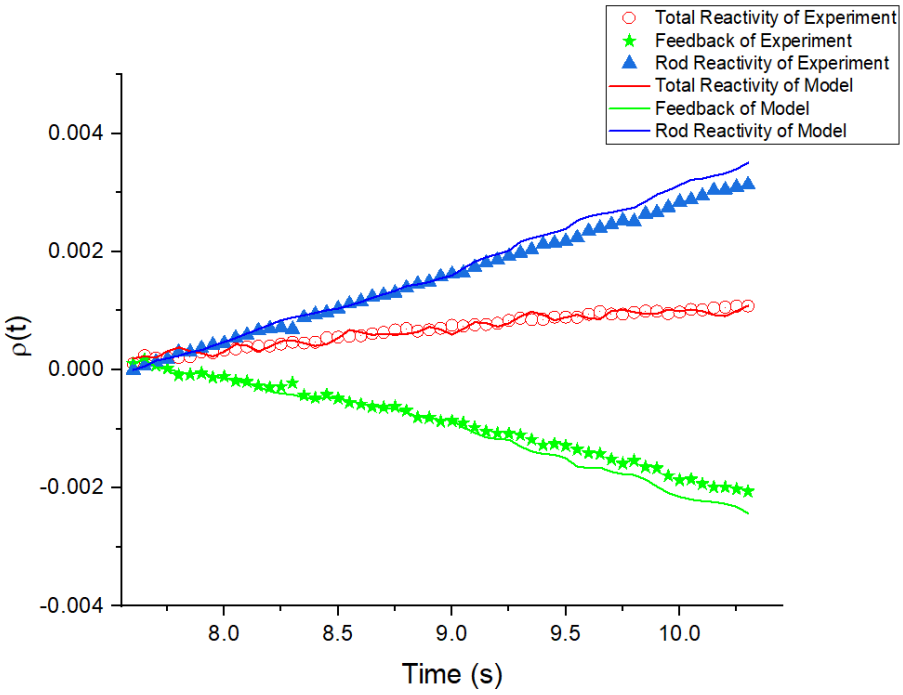

Figure 5-21. Evolution of Core Reactivity and Feedback in the Power Ramp.

As expected, the total reactivity of the core increases as the power level increase. To isolate the temperature feedback reactivity component, the worth of the T-2 rods was subtracted from the total reactivity. The feedback reactivity increasing in the negative direction of reactivity indicates an increase in core temperature as the transient progresses. The maximum deviation in feedback reactivity between the model and the experiment at the end of the power ramp was found to be 36 pcm accounting for a deviation of 16% from the total increase in the experimental feedback reactivity. This deviation is attributed to the adiabatic approximation in OpenFOAM.

6 CONCLUSION

A transient benchmark model based on the M2-CAL experiment was developed using the coupled Serpent/OpenFOAM system. The model was used to simulate the M2-CAL Transient 2580 experiment. To validate the model. The kinetic parameters for TREAT were calculated and compared to historic measurements. The steady-state benchmark model was used to evaluate the total experimental uncertainty for the M2-CAL experiment with the assumption of a distribution for the concentrations and lengths of each core variable. The hydrogen concentration was found to have a great impact on k_{eff}, and consequently, will impact the transient analysis. Only top three contributing factors to the uncertainty in k_{eff} were chosen to calculate the benchmark uncertainty for the transient benchmark, since they contribute 98.7% of the total uncertainty in the steady-state benchmark. However, their distributions were adjusted to the ranges that permit the criticality of the core.

The purpose of the M2-CAL Transient series was to quantify the power coupling factors (PCFs) for the fuel pins in the M2 and M3 tests, to determine the axial power variation in the fuel pins, and to calculate the transient correction factors (TCFs) before the initiation of the M2 and M3 tests.

The benchmark model was used to simulate the U-Zr flux wire low-level steady-state irradiation test (48-1) with a power of 90 KW. The axial power profile in the flux wire was determined and compared to the experimental measurement. The model axial profile was found to have good agreement with the experimental profile except at the upper third part of the wire. The deviation could be explained by the potential of faulty analysis applied after the test. The power coupling factor in the wire was calculated by determining the ratio of the number of fissions in the wire to the total TREAT energy. The PCFs were found to have a 16% deviation from the experiment in the steady-state wire irradiation test and 10.9% in the transient wire irradiation test. A major source of uncertainty in the determination of the PCF is the large uncertainty in the hydrogen concentration in the core, which is higher than 50% of the nominal

concentration of hydrogen. Another potential source of uncertainty in the steady-state wire irradiation test is not reporting the slow movement of the rods during irradiation. It is worth noting that the PCF is a strong function of the transient rod positions and movements.

The integral rod worth was calculated and compared to the experimental measurement and was found to agree to within 1.5%. This difference in worth has significant impact on the period after the initiation of the transient. To avoid this scenario, an equivalent amount of worth must be inserted. Consequently, the position of the rod in the model will always be slightly lower than in the experiment.

The transient benchmark model was built by coupling the Serpent model with OpenFOAM to update the temperature distribution in the core to capture the feedback mechanism in TREAT. The volumetric power distribution in the core is transferred to OpenFOAM where the heat conduction equation is solved and a temperature distribution is obtained. The temperature distribution is then fed to Serpernt to update the thermal neutron scattering libraries. In OpenFOAM, the heat transfer parameters like specific heat and thermal conductivity were introduced as equations fitted according to the experimental measurements of these parameters. Moreover, the meshing of the air cooling channels was not considered since they require finer meshes, which increases the number of meshes by several orders of magnitude. Consequently, the heat transfer process in this model assumes an adiabatic approximation. This approximation is justified by the short duration of the transient (~11 s).

The transient process was started by pulling out T-2, and establishing a stable period of 0.206 s, compared to a reported value of 0.209 s. The benchmark power trace was found to follow closely the trends of the experimental power traces. The total generated energy was reported to have a value between 206 and 177 MJ, compared to 209 ± 0.07 MJ produced by the benchmark model. At the power ramp, four transient runs with different random seeds were carried out and the results were averaged and compared to the model and experimental traces. The power ramp rate for the benchmark model, the experiment, and the four different seed runs were found to agree with each other to within 3%. In order to obtain the axial power

profile in time-dependent calculation while reaching good statistics, the number of segments in the flux wire was reduced. A steady-state wire irradiation was carried out to validate the reduction in the number of segments. The axial power for the transient wire irradiation was compared to the experimental measurement. The TCF was calculated by taking the ratio of the PCF in the steady-state irritation test to that of the transient irradiation test. A model TCF of 0.921 was calculated compared to the experimental measurement of 0.87.

The calculated final maximum temperature was found to be 6.79 K higher than the experiment. Finally, the feedback and total reactivities for the model and the experiment were calculated using the inverse point kinetics method and were found to have good agreement. The deviation between the total feedback reactivity of the model and the experiment is attributed to the implementation of the adiabatic approximation.

REFERENCES

1. Bess, J. D. and DeHart, M. D., "Baseline Assessment of TREAT for Modeling and Analysis Needs," INL/EXT-15-35372, Idaho National Laboratory, Idaho Falls, Idaho (2015).

2. Robinson, W. R. "Power Calibration Experiment for TREAT Test M2," ANL-IFR-8, Argonne National Laboratory, Argonne, Illinois (1985).

3. Bauer, T. H., Morman, J. A., Lo, R. K., Robinson, W. R., et al, "TREAT Tests M2 and M3: Experiment Information and Pretest Analysis," ANL-IFR-9, Argonne National Laboratory, Argonne, Illinois (1985).

4. TREAT: Data and Analysis," ANL-IFR-18, Argonne National Laboratory, Argonne, Illinois (1985).

5. Freund, G. A., Elias, P., MacFarlane, D. R., Geier, J. D., et al, "Design Summary Report on the Transient Reactor Test Facility (TREAT)," ANL-6034, Argonne National Laboratory, Argonne, Illinois (1960).

6. "TREAT Baseline Description Document - 1972," ANL/RAS-72-23, Argonne National Laboratory, (1972).

7. "TREAT Baseline Description Document - 1992," Z0003-00004-OJ-12, Argonne National Laboratory, (1992).

8. Robinson, W. R. and Bauer, T. H., "The M8 Power Calibration Experiment (M8CAL)," ANL-IFR-232, Argonne National Laboratory, Argonne, Illinois (1994).

9. Handwerk, J. H. and Lied, R. C., "The Manufacture of the Graphite-Urania Fuel Matrix for TREAT," ANL-5963, Argonne National Laboratory, Lemont, Illinois (1960).

10. Okrent, D., Dickerman, C. E., Gasidlo, J., O'Shea, D. M., et al, "The Reactor Kinetics of the Transient Reactor Test Facility (TREAT)," ANL-6174, Argonne National Laboratory, Argonne, Illinois (1960).

11. Iskenderian, H. P. "Post Criticality Studies on the TREAT Reactor," ANL-6115, Argonne National Laboratory, Lemont, Illinois (1960).

12. MacFarlane, D. R., Freund, G. A. and Boland, J. F., "Hazards Summary Report on the Transient Reactor Test Facility (TREAT)," ANL-5923, Argonne National Laboratory, Lemont, Illinois (1958).

13. “TREAT Transient Data Summary Sheet – Transient No. 2580,” Z0003-0040-SA-01, Argonne National Laboratory, Argonne, Illinois (1984).

14. "M2CAL Rod Worth Measurment Data Sheet" Z0003-0036-SA-04, Argonne National Laboratory, Argonne, Illinois (1984).

15. Kirn, F., Boland, J., Lawroski, H., Cook, R."" Reactor Physics Measurements in TREAT" ANL-6173, Argonne National Laboratory, Illinois, 1960.

16. "TREAT Reactor Thermocouple Information Data Sheet" Argonne National Laboratory, Illinois, 1989.
17. Robinson, W. R. "Power Calibration Experiment for TREAT Test M2" ANL-IFR-8, Argonne National Laboratory, Argonne, Illinois (1985).

18. W.R. Robinson and T. H. Bauer" Intra Laboratory Memo on the Reanalysis of the Transient Correction Factors for TREAT Tests M2 and M3" Argonne National Laboratory, Illinois, August 5, 1985.

19. L. J. Harrison, W. G. Knapp "Intra Laboratory Memo on A Better Fitted Equation for Heat Capacity of TREAT Fuel" Argonne National Laboratory, Illinois, September 26, 1977.

20. W.R. Robinson and T. H. Bauer " Power Coupling In Treat M-Series: New Experimental Results From M7cal And Updated Analyses" ANL-IFR-86 Argonne National Laboratory, Illinois, February, 1988.

21. Sorrell, N. C., Hawari, A. I., DeHart, M. D., & Bess, J. D. (2017). Investigation of Treat M2 and M3 calibration experiments for benchmark analysis. *Transactions of the American Nuclear Society*, *116*.

22. Intra-Laboratory Memo between W. C. Lipinski and R. L. McVean regarding "TREAT Reactor Instrumentation," (December 2, 1980).

23. "M2-CAL Partial Transient with Flux Wire - 200MJ – TREAT Transient Data Summary Sheet," Z0003-0040-SA-01, Argonne National Laboratory, Argonne, Illinois (1984).

24. Alcoa Distribution and Industrial Products, "Extruded Alloy 6061," www.buildlog.net/documents/Extruded_Alloy_6063.pdf (last updated 2002, last accessed 2022).

25. F. L. Pundsack, "The Properties of Asbestos. II. The Density and Structure of Chrysotile," *J. Phys. Chem.*, **60**, 361-364 (1956).

26. NASA Goddard Space Flight Center, "Earth Fact Sheet," http://nssdc.gsfc.nasa.gov/planetary/factsheet/earthfact.html (last updated 2013, last accessed 2022)

27. Keepin, George Robert, T. F. Wimett, and R. K. Zeigler. "Delayed neutrons from fissionable isotopes of uranium, plutonium and thorium." *Journal of Nuclear Energy (1954)* 6.1-2 (1957): IN2-21.

28. Internal Memo between R. W. Swanson and W. Poenitz regarding "TREAT Stack Effluence," (March 23, 1994).

29. A. E. Powell and R. W. Swanson, Internal Memo regarding "Results of TREAT Annual Confirmatory Emission Measurements," (April 13, 1994).

30. J. Lepannen, et. al., "The Serpent Monte Carlo Code: Status, Development and Applications in 2013," *Ann. Nucl. Energy*, **82**, 142-150 (2015).

31. M. B. Chadwick, et. al., "ENDF/B-VII.1 Nuclear Data for Science and Technology: Cross Sections, Covariances, Fission Product Yields and Decay Data," *Nucl. Data Sheets*, **112** (12), 2887-2996 (2011).

32. D. A. Brown, et. al., "ENDF/B-VIII.0: The 8th Major Release of the Nuclear Reactor Data Library with CIELO-Project Cross Sections, New Standards and Thermal Scattering Data," *Nucl. Data Sheets,* **148**, 1-142 (2018).

33. "ICSBEP Guide to the Expression of Uncertainties," *International Handbook of Evaluated Criticality Safety Benchmark Experiments*, NEA/NSC/DOC (95)/03, OECD/NEA, Paris, France (2008).

34. HTR-PROTEUS Pebble Bed Experimental Program Cores 1, 1A, 2, and 3: Hexagonal Close Packing with a 1:2 Moderator-to-Fuel Pebble Ratio, PROTEUS-GCR-EXP-001," International Handbook of Evaluated Reactor Physics Benchmark Experiments, NEA/NSC/DOC(2006)1, OECD/NEA, Paris, France (2017).

35. Evaluation of the Start-Up Core Physics Tests at Japan's High Temperature Engineering Test Reactor (Fully-Loaded Core), HTTR-GCR-RESR-001," *International Handbook of Evaluated Reactor*Physics Benchmark Experiments, NEA/NSC/DOC(2006)1, OECD/NEA, Paris, France (2017).

36. Bradley Heath & Colby Jensen (2020) Thermal Design of the TREAT Facility, Nuclear Technology 206:9, 1436-1448, DOI: 10.1080/00295450.2020.1725370.

37. A. I. Hawari and V. H. Gillete, "Inelastic Thermal Neutron Scattering Cross Sections for Reactor-grade Graphite," Nucl. Data Sheets, 118, 176-178 (2014).

38. D. Hughes and J. Harvey, "Neutron Cross Sections." McGraw-Hill Book Company, New York (1955).

39. Valtavirta, V., Hessan, M., & Leppänen, J. (2016). Delayed neutron emission model for time dependent simulations with the serpent 2 Monte Carlo code - First results. Physics of Reactors 2016, PHYSOR 2016: Unifying Theory and Experiments in the 21st Century, 3, 1568–1582.

40. H. G. Weller, G. Tabor, H. Jasak, and C. Fureby, "A tensorial approach to computational continuum mechanics using object-oriented techniques," *Comput. Phys.*, vol. 12, no. 6, p. 620, 1998.

41. Leppänen, J. ″Development of a dynamic simulation mode in the Serpent 2 Monte Carlo code.″ In proc. M&C 2013, Sun Valley, ID, May 5-9, 2013.

42. N. C. Sorrell and A. I. Hawari, "TREAT M2 experiment modeling for transient benchmark analysis," *Ann. Nucl. Energy*, vol. 128, pp. 398–405, 2019.

43. Duderstadt, James J., and Louis J. Hamilton. 1976. *Nuclear reactor analysis*. New York: Wiley.

44. Klotzkin, G., Swanson, R. W., Hart, P., & Harrison, L. J. (1984). Time dependence of test fuel power coupling during transient reactor test facility irradiation experiments. *Nuclear Science and Engineering*, *86*(2), 206-218.

45. N. C. Fleming et al., "Transient Reactor Test Facility (TREAT): M2 Calibration (M2CAL) Steady-State Experiments," *International Handbook of Evaluated Reactor Physics Benchmark Experiments, NEA/NSC/DOC (2006)1, OECD/NEA, Paris, France (2020).*